CONSIDERATIONS IN THE DESIGN OF SUPPORTS FOR PANELS IN FATIGUE TESTS

ERIC E. UNGAR AND KYUNG S. LEE

FOREWORD

This report was prepared by Bolt Beranek and Newman Inc., Cambridge, Massachusetts, for the Aero-Acoustics Branch, Vehicle Dynamics Division, AF Flight Dynamics Laboratory, Wright-Patterson Air Force Base, Ohio 45433, under Contract AF 33(615)-5034 "Design of Fixtures for Acoustic Fatigue Tests." The research performed is part of a continuing effort to improve sonic fatigue testing techniques. This effort is part of the Air Force Systems Command's exploratory development program. The contract was initiated under Project 4437 "High Intensity Sound Environment Simulation," Task 443703 "Development of Acoustic Testing Techniques." Mr. Nelson D. Wolf of the Aero-Acoustics Branch, FDDA, was the project engineer.

This report covers work done from May 1966 to April 1967. Contractor's report number is 1494. The manuscript was released by the authors in May 1967 for publication.

The authors are indebted to their colleagues, Dr. Terry D. Scharton and Mr. Thomas M. Yang, for the work reported in Appendix IV, and for many helpful suggestions.

This report has been reviewed and is approved.

Howard A. Magrath

HOWARD A. MAGRATH
Chief, Vehicle Dynamics Division
AF Flight Dynamics Laboratory

ABSTRACT

The question is studied of how a test panel, which represents one of an assemblage of panels in a prototype (e.g., an aircraft fuselage), should be supported, so that a fatigue test of that panel yields the same result as a test of a complete prototype. The recommendation is developed that one should test the panel of interest at the center of a three-by-three panel array, rather than by itself, in order to obtain realistic representations of the boundary stiffness, energy dissipation, and energy transport properties. Considerations in obtaining practical supports that provide approximate free, clamped, and simply supported boundary conditions are investigated and reduced to design equations, graphs, and recommendations. Extensive analyses of the effects of boundary conditions on maximum stresses in resonantly and in randomly vibrating plates and cylindrical shells are appended, as are the results of experiments and analyses concerned with the determination of damping and energy transport in multipanel structures.

TABLE OF CONTENTS

Table of Contents (continued) PAGE

Table of Contents (continued) PAGE

Table of Contents (continued) PAGE

ILLUSTRATIONS AND TABLES

Illustrations and Tables (continued)

Illustrations and Tables (continued)

INTRODUCTION

Many structural parts of aerospace craft are exposed to intense fluctuating pressure fields, which cause these parts to vibrate and hence to be subject to fatigue failure. In spite of recent advances in response prediction methods and fatigue failure theories, the state of the art has not yet reached the point where one can obtain useful predictions of the fatigue life of realistic structures exposed to realistic pressure fields, without carrying out appropriate sonic fatigue tests.

One may in essence distinguish between three types of fatigue and related noise and vibration test: proof tests, development tests, and research tests. In proof tests one attempts to simulate actual field conditions in order to evaluate the probable in-service performance of a prototype. Development tests are somewhat similar to proof tests, but generally are performed on more preliminary configurations and are usually used to evaluate the effect of changes or to compare alternate designs. Research tests, on the other hand, are performed primarily to check theoretical predictions or to provide data on which improve theories can be based.

Ideally, one should carry out all proof tests and probably most development tests on complete vehicles, or at least on complete major substructures, since one generally cannot hope to simulate all of the effects of components which are omitted in tests of smaller structural parts. However, sonic fatigue testing of large structural assemblies is extremely costly, and often entirely impractical, in view of the limited availability of suitable test facilities. One must therefore usually confine himself to testing only some representative structural parts, such as a panel or an assemblage of panels, and immediately face the question of how to treat the boundaries of these structural parts so as to simulate the effects of the missing adjacent structures. It is to this question that the initial sections of the present report are addressed.

Whereas in proof and development tests panel supports must serve to simulate the effects of adjacent structures, panel supports in research tests are usually required merely to provide

predictable and repeatable boundary conditions, which should preferably lend themselves to convenient mathematical representation. The final sections of the present report deal with some of the greatest problems one encounters in attempting to approximate ideal free, clamped, and simply supported boundaries.

PANEL SUPPORTS FOR PROOF AND DEVELOPMENT TESTS

Simulation Requirements

In proof and development testing one desires to "simulate field conditions"; that is, one wants to obtain the same failures in the laboratory as are produced by field conditions. Since failures are known to be correlated with response parameters, simulation of field conditions therefore in essence amounts to reproduction of the salient (failure-producing) features of field responses.

Clearly, more is required than simulation of the excitation that acts on a given panel. The response of a panel which is part of a larger structure may be expected to depend not only on the excitation that acts on that particular panel and on parameters of that panel, but also on the vibrations of adjacent panels and on parameters of the reinforcing members that separate the panels. All of these items need to be considered in the design of proof and development tests.

If one can somehow simulate panel responses, at least in regard to those parameters which one desires to study, then one does not need to consider excitations and boundary effects at all. For example, if one has enough field or laboratory data on the vibrations of a panel on a prototype vehicle, then one may (at least in concept) arrive at a corresponding panel test by a trial-and-error process in which the excitations and panel supports are adjusted until the actual panel response is reproduced to the desired degree. However, proof tests and development tests usually are no longer needed once a complete prototype is available from which the necessary data for designing panel tests can be obtained, and the analytical development of such data is still largely beyond the present state of the art. Thus, the central problem in the design of proof and development tests of panels amounts to: How can one simulate a panel response in the laboratory, in absence of the structures that are in the prototype adjacent to the panel of interest, and without fully knowing the panel response beforehand?

Panel Edge Support Stiffnesses

From elementary analyses one may conclude that boundary conditions affect the stress distributions and the maximum stresses in panels subject to prescribed excitations. Thus, in any simulation one should logically be concerned with reproducing the boundary conditions that are effective in the prototype.

The stiffness constraints that act on a given panel edge in a prototype structure rarely are simple, and usually are contributed both by the edge reinforcing structure (such as a beam, stringer, ring, or bulkhead) and by the adjacent panels. Because these stiffness contributions are complex and generally cannot be fully predicted (and therefore not well simulated) without a great deal of testing, one desires to know the effect that misrepresentation of these edge stiffnesses has on the results of proof and development tests.

The results of an extended study of the effect of edge support stiffnesses on the maximum principal stresses in vibrating panels are presented in Appendixes I-III. Appendix I introduces the "dynamic edge effect" concept, on the basis of which the studies of support stiffness effects are carried out, and applies this concept to study how the ratio of the maximum stress near a panel edge to the maximum stress in a region several wavelengths from the panel boundaries varies with the rotational and lateral (translational) stiffnesses of the panel boundary supports. Appendix I concerns itself only with single modes at a time, whereas Appendix II deals with the multimodal responses to random excitation. Appendixes I and II pertain to flat plates, whereas Appendix III presents similar, but less complete results pertaining to cylindrical shells.

From the results presented in Appendixes I and II one may deduce that generally the maximum stress near an edge exceeds the maximum stress in the interior region of the panel (i.e., far from the panel edges) only if

$$\alpha_r^{-2} + \alpha_t^{-2} < 2 \qquad (1)$$

where α_r and α_t are dimensionless panel support stiffness parameters defined as

$$\alpha_r = K_r/2D\ k_p \quad , \quad \alpha_t = K_t/2D\ k_p^3 \tag{2}$$

in terms of the rotational and translational spring constants K_r and K_t of the supports, per unit edge length. The symbol D denotes the panel's flexural rigidity, and k_p represents a wavenumber which is defined by

$$k_p^2 = (2\pi/\lambda_x)^2+(2\pi/\lambda_y)^2 \approx \omega\sqrt{m/D} \quad , \tag{3}$$

where ω denotes the radian frequency (of a mode or of the midpoint of a frequency band being considered), and m represents the panel mass per unit area. Also, λ_x and λ_y represent typical wavelengths associated with the panel vibrations, in directions parallel and perpendicular to the edge under consideration.

Substitution of Eqs. (2) and (3) into Eq. (1) yields

$$\omega\sqrt{mD^3}\left[\frac{\omega^2 m/D}{K_t^2} + \frac{1}{K_r^2}\right] < 1/2 \tag{4}$$

for the approximate condition under which the maximum stress near an edge exceeds the maximum "interior" stress. Inspection of Eq. (4) leads one to conclude that the maximum edge stress (in the absence of stress raisers, such as holes and rivets) exceeds the maximum interior stress only for relatively large values of the spring constants K_t and K_r — and then only for low frequencies. Thus, one finds that for a rather wide range of frequencies and edge support stiffnesses the greatest stresses occur in the panel regions remote from the edges and are independent of the edge conditions, and one then expects that accurate simulation of edge support stiffnesses often may not be required.

The foregoing result has been derived for flat panels, but as shown in Appendix III, it also holds for cylindrical shells at frequencies (wavenumbers) that are high enough so that membrane stresses are insignificant as compared to flexural stresses. At lower frequencies and wavenumbers membrane forces effect the shell motions significantly, and proper simulation of appropriate membrane boundary conditions may generally be expected to be required, in addition to simulation of the usual flexural boundary conditions.

Energy Dissipation and Transport Properties

It is well known that the response of a panel depends not only on its stiffness and mass properties, but also — and particularly in the presence of random excitation — on its "damping." Damping here refers to the panel's capacity for ridding itself of mechanical energy, and in the most general sense this includes both dissipation of energy and transport of energy to adjacent structures. Simulation of damping thus may be expected to be important, and generally also to present some difficult problems.

Rough estimates of the energy dissipation capabilities of a panel can readily be obtained from available information (for example, Refs. 1-3) or from measurements carried out on a sample panel. Desired amounts of damping may readily be simulated by use of damping materials applied to the test panels; however, such damping material applications must be made judiciously, so as not to distort the stress distributions excessively.

On the other hand, relatively little quantitative information is available concerning the transport of mechanical energy from a panel to its neighbors. It has been shown theoretically that the time-average power flow from one panel to an adjacent one is proportional to the difference between the average kinetic energies per mode of the two panels, providing that the excitations acting on the two panels are steady and uncorrelated, and provided that no energy is dissipated by the coupling (e.g., the reinforcing beam) between the two panels (Ref. 4). Experiments have shown that this proportionality holds approximately, even if the theoretically established conditions for its applicability are not fully satisfied, and also if more than just two connected panels are involved (Ref. 5).

Unfortunately, there exists as yet no valid theoretical basis for prediction of the "power flow coefficients," i.e. of the coefficients of proportionality between power flow and average modal energy difference. These coefficients may be determined experimentally, from a series of measurements on separate structural samples consisting of two panels separated by a reinforcing beam (Ref. 5). Several approaches to measuring these coefficients and dissipative damping on larger panel arrays (with an eye toward measurements to be performed on complete prototypes) have been explored and are reported in Appendix IV; however, these approaches were generally rather unsuccessful.

If two adjacent panels are excited so that they have the same average modal kinetic energy, then there is no net power flow between them, according to the foregoing discussion. As reported in Appendix IV, it has been verified experimentally that power flow is indeed blocked by energy matching (and it has been demonstrated that other means for blocking power flow, such as masses and stiffeners added to the stiffeners between adjacent panels, are ineffective). A panel, which in a structural prototype is surrounded on all sides by similar panels that are similarly excited, thus transfers no net energy to its neighbors, and its damping is due only to its energy dissipation properties. The damping of such a panel may be estimated relatively readily, and thus simulated without great difficulty, as previously mentioned. However, the total damping of a panel that is adjacent to dissimilar or dissimilarly excited panels is affected also by energy transport, and cannot reaily be estimated.

Recommended Configuration

As pointed out in the previous paragraphs, prediction, measurement, and simulation of the "damping" due to energy transport present serious difficulties. Although exact simulation of the stiffnesses of panel boundary structures may not be required if the panels of interest are homogeneous and if the reinforcements do not contribute stress concentrations, the simulation accuracy requirements may be greater for realistic inhomogeneous panels and in the presence of such stress raisers as welds or rivets at the boundaries. In addition, reinforcing structures (e.g., beams, stringers, rings) also exhibit dynamic behavior (e.g., flexural, torsional, and coupled resonances) which cannot readily be simulated without reproducing the prototype reinforcing structures.

All of the foregoing considerations point to the undesirability of testing a single panel by itself, and indicate the utility of using a larger array of panels. Perhaps the most convenient array one may use consists of a three-by-three arrangement of nine panels (see Fig. IV-2, page 99) where only the center panel is the one to be tested under realistic conditions, and the other panels merely serve to provide the proper boundary conditions (in terms of stiffness, energy dissipation, and energy transport) for the center one. The reinforcing beams in such an array should correspond to the prototype in detail, as should the panels, of course, so as to reproduce all potential stress concentrations.

In sonic fatigue (or related noise and vibration) tests of such a nine-panel array, the entire array should be exposed to the excitation that the corresponding portion of the prototype is expected to experience. Since extreme gradients in excitation level generally do not occur, such tests may be expected to reproduce relatively realistically the responses, and thus also the energy transport properties to and from the center panel.

In cases where use of a nine-panel array is impractical, use of a five-panel array (obtained by removing the four corner panels from a nine-panel configuration) may suffice. In a nine-panel array relatively little energy generally may be expected to flow directly from the center panel to the corner ones (Ref. 5), but possibly significant energy flow may occur from the corner to the side panels. Removal of the corner panels thus may reduce the vibration levels of the side panels, and it may be necessary to increase the excitations acting on these panels to make up for this level reduction. One generally need not extend the reinforcing beams beyond the nine-panel or five-panel array dimensions or worry about providing special terminations for these beams, since, as shown in Appendix IV, no appreciable energy transport occurs along the beams and terminations have little effect on the vibrations of the center test panel.

If exposure of the entire nine- or five-panel configuration to sonic excitation is impractical, one may expose only the center panel, and excite the surrounding panels to the proper vibration levels by means of shakers. Here, however, one must determine (perhaps by calculations, for example, based on statistical energy analysis, Ref. 4) what the proper vibration levels are, and one must face the possibility that the spatial distributions of the vibration fields of the various panels will be simulated improperly.

The foregoing discussion applies for panel arrays in which curvature effects are negligible, i.e., for flat arrays at all frequencies and for parts of cylindrical shells above the "breathing" or "ring frequency" f_r, where

$$f_r = c_L/\pi d \qquad (5)$$

in terms of the longitudinal wave velocity c_L of the shell material and the diameter d of the shell. Additional simulation difficulties occur for curved structures at frequencies below f_r, since then membrane effects become important and affect both the vibrations and the associated stresses. Under such conditions, use of some

tensioning arrangement is indicated to simulate shell membrane tension in the circumferential direction; however, use of a complete closed shell section would seem to be preferable, when possible.

PANEL SUPPORTS FOR RESEARCH TESTS

Simulation Requirements

Research tests usually have the purpose of exploring the agreement of experimental results with theoretical predictions, or of generating new data. Thus, panel supports for research tests must provide predictable and repeatable boundary conditions, which lend themselves to exact mathematical analysis.

In research tests one usually attempts to approximate as closely as possible ideally clamped, simply supported, or free boundary conditions, which imply the imposition of certain well-known restrictions on the displacements, rotations, forces, and moments at the panel edges. How well some practical panel edge support structures approach these ideal conditions is studied in Appendix V and summarized below.

It must also be kept in mind, however, that ideal free, simply supported, or clamped boundaries do not permit the transfer of mechanical energy across the panel edges. Because of the finite stiffnesses of realistic support structures, these cannot impede the flow of energy completely. Thus, support structures may be expected to affect the effective damping of test panels, unless extreme care is taken in the design of the panels and their test fixtures. Corresponding recommendations appear at the end of this section.

String-Supports (Free Boundary Simulation)

The most common practical method for simulating free boundaries consists of suspending a test panel from long strings or cables attached at one or two edges, so that the strings and the test panel hang vertically.

In order for a string not to affect the motion of a panel significantly, the lateral impedance of the string must be considerably smaller than the driving point impedance of a panel edge. As shown in Appendix V, a string with negligible flexural

stiffness, for which

$$T^2/E_S I_S \rho_S A_S \omega^2 \ll 1 \quad , \tag{6}$$

will not affect the panel motions significantly if the condition

$$\rho_S A_S T/\rho_P h_P D_P \ll 1 \tag{7}$$

is satisfied. Here T represents the tension in the string, and $E_S I_S$ its flexural stiffness (where E_S is the elastic modulus of the string material and I_S the string's cross-sectional moment of inertia). A_S represents the string's cross-sectional area, ρ_S the density of the string material, and ω the radian frequency; the symbols ρ_P, h_P, D_P denote the density of the panel material, the panel thickness, and the panel's flexural rigidity, respectively.

The use of cables or strings whose flexural stiffness is not negligible — that is, whose properties do not satisfy the inequality (6) — is generally not advisable, except perhaps at very low frequencies. If a supporting cable has considerable flexural stiffness, then this stiffness can lead to relatively high cable impedances (at anti-resonances), and correspondingly to undesirably large effects on the panel responses.

Supporting a test panel in a cutout in a "baffle" by means of layers of a soft material (such as plastic or rubber foam) around its edges, or by the use of tapes (e.g., plastic or fabric adhesive tapes) is also deemed to be generally inadvisable. Such supports may be expected to provide considerable amounts of extraneous damping, and to exhibit anti-resonances at which panel motions may be inhibited excessively.

Clamp Design ("Built-In" Boundary Simulation)

In attempting to obtain the best possible approximations to ideally clamped or "built-in" boundaries, researchers have generally machined the supports and test pieces from the same piece of metal, and have designed the support portion of the resulting single piece of metal to be much more massive than the test portion. (See Refs. 6, 7 for example.) However, the construction of supports and test panels from the same piece of material tends to be costly, so that on this basis one may prefer to use bolted supports instead.

A bolted support, where the edge of a test panel is clamped between two massive bolted-together support strips, may be made to behave like an ideally machined one if the bolt tension is great enough and if the bolts are closely enough spaced so that no (normal or tangential) relative motions occur. The basis for designing such bolted supports is presented in Appendix V, together with a discussion of how to optimize such designs.

Flexures (Simply Supported Boundary Simulation)

Simple supports ideally have infinite lateral (translational) and zero rotational stiffness; they generally are the most difficult to approximate in practice. "Knife-edge" supports come close to satisfying the stiffness requirements, but unfortunately are impractical for panels. If one uses knife edges on only one face of a panel (naturally, on the bottom face of a horizontal panel), then one finds that the corners of the panel leave the supports under the static loading of its own weight (Ref. 8), and also at the low modes — even for small amplitudes. Use of knife edges on both faces of a panel is generally inadvisable, because of the moment constraint that is imposed by two opposed knife edges (particularly if they are not precisely aligned).

The use of short leaf-spring-like sections, made by milling slots into a parent panel and leaving only thin strips of metal to support the center test portion, has been explored to some extent (Ref. 9). Such arrangements deviate from the ideal in that they permit a generally not insignificant amount of lateral motion, and in addition have a tendency to fatigue before the main test panel unless extreme care is taken in their design and production (Ref. 9). "Flexures," consisting essentially of two leaf springs at right angles to each other, may be used to reduce drastically the lateral motions that the milled-slot arrangement permits, and have been put to some uses (Ref. 10) unrelated to fatigue testing.

As demonstrated in Appendix V on the basis of a simple analysis, flexures are generally not useful for the testing of panels over broad frequency ranges, because of the resonant behavior they exhibit. At any one of its anti-resonances a leaf spring may be expected to exert a considerable moment constraint on the test panel and thus not to act like a simple support. These resonant and anti-resonant characteristics might be overcome by the use of flexures made up of very long and very highly damped leaf-springs; however, such springs would be

relatively soft in their axial directions and would not present the desired lateral stiffness to the panel edge.

Recommendations

Of the various types of commonly used ideal boundary conditions, free conditions may be simulated most readily, as evident from the foregoing discussion. Therefore, free boundary conditions should be used for research tests where possible.

Clamped boundaries may be simulated with greater difficulty, but good approximations may be obtained by use of properly designed clamping arrangements. Such an arrangement must be both stiff and heavy, and the entire support-and-panel assembly should be suspended from strings, in order to minimize the dissipation of energy due to support motions.

Simple supports are the most troublesome of all; there exists no adequate practical means for simulating them over extended frequency ranges. Therefore, in spite of the relative simplicity of the associated analyses, one should strive to avoid the use of simple supports.

CONCLUDING REMARKS

The present report constitutes an attempt at setting down rational guidelines for the selection and design of panel fatigue test fixtures and is based on heuristic deductions, on the results of extended analyses, and on some exploratory experimental data.

One may be reasonably confident that the recommendations which appear in this report are generally valid. However, one should keep in mind that the analyses that were carried out are not completely general, and that the exploratory experiments were relatively limited. In particular, most of the analytical work presented in the appendixes applies to homogeneous isotropic rectangular flat panels without stress concentrations; additional studies, particularly of anisotropic panels having various common types of stress concentrations undoubtedly would yield instructive results. Further work on curved panels, which constitute parts of shells, appears also to be needed rather urgently; because of the complexity of the associated analyses, relatively little progress has so far been made in this area.

There is evidently also a need for further experimental work to study the spreading of energy in multi-panel structures, and to develop techniques for the prediction and measurement of this spreading. The exploratory experiments reported here, as well as related prior ones, were performed on geometrically simple (generally flat) panels with epoxy-bonded reinforcements of simple cross-section. More work is needed, particularly on less regularly shaped and curved panels with riveted-on reinforcing beams of Z- or C-shaped cross-sections, which are typical of aerospace vehicle construction.

The design of fixtures to support panels in fatigue tests continues to be partly art and partly science. It is hoped that the present report will help to swing the pointer a little farther toward the science side, but more work is needed before this swing can be made very pronounced.

REFERENCES

1. Structural Damping, J.E. Ruzicka, Ed. (Am. Soc. Mech. Engrs., New York, 1959).

2. E.E. Ungar, "Energy Dissipation at Structural Joints; Mechanisms and Magnitudes," FDL-TDR-64-98, Aug. 1964.

3. E.E. Ungar and J.R. Carbonell, "On Panel Vibration Damping due to Structural Joints," AIAA J. 4: 1385-1390, Aug. 1966.

4. E.E. Ungar, "Fundamentals of Statistical Energy Analysis of Vibrating Systems," AFFDL-TR-66-52, May 1966.

5. E.E. Ungar, N. Koronaios, and J.E. Manning, "Application of Statistical Energy Analysis to Vibrations of Multi-Panel Structures," AFFDL-TR-67-79, May 1967.

6. R.R. McWithey and R.J. Hayduk, "Damping Characteristics of Built-up Cantilever Beams in a Vacuum Environment," NASA TN D-3065, Nov. 1965.

7. J.C. Heine, "The Stress and Frequency Dependence of Material Damping in Some Engineering Alloys," Sc.D. Thesis, Massachusetts Institute of Technology, June 1966.

8. S. Timoshenko and S. Woinowsky-Krieger, Theory of Plates and Shells (McGraw-Hill Book Co., Inc., New York, 1959), 2nd Ed., Chap. 5.

9. I. Dyer, P.W. Smith, Jr., C.I. Malme, and C.M. Gogos, "Sonic Fatigue Resistance of Structural Designs," ASD TR 61-262, Mar. 1961.

10. J.M. Paros and L. Weisbrod, "Flexure Hinges," Machine Design 37: 131-156, Nov. 1965.

DEFINITION OF SYMBOLS USED IN APPENDIXES I AND II

A	Plate area
B_1, B_2	Constants
b	Plate length in y-coordinate direction
$C_o, C_1, \cdots C_4, C_B$	Constants
C_p	Pressure cross-correlation function; see Eq. (1) of Appendix II
$D = \frac{Eh^3}{12(1-\nu^2)}$	Flexural rigidity of plate
D_1, D_2, D_3	See Eqs. (41) of Appendix I
$d_1(\xi)$, $d_2(\zeta)$	Spatial correlation functions; see Eq. (28) of Appendix II
E	Young's modulus
E_1, E_2, E_3	See Eqs. (45) of Appendix I
F_{mnrs}	See Eq. (30) of Appendix II
$F_1(\tau, \omega_{mn}, \omega_{rs})$	See Eq. (36) of Appendix II
$F_2(\omega_{mn}, \omega_{rs})$	See Eq. (36) of Appendix II
$f(\tau)$	Temporal correlation function; see Eq. (28) of Appendix II
G, H, J	Functions of β; defined in Eq. (17) of Appendix I
G_{mr}	See Eq. (34) of Appendix II

Symbols (continued)

h	Plate thickness
I_{mnrs}	Response integral; see Eq. (15) of Appendix II
K_m	See Eq. (34) of Appendix II
K_r, K_t	Support rotational and translational stiffnesses, per unit edge length
k_o	Wavenumber parameter; defined in Eq. (3) of Appendix I
k_p	Wavenumber parameter; defined in Eq. (17) of Appendix I
k_x, k_y	Wavenumbers in x and y directions, respectively
L	Average plate edge length
L_{xy}	Linear differential operator; see Eq. (12) of Appendix II
ℓ	Correlation length; see Eq. (32) of Appendix II
M	$= \max[J, \nu+\beta^2]$; see Eq. (27) of Appendix I
m, m_o	Mass per unit area of plate
N	Stress factor; defined in Eq. (19) of Appendix I
N_c	Number of modes in coherent group
N_g	Number of incoherent mode groups
N_o	Number of resonantly excited modes
n_ω	Modal density

Symbols (continued)

$\langle p^2 \rangle_t$	Temporal mean square pressure; see Eq. (4) of Appendix II
$\langle p^2 \rangle_s$	Spatial mean square pressure; see Eq. (5) of Appendix II
$p(x,y,t)$	Pressure distribution on plate
Q	Plate parameter; see Eq. (17) of Appendix II
R	Ratio of maximum stresses; see Eq. (24) of Appendix I
S_{mnrs}	See Eq. (30) of Appendix II
T_{mn}	Response functions; see Eq. (9) of Appendix II
W_p	Cross-power spectral density of $p(x,y,t)$; see Eq. (3) of Appendix II
W_w	Cross-power spectral density of deflection w
w	Lateral flexural deflection of plate
x_o	Constant
x,y	Cartesian coordinates parallel to plate edges
Y, Y_e, Y_B	Deflection functions; defined in Eqs. (2), (6), and (10) of Appendix I
α_r, α_t	Stiffness parameters; defined in Eq. (17) of Appendix I
γ_{mr}	See Eq. (34) of Appendix II

Symbols (continued)

Δ	Parameter defined in Eq. (17) of Appendix I
$\Delta\omega$	Bandwidth of excitation frequency band
δ_{ij}	Kronecker delta (takes one unit value if i=j; is zero otherwise)
ζ	Spatial separation in y-direction; see Eq. (2) of Appendix II
η	Loss factor of plate
Λ_x, Λ_y, Λ_{xy}	Stress parameter; defined in Eq. (19) of Appendix I
ν	Poisson's ratio
ξ	Spatial separation in x-direction; see Eq. (2) of Appendix II
σ_x, σ_y	Normal stresses in x,y coordinate directions
τ	Time separation; see Eq. (2) of Appendix II
τ_{xy}	Shear stress
$\phi_{mn}(x,y)$	Natural mode shape functions
ω	Circular frequency
ω_c	Center frequency of excitation band
ω_{mn}	Natural frequency of mn mode

APPENDIX I

EFFECT OF BOUNDARY CONDITIONS ON MAXIMUM MODAL STRESSES IN PLATES

THE DYNAMIC EDGE EFFECT IN PLATES

Bolotin's Asymptotic Method

It is well-known that the mode shapes of uniform rectangular plates are essentially sinusoidal, except in the immediate vicinity of the plate boundaries (Ref. 1). Accordingly, Bolotin has developed a method of analysis based on approximate mode shapes, which satisfy specified boundary conditions and which approach sinusoids in the plate "interior region," many wavelengths from the boundaries (Fig. I-1).

Bolotin has shown (Ref. 2) that one may represent the deflection $w(x,y)$ of a plate in the region near a boundary that is parallel to the x-axis as

$$w(x,y) = Y(y) \sin k_x(x-x_o) \qquad (1)$$

where the function $Y(y)$ must be of the form

$$Y(y) = C_o\left[\sin k_y y + B_1 \cos k_y y + B_2 e^{-k_o y}\right] \quad , \qquad (2)$$

with

$$k_o = \sqrt{2k_x^2 + k_y^2} \qquad (3)$$

in order to satisfy the classical equation of free vibrations of plates,

$$D\nabla^4 w - m\omega^2 w = 0 \quad , \qquad (4)$$

and in order to approach a sinusoidal form asymptotically (for large values of x). In the foregoing expressions, k_x and k_y represent the wavenumbers associated with the plate mode shapes

in the interior region, and C_o, B_1, and B_2 are constants. B_1 and B_2 may be evaluated from boundary conditions; C_o is of no interest, since mode shapes are defined only within an arbitrary multiplicative constant.

The $B_2e^{-k_oy}$ term represents the "dynamic edge effect," and the region within which this term is significant as compared to the other two terms of Eq. (2) has been called the "dynamic edge effect region."

Bolotin has also demonstrated (Refs. 2,3) that one generally obtains very good approximations to the natural frequencies if one uses the expression

$$\omega = (k_x^2+k_y^2)\sqrt{D/m} \quad , \tag{5}$$

which follows from substitution of the asymptotic form of Eq. (2) into Eq. (1), and from substitution of the result into Eq. (4).

Errors in Stresses from Edge Effect Calculations

Bolotin and his associates have used the foregoing dynamic edge effect concept and his related "asymptotic method" to study natural frequencies of plates and to analyze edge stresses for some special cases. Although they studied the errors in the natural frequencies calculated by this method, no one seems to have been concerned with the errors in the corresponding mode shapes and in the stress distributions associated with these mode shapes. Since the primary concern here is with stresses, at least a brief investigation of the errors in the mode shapes and stresses is indicated. Such an investigation appears in the following paragraphs.

The simplest problem one might consider is that of a rectangular plate which is simply supported on all edges. For such a plate it turns out that the dynamic edge effect is degenerate, and that Bolotin's method gives mode shapes which coincide exactly with the exact mode shapes.

More instructive results may be obtained by considering a rectangular plate which is simply supported on only two opposite edges (x=0 and x=a) and clamped at the other two edges

(y=0 and y=b). For such a plate, the (exact) general solution of Eq. (4) may be expressed as

$$w = Y_e(y) \sin k_x x \quad ;$$

$$Y_e(y) = C_1 \sin k_y y + C_2 \cos k_y y \tag{6}$$

$$+ C_3 \sinh k_o y + C_4 \cosh k_o y \quad ,$$

where the C's are constants.

Application of the clamped edge conditions

$$Y_e(0) = Y_e(b) = Y_e'(0) = Y_e'(b) = 0 \quad , \tag{7}$$

where the prime denotes differentiation, to the second of Eq. (6) permits one to evaluate all but one of the C's and yields the mode shape function

$$\frac{Y_e}{C_1} = \left[\sin k_y y - \frac{k_y}{k_o} \sinh k_o y\right] - \frac{\sin k_y b - \frac{k_y}{k_o} \sinh k_o b}{\cos k_y b - \cosh k_o b} \left[\cos k_y y - \cosh k_o y\right] \tag{8}$$

and the relation

$$\cos k_y b \cosh k_o b - \frac{k_x^2}{k_o k_y} \sinh k_o b \sin k_y b = 1 \tag{9}$$

which the wavenumbers must satisfy.

Bolotin's asymptotic method, when applied to the same problem, yields

$$\frac{Y_B}{C_B} = \sin k_y y - \frac{k_y}{k_o}\left(\cos k_y y - e^{-k_o y}\right) \quad , \quad \text{for } 0<y<b/2 \qquad (10)$$

instead of Eq. (8) and

$$k_y \tan(k_y b/2)+k_o = 0 \quad \text{(for symmetric* mode shapes)}$$
$$k_o \tan(k_y b/2)+k_y = 0 \quad \text{(for anti-symmetric* mode shapes)} \qquad (11)$$

instead of Eq. (9). Here C_B is an arbitrary constant, as is C_1 in Eq. (8). The subscript B in Y_B is intended to differentiate the result from Bolotin's method from the exact mode shape function Y_e.

One finds that Eqs. (8) and (9) approach Eqs. (10) and (11), respectively, as k_x and k_y take on large values. Thus, the greatest difference between the two solutions may be expected to occur for the smallest values of k_x and k_y; i.e., for the fundamental mode. Table I shows the results of corresponding calculations for a square panel, with the constants C_1 and C_B adjusted so that $Y_e(b/2)=Y_B(b/2)=1$. The difference between Bolotin's and the exact mode shape is seen to be small.

The stress components σ_x, σ_y, τ_{xy} [in Timoshenko's notation (Ref. 4)] in the outermost fibers of a homogeneous isotropic plate of thickness h obey the well-known relations

$$\pm \frac{h^2}{6D}\sigma_x = w_{xx}+\nu\, w_{yy}$$
$$\pm \frac{h^2}{6D}\sigma_y = w_{yy}+\nu\, w_{xx} \qquad (12)$$
$$\pm \frac{h^2}{6D}\tau_{xy} = (1-\nu^2)w_{xy}$$

---

*About y = b/2.

where the subscripts on w denoted partial differentiation, and where ν represents Poisson's ratio. One may thus calculate the stresses associated with a given mode shape by substituting the corresponding mode shape function into Eq. (12).

Although it has already been shown that the exact mode shape function $Y_e(y)$ is closely approximated by the corresponding function $Y_B(y)$ obtained from Bolotin's method, the errors in the stresses may be greater, since the stresses involve the second derivatives of the shape functions — and these errors require some further study.

By differentiation of Eqs. (8) and (10) one may obtain

$$\frac{Y_e''+k_y^2 Y_e}{C_1\left(k_y^2+k_o^2\right)} = -\frac{k_y}{k_o}\sinh k_o y + \frac{\sin k_y b-\frac{k_y}{k_o}\sinh k_o b}{\cos k_y b-\cosh k_o b}\cosh k_o y \qquad (13)$$

and

$$\frac{Y_B''+k_y^2 Y_B}{C_B\left(k_y^2+k_o^2\right)} = \frac{k_y}{k_o} e^{-k_o y} \quad . \qquad (14)$$

One may again determine that the asymptotic values (i.e., the values as k_x, $k_y \to \infty$) of the right-hand sides of Eqs. (13) and (14) are identical, and thus that the greatest difference between them is obtained for the lowest mode. Values of Y_e'' and Y_B'' calculated for this mode are indicated in Table I. Good agreement between the approximate and exact solution may again be noted, indicating that one introduces little error if one calculates stresses from Bolotin's instead of the exact mode shapes.

TABLE I

COMPARISON OF EXACT AND BOLOTIN'S APPROXIMATE MODE SHAPE FUNCTIONS, FOR FUNDAMENTAL MODE OF CLAMPED-CLAMPED SUPPORTED-SUPPORTED SQUARE PLATE

y/b	Y_e	Y_B	$Y_e'' b^2$	$Y_B'' b^2$
0.0	0	0	52.69	53.40
0.05	.0357	.0364	22.22	22.67
0.1	.1280	.1307	13.38	13.59
0.2	.4057	.4136	- 2.58	- 2.72
0.3	.7020	.7136	-15.00	-15.79
0.4	.9202	.9305	-23.29	-24.28
0.5	1.000	1.000	-26.15	-27.44

Analysis of this special case thus indicates that Bolotin's asymptotic method gives the mode shapes and the associated stress distributions within tolerable error bounds. Although this method was developed primarily for the higher modes, the present results encourage one to use the proposed approximate method also for the lowest modes.

EVALUATION OF BOUNDARY EFFECTS ON MAXIMUM STRESSES

Translational and Rotational Edge Constraints

In order to study the effect of changes in the plate edge constraints on the plate stresses it is convenient to consider two spring-like boundary conditions: 1) A rotational spring condition, characterized by spring constant K_r, which provides a moment (per unit edge length) proportional to the edge rotation; 2) a translational spring, described by spring constant K_t, which provides a lateral force (per unit edge length) proportional to the edge deflection.

From the well-known plate moment and shear force expressions (Ref. 4) one finds that these spring constants are related to the plate deflection as

$$\begin{aligned} K_r[w_y]_{y=0} &= D[w_{yy}+\nu\, w_{xx}]_{y=0} \\ -K_t[w]_{y=0} &= D[w_{yyy}+w_{xxy}]_{y=0} \end{aligned} \tag{15}$$

where the subscripts on the w's denote partial differentiation. Substitution of Eq. (2) into (15) permits one to evaluate the constants B_1 and B_2, and to write

$$\begin{aligned} -B_1\Delta &= B_2\Delta+2G(G+2\alpha_r H) \\ -B_2\Delta &= 4\alpha_r\alpha_t G^2 + J \end{aligned} \tag{16}$$

where

$$\begin{aligned} &G \equiv \sqrt{1+\beta^2} \quad , \quad H \equiv \sqrt{1+2\beta^2} \quad , \quad J \equiv 1+\nu\beta^2 \\ &\Delta \equiv JH-4\alpha_t G^2(G+\alpha_r H) \\ &\alpha_r \equiv K_r/2Dk_p \quad , \quad \alpha_t \equiv K_t/2Dk_p^3 \\ &\beta \equiv k_x/k_y \quad , \quad k_p^2 \equiv k_x^2+k_y^2 = G^2k_y^2 \quad . \end{aligned} \tag{17}$$

Stresses

The normal and shear stresses in the outermost fibers of the plate may be computed from the deflection w according to Eq. (12). From these stresses one may determine the maximum principal stress σ_p by use of the general relation

$$2\sigma_p(x,y) = |\sigma_x|+|\sigma_y|+\sqrt{\left[|\sigma_x|-|\sigma_y|\right]^2+4\tau_{xy}^2} \quad . \tag{18}$$

By substitution of Eqs. (1) and (2) into (12) one may obtain expressions for the stress distribution throughout the entire plate. However, the "edge stresses" (at the plate edge y=0) and the "asymptotic stresses" (at y=∞) are of particular interest here. If one defines

$$\Lambda_x = N|\sigma_x| \quad , \quad \Lambda_y = N|\sigma_y| \quad , \quad \Lambda_{xy} = N|\tau_{xy}|$$
$$N \equiv |h^2/6D\ k_y^2 C_o \cos k_x(x-x_o)| \tag{19}$$

and lets the added subscripts e and a refer to the edge and to the space-wise maximum asymptotic stresses, respectively, then one may write

$$\Lambda_{x,e} = |-(\nu+\beta^2)B_1 + (\nu H^2-\beta^2)B_2|$$
$$\Lambda_{y,e} = |-J\ B_1 + (H^2-\nu\beta^2)B_2| \tag{20}$$
$$\Lambda_{xy,e} = |(1-\nu)\beta\ (1-HB_2)|$$

and

$$\Lambda_{x,a} = \left|\left(\nu+\beta^2\right)\sqrt{1+B_1^2}\right|$$

$$\Lambda_{y,a} = \left|J\sqrt{1+B_1^2}\right| \qquad (21)$$

$$\Lambda_{xy,a} = \left|\left(1-\nu\right)\beta\sqrt{1+B_1^2}\right| \quad .$$

One may then study the relative magnitudes of the edge stresses and the maximum asymptotic stresses by comparing Eqs. (20) and (21).

Since the normal stresses vary as sin $k_x(x-x_o)$, whereas the shear stress varies as cos $k_x(x-x_o)$, the maximum normal and shear stresses do not occur at the same locations. At those locations where the normal stresses take on their greatest values, the shear stress vanishes; the greatest principal stress there is equal to the greater of the two normal stresses, in view of Eq. (18).

From Eq. (21) one can deduce that $\Lambda_{xy,a}$ always is smaller than either $\Lambda_{x,a}$ or $\Lambda_{y,a}$, or both. Hence, the maximum principal stress in the asymptotic region is given by

$$\left(\Lambda_{p,a}\right)_{max} = \text{Max}\left[\left|\Lambda_{x,a}\right| \quad , \quad \left|\Lambda_{y,a}\right|\right] \quad . \qquad (22)$$

By maximizing (with respect to x) the expression for the principal stress obtained from Eqs. (18) and (19), one finds that the maximum principal edge stress obeys the following expression, provided that $\Lambda_y > \Lambda_x$:

$$\left(\Lambda_{p,e}\right)_{max} = \begin{cases} \Lambda_y & \text{for } \Lambda_{xy}^2 \leq \left(\dfrac{\Lambda_y-\Lambda_x}{2}\right)\Lambda_y \\ \Lambda_{xy}\sqrt{\dfrac{\Lambda_{xy}^2+\Lambda_x\Lambda_y}{\Lambda_{xy}^2-\left(\dfrac{\Lambda_x-\Lambda_y}{2}\right)^2}} & \text{for } \Lambda_{xy}^2 > \left(\dfrac{\Lambda_y-\Lambda_x}{2}\right)\Lambda_y \end{cases} \qquad (23)$$

The added subscript e is implied for all Λ's on the right-hand side of Eq. (23). Equation (23) may be made to apply for $\Lambda_x > \Lambda_y$ by interchanging all x and y subscripts.

Ratio of Maximum Edge and Interior Stresses

The "asymptotic stresses" are those associated with the sinusoidal mode shapes that approximate the plate deflection in regions remote from any boundary, and are thus independent of the boundary conditions. The "edge stresses," on the other hand, depend very markedly on the boundary conditions. Thus, the stress ratio

$$R = \frac{\left(\sigma_{p,e}\right)_{max}}{\left(\sigma_{p,a}\right)_{max}} \tag{24}$$

may be taken as a convenient measure of the effect of boundary conditions on the maximum stresses.

In view of the form of Eq. (2), it is conceivable that the greatest stresses may occur not directly at the edge, but rather at some other position within one wavelength from the edge. One might thus argue that the ratio R is not representative of the greatest stress. However, by examining the expressions for the stress distributions in detail one can show that for the higher modes the actual maximum stress differs only negligibly from the maximum edge stress.

STRESS RATIOS FOR LIMITING CASES

Infinite Translational Stiffness

For the case where the plate edge is not permitted to deflect, and where the plate edge rotation is opposed by a rotational spring of finite stiffness K_r, one may let $K_t \to \infty$ in Eqs. (16) and (17) and obtain

$$B_2 = -B_1 = \frac{\alpha_r}{G + \alpha_r H} \equiv B \quad . \tag{25}$$

Then Eqs. (20)-(22) yield

$$\begin{aligned} \left(\Lambda_{p,a}\right)_{max} &= \sqrt{1+B^2}\ M \\ \Lambda_{x,e} &= 2\nu G^2 B \\ \Lambda_{y,e} &= 2G^2 B \\ \Lambda_{xy,e} &= (1-\nu)\beta(1-BH) \end{aligned} \tag{26}$$

where

$$M \equiv \max[J,\ \nu+\beta^2] \quad . \tag{27}$$

If one substitutes Eq. (26) into Eqs. (23) and (24) [and notes that $\Lambda_y > \Lambda_x$ if $1>\nu$, which is always true], then one obtains

$$R = \begin{cases} \dfrac{2G^2 B}{M\left(1+B^2\right)^{1/2}} & \text{for } \alpha_r > \alpha_{ro} \\ \dfrac{\beta G\left[\beta^2\left(1-\nu^2\right)+4\nu\alpha_r^2 G^2\right]^{1/2}}{M\left[\alpha_r^2+\left(G+\alpha_r H\right)^2\right]^{1/2}\left[\beta^2-\alpha_r G^2\right]^{1/2}} & \text{for } \alpha_r < \alpha_{ro} \end{cases} \tag{28}$$

where

$$\alpha_{ro} \equiv \frac{\beta}{G}\sqrt{\frac{1-\nu}{2}} \quad . \tag{29}$$

One may show that the ratio of the two bracketed expressions of Eq. (28) that begin with β^2 takes on its maximum value for $\alpha_r = \alpha_{ro}$, and that for $\alpha_r \leq \alpha_{ro}$ Eq. (28) implies

$$R \leq \frac{\beta G \sqrt{2(1-\nu)}}{M\left[\alpha_r^2+\left(G+\alpha_r H\right)^2\right]^{1/2}} \leq \frac{\beta\sqrt{2(1-\nu)}}{M} \leq \frac{\sqrt{2(1-\nu)}}{1+\nu} \quad . \qquad (30)$$

The right-most of the foregoing expressions is less than unity for $\nu \geq 0.23$, which holds for most structural materials. Thus, one may conclude that R is less than unity if $\alpha_r < \alpha_{r_0}$; i.e., that the greatest asymptotic principal stress then exceeds the greatest principal edge stress.

From Eq. (28) one may obtain contours of constant R in the α_r-β plane. The most important of these contours, the one for R=1, is sketched in Fig. I-2 (for ν=0.3). Figure I-2 permits one to tell at a glance whether the edge stresses or the asymptotic stresses predominate for a given reduced rotational constraint stiffness α_r and for a given wavenumber ratio β.

In the R<1 region of Fig. I-2 the asymptotic stresses predominate. Since these are independent of the boundary conditions, changes of the constraint stiffness (within this region) will not affect the dominant stresses, and thus will have no effect on the fatigue life of the plate.

Infinite Rotational Stiffness

For the case where the plate edge rests on an "elastic foundation" but is constrained so that its slope in direction perpendicular to the edge remains zero, one may let $K_r \to \infty$ in Eqs. (16) and (17). One then obtains

$$B_1 = -B_2 + 1/\alpha_t G \quad , \quad B_2 = 1/H \qquad (31)$$

and Eqs. (20) and (21) yield

$$\Lambda_{x,e} = \left|2\nu G^2/H - (\nu+\beta^2)/\alpha_t G\right|$$

$$\Lambda_{y,e} = \left|2G^2/H + J/\alpha_t G\right| \qquad (32)$$

$$\Lambda_{xy,e} = 0 \quad , \quad (\Lambda_{p,a})_{max} = M\sqrt{1+B_1^2} \quad .$$

Since the edge shear stress vanishes here, the greatest principal edge stress is always equal to the greater of the two normal stresses. Detailed examination of the above expressions indicates that $\Lambda_{x,e}>\Lambda_{y,e}$ for

$$(1-\beta^2)H/2G^3 < \alpha_t < H/2G \tag{33}$$

and that otherwise $\Lambda_{x,e}<\Lambda_{y,e}$.

One may again form the stress ratios R and obtain contours of constant R in the α_t-β plane. Figure I-3 shows the R=1 contour, together with limits for the dominance of the σ_x and σ_y normal stresses.

Zero Rotational Stiffnesses

For the case where the moment-stiffness at the plate edge is zero, and where the plate edge translation is opposed by a restraint of finite stiffness K_t, one may let $K_r \to 0$ in Eqs. (16) and (17) and obtain

$$B_2 = -(1+\mu\beta^2)/\Delta_t = -J/\Delta_t$$
$$B_1 = B_2(2G^2/J-1) \tag{34}$$

where

$$\Delta_t \equiv JH-4\alpha_t G^3 \quad . \tag{35}$$

Then Eqs. (20) and (21) yield

$$\Lambda_{x,e} = 2G^2\beta^2(1-\nu^2)/\Delta_t \quad , \quad \Lambda_{y,e} = 0$$

$$\Lambda_{xy,e} = (1-\nu)\beta[1+JH/\Delta_t] \tag{36}$$

$$(\Lambda_{p,a})_{max} = M[1+(2G^2-J)^2\,\Delta_t^{-2}]^{1/2} \quad .$$

Since here $\Lambda_{y,e}=0$, the greatest principal edge stress is equal either to $\Lambda_{x,e}$ or to the principal stress as obtained from Eq. (23), which here reduces to

$$\Lambda_{p,e} = \Lambda_{xy,e}[1-(\Lambda_{x,e}/2\Lambda_{xy,e})^2]^{-1/2} \quad . \tag{37}$$

Detailed examination reveals that the greatest value of the principal stress given by Eq. (37) is always less than the corresponding maximum of the asymptotic stress $(\Lambda_{p,a})_{max}$. Therefore, one needs only to compare $\Lambda_{x,e}$ and $(\Lambda_{p,a})_{max}$. One finds that $\Lambda_{x,e}>(\Lambda_{p,e})_{max}$ if

$$|2G\sqrt{\alpha_t}-JH/G^2|<\beta(1+\nu)/\sqrt{2} \quad . \tag{38}$$

The stress ratio R, as defined in Eq. (24), here becomes

$$R = \frac{2\beta^2G^2\left(1-\nu^2\right)}{M\left[\Delta_t^2+\left(2G^2-J\right)^2\right]^{1/2}} \quad . \tag{39}$$

The region of the α_t-β plane in which $R\geq 1$ may be determined by setting R=1 in Eq. (39). One finds that $R\geq 1$ for

$$\alpha_t<D_1/2+\sqrt{(D_3/M)^2-D_2^2}$$
$$\alpha_t>D_1/2-\sqrt{(D_3/M)^2-D_2^2} \tag{40}$$

where

$$D_1 = JH/2G^3 \quad , \quad D_3 = \beta^2(1-\nu^2)/2G$$
$$D_2 = (2G^2-J)/4G^3 \quad . \tag{41}$$

The above expressions define a strip region centered along the line $\alpha_t=D_1/2$, on which the denominators of the expressions for the constants B_1 and B_2 vanish identically. Figure I-4 shows the contour of R=1, together with the discontinuity line $\alpha_t=D_1/2$ in the α_t-β plane.

Zero Translational Stiffness

For the case where the shear force at the plate edge is zero, and where the plate edge rotation is opposed by a rotational restraint of finite stiffness K_r, one may set $K_t=0$ in Eqs. (16) and (17) to obtain

$$B_1 = -[B_2+4\alpha_r G/J+2G^2/JH]$$
$$B_2 = -1/H \quad . \tag{42}$$

Then Eqs. (20) and (21) reduce to

$$\Lambda_{x,e} = \frac{4G}{J}\left[\alpha_r(\nu+\beta^2) + \frac{(1-\nu^2)\beta^2 G}{2H}\right]$$
$$\Lambda_{y,e} = 4\alpha_r G \quad , \quad \Lambda_{xy,e} = 2(1-\nu)\beta \tag{43}$$
$$\Lambda_{p,a} = \frac{4MG}{J}\left[\left(\alpha_r+\frac{2G^2-J}{4GH}\right)^2 + \left(\frac{J}{4G}\right)^2\right]^{1/2} \quad .$$

One may find the greatest principal edge stress from the above expressions by the method illustrated in the development of Eq. (23). One can show, after much manipulation, that only $\Lambda_{x,e}$ can yield values of the stress ratio R which exceed unity. The corresponding stress ratio may be expressed as

$$R = \frac{(\nu+\beta^2)}{M} \frac{[\alpha_r+E_3]}{\sqrt{(\alpha_r+E_1)^2+E_2^2}} \tag{44}$$

where

$$E_1 = (2G^2-J)/4GH \quad , \quad E_2 = J/4G$$
$$E_3 = \beta^2 G(1-\nu^2)/2H(\beta^2+\nu) \quad . \tag{45}$$

The contour of R=1 and region for R>1 and R<1 are shown in Fig. I-5.

Observations

In addition to the delineation of the R>1 and R<1 regions presented in Figs. I-2 – I-5, the foregoing analysis of the limiting cases has shown the following:

1. The maximum principal edge stress which exceeds the maximum principal asymptotic stress is equal either to σ_x or to σ_y.

2. If either one of the edge stiffnesses is infinite, then the edge stress σ_y dominates in the R>1 region.

3. If either one of the edge stiffnesses is zero, then the edge stress σ_x dominates in the R>1 region.

STRESS RATIOS FOR GENERAL CASES

Simplifying Assumption

The previous section, which dealt with the maximum stresses in panels where only one of the two types of edge stiffnesses is finite (the other being zero or infinite), sheds light on the approach one may take to deal with the most general case of concern here. Since the general expressions for the edge stresses have already been developed, one needs only to carry out the maximizations required to determine the greatest principal edge stress, and then to delineate those regions in the edge-stiffness and wavenumber-ratio (α_r, α_t, β) space where the "edge-to-asymptotic" stress ratio R, as defined in Eq. (24) exceeds unity. This procedure is quite straightforward in principle, but requires an excessive amount of algebraic manipulation. Hence, it is useful to introduce some plausible assumptions, the validity of which may be inferred from the previous analyses of the limiting cases.

The previous studies have shown that in the limiting edge-stiffness cases the shear stress at the panel edge plays no role in establishing the maximum principal edge stress. Thus, it seems reasonable to assume that this shear stress is only rarely significant in the more general case, and to take the statement that "The maximum principal edge stress which exceeds the maximum principal asymptotic stress is equal either to σ_x or to σ_y" to hold in general.

With the aforementioned assumption the analysis is greatly simplified. By combining Eqs. (16), (20), and (21) one obtains

$$\begin{aligned}
\Lambda_{x,e}|\Delta| &= 2G\left|-\nu G\left(4\alpha_r\alpha_t G^2+J\right) + \left(\nu+\beta^2\right)\left(2\alpha_r H+G\right)\right| \\
\Lambda_{y,e}|\Delta| &= 4\alpha_r G\left|-2\alpha_t G^3+HJ\right| \qquad (46) \\
\Lambda_{p,a}|\Delta| &= M\left\{\left[4\alpha_r G\left(\alpha_t G-H\right) + J-2G^2\right]^2 + \Delta^2\right\}^{1/2} .
\end{aligned}$$

From the comparison of the expressions for $\Lambda_{x,e}$ and $\Lambda_{y,e}$ it follows that

$$\begin{aligned} \Lambda_{y,e} &> \Lambda_{x,e} \quad \text{if} \quad \alpha_r > \alpha_1 \text{ and/or } \alpha_r > \alpha_2 \\ \Lambda_{y,e} &< \Lambda_{x,e} \quad \text{if} \quad \alpha_r < \alpha_1 \text{ and/or } \alpha_r < \alpha_2 \end{aligned} \tag{47}$$

where

$$\alpha_1 \equiv \frac{\beta^2(1-\nu)}{2G[2\alpha_t G - H]} \ , \ \alpha_2 \equiv \frac{\beta^2 G^2(1+\nu)}{2G[(1-\beta^2)H - 2\alpha_t G^3]} \ . \tag{48}$$

One finds that the stress ratio R always is less than unity if $\alpha_r > \alpha_2$. Since one here is concerned only with those conditions which yield R>1, one needs to deal only with those cases where $\alpha_r < \alpha_2$.

It is convenient to divide the entire range of edge-support conditions into two classes, depending on the relative magnitudes of α_r and α_1 (where α_1, of course, is a function of the translational stiffness parameter α_t). Cases where $\alpha_r > \alpha_1$ may be called rotationally "clamped-like," those where $\alpha_r < \alpha_1$ may be called "free-like."

Clamped-Like Edges

For $\alpha_r > \alpha_1$ Eq. (46) indicates that $\Lambda_{y,e} > \Lambda_{x,e}$. One then finds that

$$R = \frac{4\alpha_r G\left[2\alpha_t G^3 - HJ\right]}{M\left\{\left[4\alpha_r G\left(\alpha_t G - H\right) + J - 2G^2\right]^2 + \Delta^2\right\}^{1/2}} \ . \tag{49}$$

The surface on which R=1 in the (α_r, α_t, β) space* is sketched in Fig. I-6; the regions where R exceeds or is less than unity are also indicated in that figure.

Free-Like Edges

For $\alpha_r<\alpha_1$, Eq. (46) indicates that $\Lambda_{x,e}>\Lambda_{y,e}$. In this case one finds that

$$R = \frac{2G}{M} \cdot \frac{\left(\nu+\beta^2\right)\left(2\alpha_r H+G\right) - \nu G\left(4\alpha_r\alpha_t G^2+J\right)}{\left\{\Delta^2+\left[4\alpha_r G\left(\alpha_t G-H\right) + J-2G^2\right]^2\right\}^{1/2}} \quad . \qquad (50)$$

Figure I-7 shows the corresponding R=1 surface in (α_r, α_t, β) space and indicates the regions where R>1 and R<1.

*In Fig. I-6 β is shown as a function of $1/\alpha_t$ and $1/\alpha_r$ (instead of α_t and α_r), in order to display the limiting surfaces more clearly.

REFERENCES FOR APPENDIX I

1. F.V. Hunt, "Stress and Strain Limits on the Attainable Velocity in Mechanical Vibration," J. Acoust. Soc. Am. 32: 1123-1128 (1960).

2. V.V. Bolotin, "Dynamic Edge Effect in the Oscillation of Plates," Inzhenernyi Sbornik 31: 3-14 (1960) (In Russian).

3. V.V. Bolotin, B.P. Makarov, G.V. Mishenkov, and Iu. Iu. Shveiko, "An Asymptotic Method for the Study of Natural Frequencies of Elastic Plates," Sbornik Raschety na Prochnost', Vol. 6, Mashgiz (1960) (In Russian).

4. S. Timoshenko, Theory of Plates and Shells (McGraw-Hill Book Company, Inc., New York, 1940).

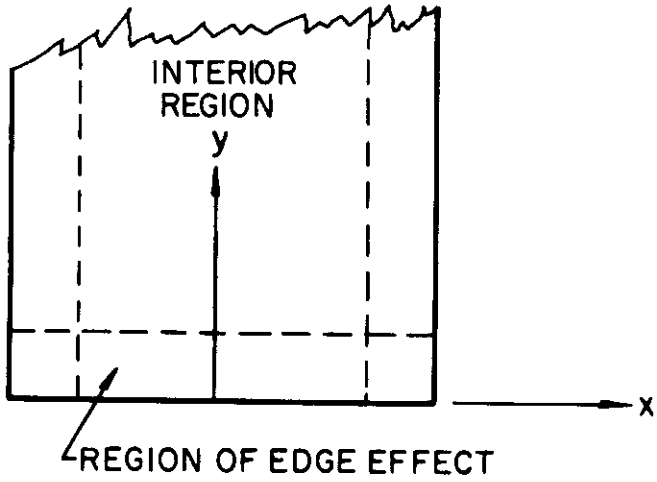

FIG. I-1 INTERIOR AND EDGE EFFECT REGIONS OF PLATE

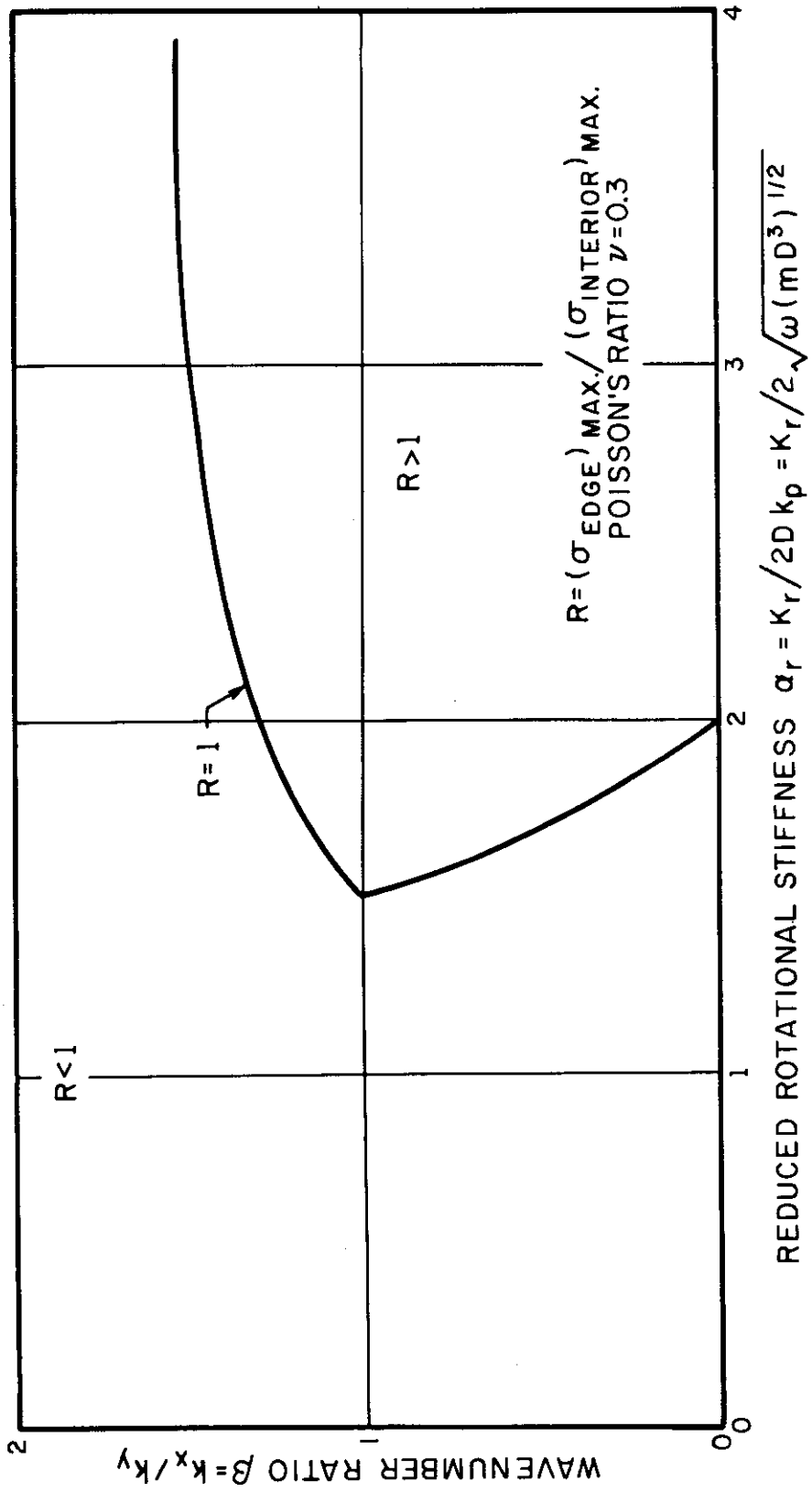

FIG. I-2 EDGE AND INTERIOR STRESS DOMINANCE IN PLATES WITH EDGES CONSTRAINED TO ZERO LATERAL DEFLECTION ($K_t = \infty$)

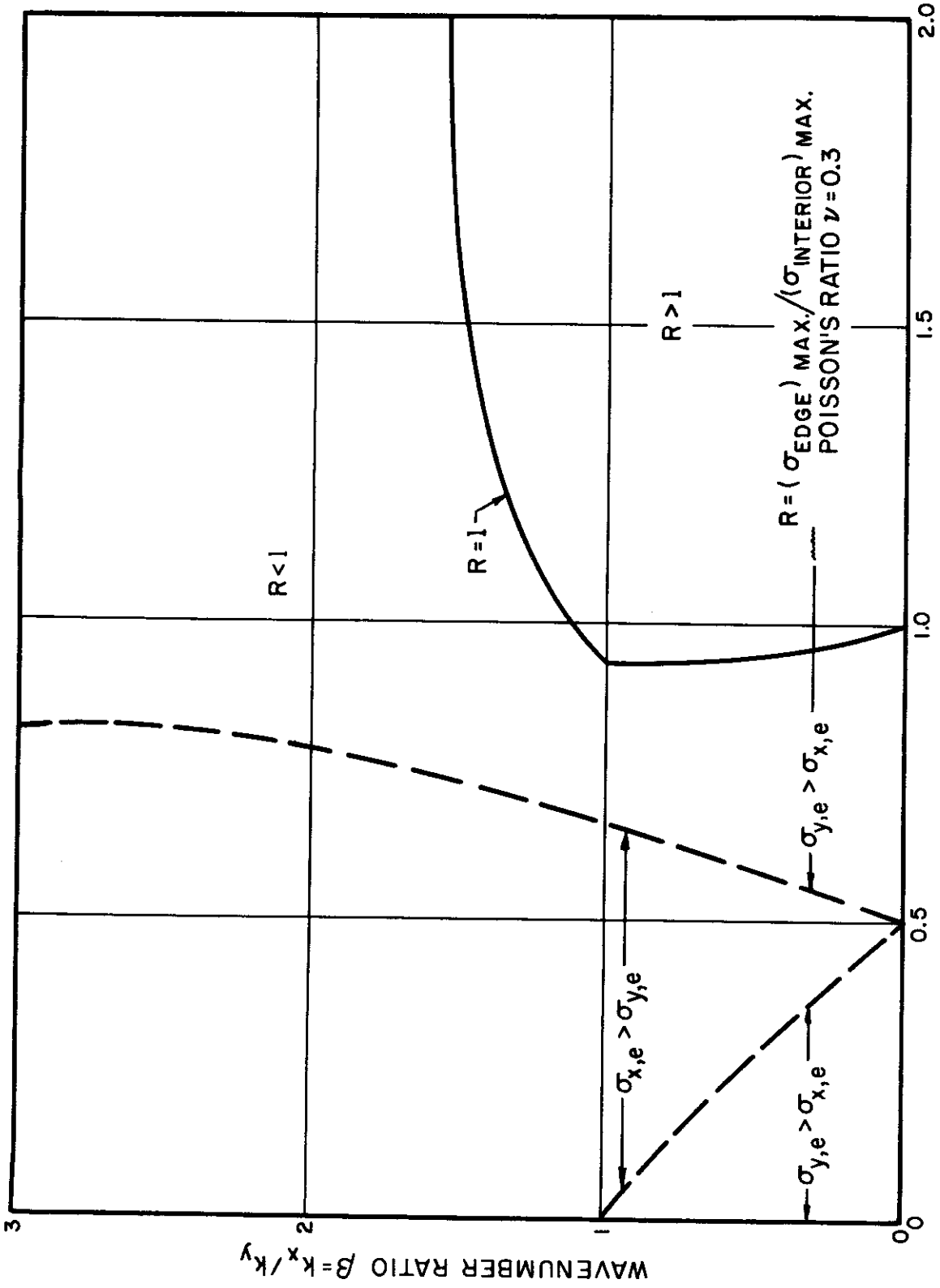

FIG. I-3 EDGE AND INTERIOR STRESS DOMINANCE IN PLATES WITH EDGES CONSTRAINED TO ZERO ROTATION ($K_r = \infty$)

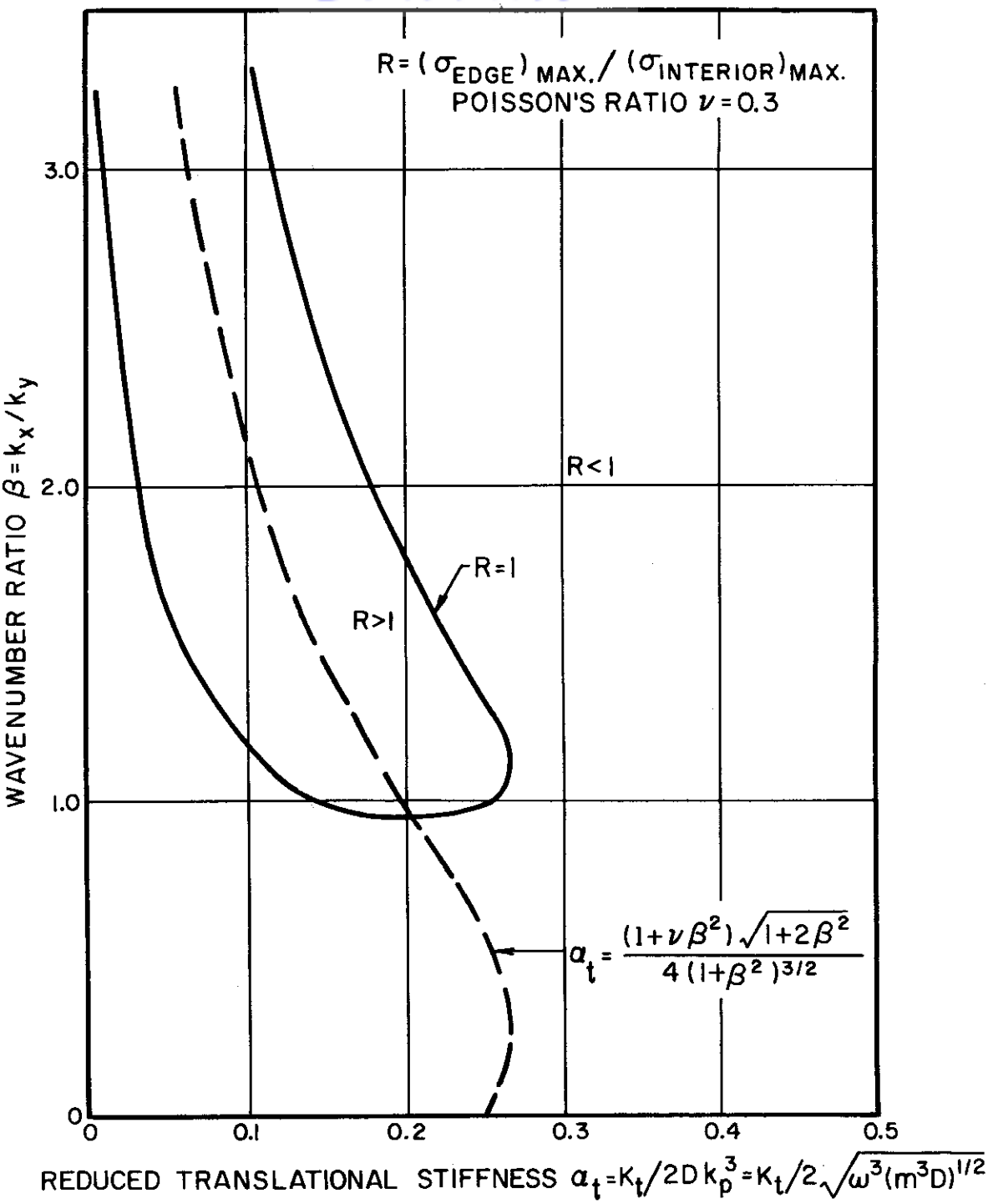

FIG. I-4 EDGE AND INTERIOR STRESS DOMINANCE IN PLATES WITH MOMENT-FREE EDGES ($K_r = 0$)

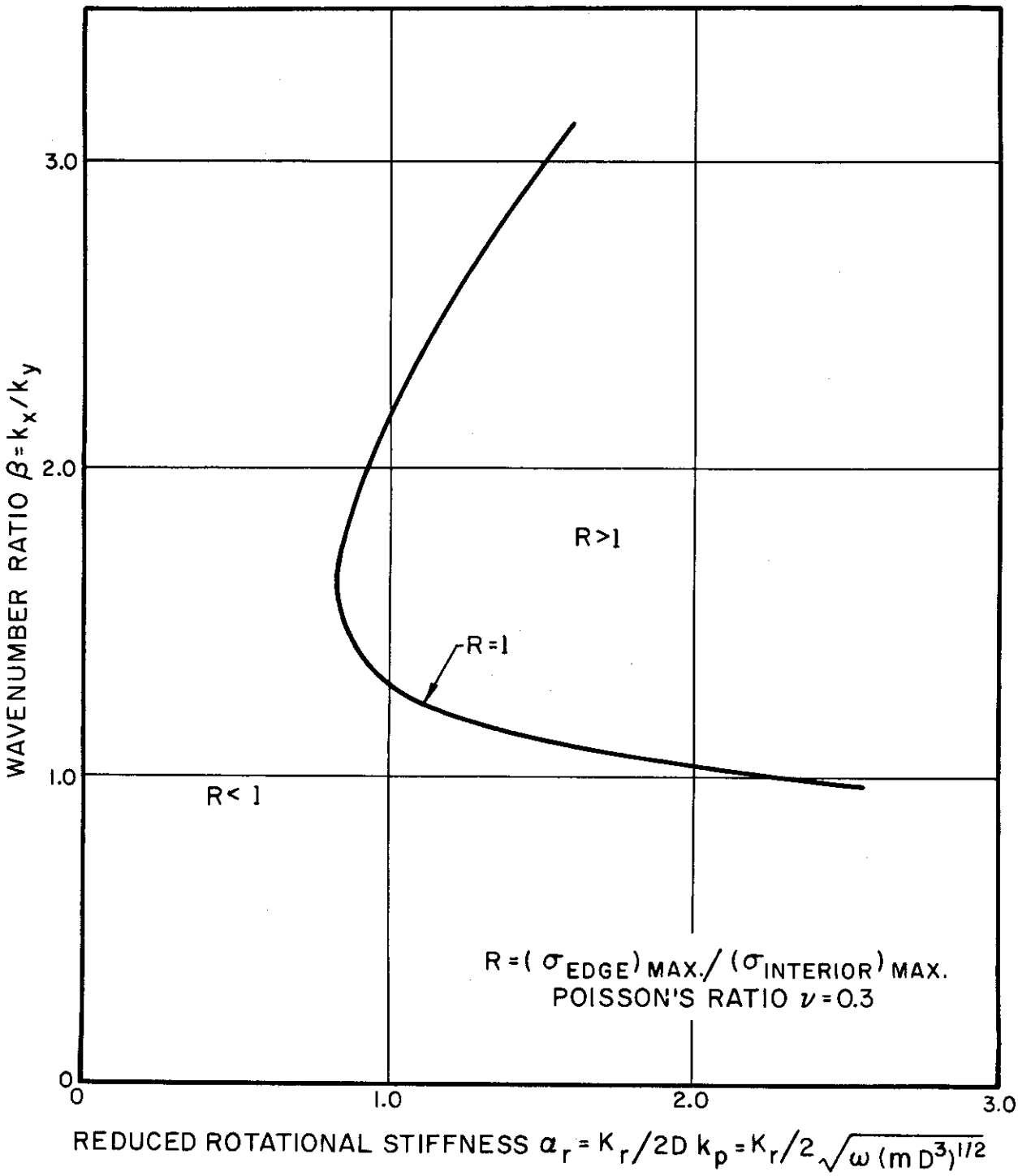

FIG. I-5 EDGE AND INTERIOR STRESS DOMINANCE IN PLATES WITH SHEAR-FORCE-FREE EDGES ($K_t = 0$)

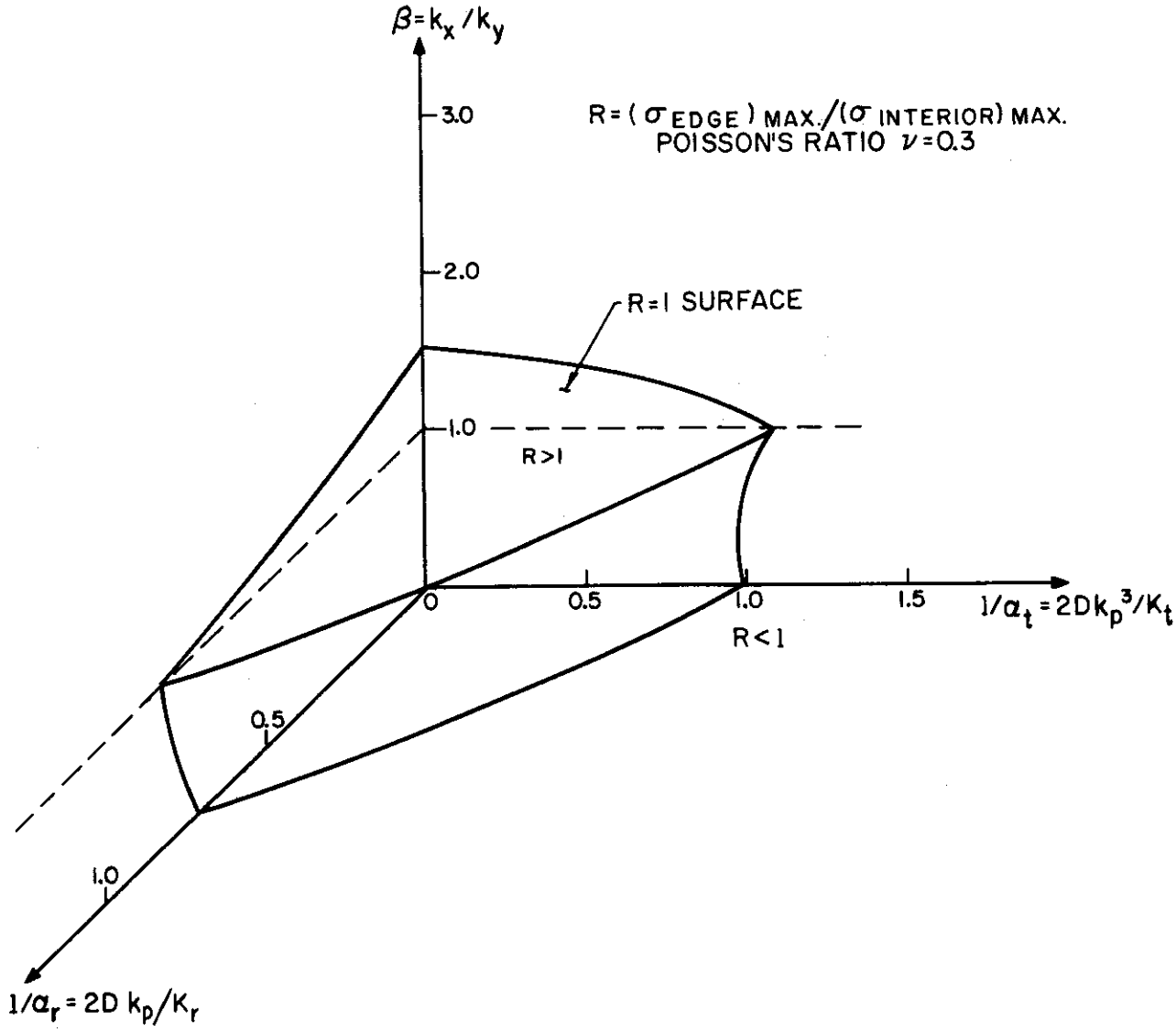

FIG. I-6 REGIONS OF EDGE AND INTERIOR STRESS DOMINANCE IN PLATES WITH ROTATIONALLY "CLAMPED-LIKE" EDGES ($\alpha_r > \alpha_1$)

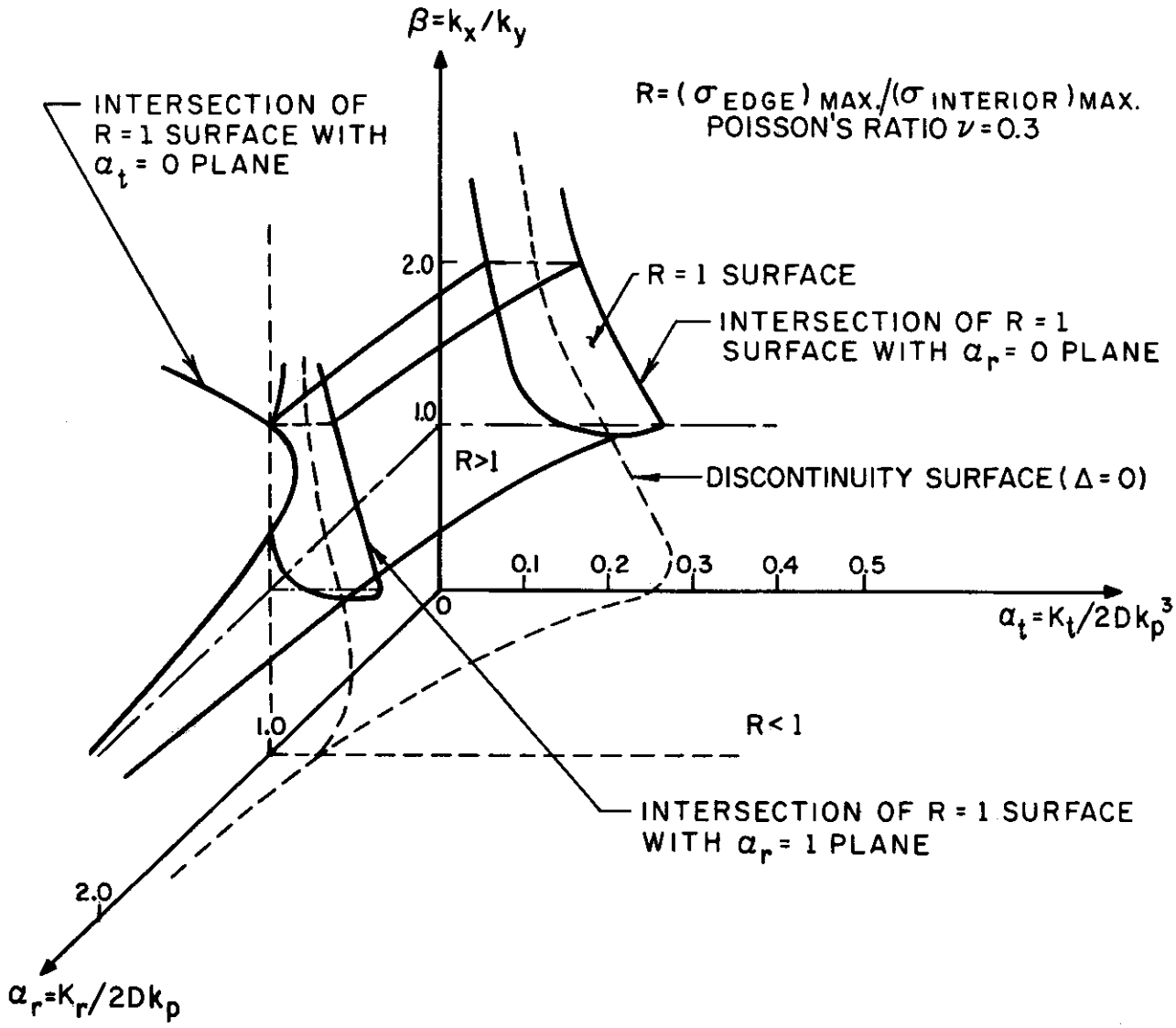

FIG. I-7 REGIONS OF EDGE AND INTERIOR STRESS DOMINANCE IN PLATES WITH ROTATIONALLY "FREE-LIKE" EDGES ($\alpha_r < \alpha_t$)

APPENDIX II

EFFECTS OF BOUNDARY CONDITIONS ON MAXIMUM STRESSES IN RANDOMLY VIBRATING PLATES

INTRODUCTION

The vibrations of an elastic plate which is subject to broad-band excitation, at frequencies that are well above the fundamental plate resonance, may be described in terms of the sums of the responses of all modes. The effects of translational and rotational boundary stiffnesses on maximum plate stresses then can, in principle, be studied by the same method as was employed in Appendix I for the analysis of stresses associated with single modes. However, the analysis of multimodal responses presents some difficulties which makes the foregoing approach impractical. Unlike in the single modal case, the ratio of maximum edge to maximum interior stress in the multimodal case depends markedly on the character of the excitation field. This dependence not only complicates the general analysis, but also makes finding of the maximum stresses very difficult.

In order to circumvent the aforementioned difficulties, the present appendix makes use of a different approach than Appendix I. Instead of superposing modal responses, the present appendix develops a general expression which describes the temporal mean square response of a plate subject to a random pressure field, then determines the spatial maximum of this temporal mean square response by a statistical method, and finally examines the effect of edge conditions on this maximum.

RANDOM VIBRATIONS

There exists much literature on the calculation of dynamic responses of elastic structures to random pressure fields (Refs. 1,2). It is useful to restate here briefly some of the most important results, for the sake of clarity and completeness.

All of the work discussed here pertains to uniform homogeneous isotropic flat plates, with thickness h, flexural rigidity D, Poisson's ratio ν, and mass m_o per unit area. Structural damping is treated by permitting the plate rigidity

to take on complex values (Ref. 3), and the corresponding loss factor η is taken to be small and independent of frequency. The excitation fields are considered to be stationary, homogeneous, and ergodic random processes.

Characterization of Excitation Pressure

The cross-correlation function C_p of the pressure $p(x,y,t)$ is defined as

$$C_p(\xi,\zeta,\tau) = \lim_{T\to\infty} \frac{1}{2T} \int_{-T}^{T} p(x,y,t)p(x',y',t+\tau)\, d\tau \qquad (1)$$

where

$$\xi = x-x' \quad , \quad \zeta = y-y' \quad , \quad \tau = t-t' \quad . \qquad (2)$$

Also, x and y (and x' and y') represent Cartesian coordinates in the plane of the plate, and t (and t') denotes time.

The cross power spectral density W_p of p is defined as the Fourier transform of the cross-correlation function; so that

$$W_p \equiv (2\pi)^{-1/2} \int_{-\infty}^{\infty} C_p e^{-i\omega\tau} d\tau \quad , \quad C_p = (2\pi)^{-1/2} \int_{-\infty}^{\infty} W_p e^{i\omega\tau} d\omega \quad . \qquad (3)$$

The temporal mean square value of p is denoted by $\langle p^2 \rangle_t$ and obeys

$$\langle p^2 \rangle_t = C_p(0,0,0) = (2\pi)^{-1/2} \int_{-\infty}^{\infty} W_p(0,0,\omega)\, d\omega \quad . \qquad (4)$$

The spatial mean square value of p is represented by $\langle p^2 \rangle_s$ and is defined by

$$\langle p^2 \rangle_s = \frac{1}{A} \int_A p^2 \, dA \quad , \tag{5}$$

where A denotes the plate area.

Response Quantities

If the deflection $w=\bar{w}(x,y)e^{i\omega t}$ of a damped elastic plate exposed to a sinusoidal pressure field $p=\bar{p}(x,y)e^{i\omega t}$ is taken to obey the classical thin plate equation (Ref. 3)

$$D(1+is\eta)\nabla^4 \bar{w} - m_o \omega^2 \bar{w} = \bar{p} \quad , \tag{6}$$

where

$$s = \operatorname{sgn} \omega = \omega/|\omega| \quad , \tag{7}$$

then the cross power spectral density W_w of the plate deflection w may be written as

$$W_w = \sum\sum\sum\sum_{mnrs} \frac{\Phi_{mn}\Phi_{rs}}{m_o^2 T_{mn} T_{rs}^*} W_{Q,mnrs} \quad , \tag{8}$$

where the asterisk (*) indicates the complex conjugate of the quantity to which it is appended, and where

$$\begin{aligned} T_{mn} &\equiv (\omega_{mn}^2 - \omega^2) + is\eta\, \omega_{mn}^2 \\ W_{Q,mnrs} &\equiv \int_A \int_A W_p \, \Phi_{mn}(x,y)\Phi_{rs}(x',y') \, dxdy \, dx'dy' \quad . \end{aligned} \tag{9}$$

The functions Φ_{mn} represent the normalized natural mode shapes, which satisfy the modal equation

$$D\nabla^4\Phi_{mn} - \omega_{mn}^2 \, m_o \Phi_{mn} = 0 \quad , \tag{10}$$

(where ω_{mn} represents the natural frequency associated with the mn mode) as well as the prescribed boundary conditions and the normalization condition

$$\int_A \Phi_{mn}(x,y)\Phi_{rs}(x,y) \, dA = \delta_{mr}\delta_{ns} \quad , \tag{11}$$

where δ_{mr}, δ_{ns} are Kronecker deltas. For any structural response quantity U (such as stress), which is related to the natural mode shapes as

$$U_{mn} = L_{xy} \, \Phi_{mn} \quad , \tag{12}$$

in terms of a linear differential operator Lxy, which contains only the spatial coordinates, one may express the spectral density of that response quantity as

$$W_U = \sum\sum\sum\sum_{mnrs} \frac{U_{mn} \, U_{rs}}{m_o^2 T_{mn} T_{rs}^*} \, W_{Q,mnrs} \quad . \tag{13}$$

From an equation analogous to Eq. (4) one may then find the temporal mean square response to be given by

$$\langle U^2 \rangle_t = \sum\sum\sum\sum_{mnrs} m_o^{-2} \, U_{mn} \, U_{rs} \, I_{mnrs} \quad , \tag{14}$$

where

$$I_{mnrs} \equiv (2\pi)^{-1/2} \int_{-\infty}^{\infty} \frac{W_{Q,mnrs}}{T_{mn} T_{rs}^*} \, d\omega \quad . \tag{15}$$

MAXIMUM STRESSES

Edge and Interior (Asymptotic) Stresses

The temporal mean square values of the edge and asymptotic stresses may be found by the direct application of the foregoing results. From the discussion of single modal responses (Appendix I), one may observe that the stresses associated with the mn mode at the plate edge and in the plate interior may be written

$$\begin{aligned}
\sigma_{x,e,mn} &= Q\,\bar{\omega}_{mn}\,R_{x,mn}\,\sin k_m(x-x_o) \\
\sigma_{y,e,mn} &= Q\,\bar{\omega}'_{mn}\,R_{y,mn}\,\sin k_m(x-x_o) \\
\sigma_{x,a,mn} &= Q\,\bar{\omega}_{mn}\,\sin k_m(x-x_o)\,\sin k_n(y-y_o) \\
\sigma_{y,a,mn} &= Q\,\bar{\omega}'_{mn}\,\sin k_m(x-x_o)\,\sin k_n(y-y_o)
\end{aligned} \tag{16}$$

where

$$\begin{aligned}
Q &\equiv 12\sqrt{mD/ah^4}\quad , \quad \beta_{mn} = k_m/k_n \\
\bar{\omega}_{mn} &\equiv \omega_{mn}\left[\frac{\nu+\beta_{mn}^2}{1+\beta_{mn}^2}\right] \quad , \quad \bar{\omega}'_{mn} \equiv \omega_{mn}\left[\frac{1+\nu\beta_{mn}^2}{1+\beta_{mn}^2}\right]
\end{aligned} \tag{17}$$

and where the R's denote ratios of maximum edge to maximum interior stresses:

$$R_{x,mn} \equiv \frac{\left[\sigma_{e,mn,x}\right]_{max}}{\left[\sigma_{a,mn,x}\right]_{max}} = \frac{1}{\sqrt{1+B_1^2}} \left| -B_1 + B_2 \left[1 - \frac{2\beta_{mn}^2 (1-\nu)}{\nu+\beta_{mn}^2} \right] \right|$$

$$R_{y,mn} = \frac{\left[\sigma_{e,mn,y}\right]_{max}}{\left[\sigma_{a,mn,y}\right]_{max}} = \frac{1}{\sqrt{1+B_1^2}} \left| -B_1 + B_2 \left[1 + \frac{2\beta_{mn}^2 (1-\nu)}{1+\beta_{mn}^2} \right] \right| \quad . \tag{18}$$

Here B_1 and B_2 are functions of ν and β_{mn}, as defined in Eq. (16) of Appendix I.

Response Maxima; Dependence on Modal Coherence

If one attempts to determine the spatial maximum of the temporal mean square response by application of the classical maximization process, one finds that the locations and the magnitudes of the response maxima depend strongly on the excitation. Also, except in the somewhat degenerate case where a few modes dominate the plate motion, use of the classical process generally proves to be too tedious. Fortunately, one may arrive at a simple development based on the recently obtained result (Ref. 4) which indicates that the probability of the occurrence of response concentrations (i.e., of locations on the plate where all excited modes have their stress maxima) is nearly equal to unity.

It is convenient to rewrite Eq. (14) as

$$\langle U^2 \rangle_t = \sum_{mnrs} \sum \sum \sum \Gamma_{mnrs} I_{mnrs} \Phi_{mn} \Phi_{rs} \quad , \tag{19}$$

in terms of Γ_{mnrs}, a coefficient that depends on the L_{xy} operator of Eq. (12) which describes the relation of the response quantity U to the deflections. One finds that one may express the spatial maximum of this temporal mean square response (in the light of the aforementioned response concentration argument) as

$$\mathrm{Max}\left[\langle U^2 \rangle_t\right] = \sum_{mnrs} \sum \sum \sum \Gamma_{mnrs} I_{mnrs} \mathrm{Max}\left[\Phi_{mn} \Phi_{rs}\right] \quad . \tag{20}$$

The notation Max[ ] is used here and henceforth to designate maximization with respect to space.

The evaluation of the sums of Eq. (20) may be greatly simplified if the modal excitation coefficients I_{mnrs} are grouped into classes according to the magnitude of the cross-product contributions relative to that of the self-product contributions. If one designates as "uncorrelated" (or incoherently responding) those modes whose self-product contributions to the maximum response greatly exceed their cross-product contributions, and correspondingly designates as "correlated" (or coherently responding) those modes whose self- and cross-product contributions are of the same order of magnitude, then one may arrive at the following statements concerning the maximum response:

1) If all (resonantly excited) modes are uncorrelated, then

$$\text{Max}[\langle U^2\rangle_t] \approx \sum_{mn}\sum \Gamma_{mnmn} I_{mnmn} \text{Max}[\Phi_{mn}^2] \approx 4\langle U^2\rangle_{t,s} \quad . \tag{21}$$

2) If all N_o of the excited modes are correlated, then

$$\begin{aligned} \text{Max}[\langle U^2\rangle_t] &\approx \sum_{mnrs}\sum\sum\sum \Gamma_{mnrs} I_{mnrs} \text{Max}[\Phi_{mn}\Phi_{rs}] \\ &\approx N_o \sum_{mn}\sum \Gamma_{mnmn} I_{mnmn} \text{Max}[\Phi_{mn}^2] \\ &\approx 4N_o\langle U^2\rangle_{t,s} \quad . \end{aligned} \tag{22}$$

3) If the N_o excited modes are made up of N_g modal groups, where each group contains N_c modes which are correlated with each other, but uncorrelated with modes outside the group, then

$$\text{Max}[\langle U^2\rangle_t] \approx N_g N_c \sum_{mn}\sum \Gamma_{mnmn} I_{mnmn} \text{Max}[\Phi_{mn}^2] \approx 4N_g N_c \langle U^2\rangle_{t,s} \quad . \tag{23}$$

The last form of each of Eqs. (21)–(23) is obtained by considering double-sinusoidal mode shapes, like those indicated in the last two of Eq. (16). [The form of Eq. (23) also follows from the temporal and spatial mean square, which obeys

$$\langle U^2 \rangle_{t,s} = \sum_{mn}\sum \Gamma_{mnmn} I_{mnmn} \langle \Phi^2_{mn} \rangle_s \quad , \tag{24}$$

as may readily be obtained from Eq. (19).]

Maxima of Mean Square Stresses

The foregoing development and the indication that response concentrations are expected to occur with unity probability (Ref. 4) permits one to evaluate various stress maxima.

By combining Eqs. (14) and (16) one may find the mean square stresses to obey

$$\begin{aligned}
\langle \sigma^2_{x,e} \rangle_t &= \sum_{mnrs}\sum\sum\sum \Gamma_\sigma I_{mnrs} \bar{\omega}_{mn} \bar{\omega}_{rs} R_{x,mn} R_{x,rs} \phi_{mr} \\
\langle \sigma^2_{y,e} \rangle_t &= \sum_{mnrs}\sum\sum\sum \Gamma_\sigma I_{mnrs} \bar{\omega}'_{mn} \bar{\omega}'_{rs} R_{y,mn} R_{y,rs} \phi_{mr} \\
\langle \sigma^2_{x,a} \rangle_t &= \sum_{mnrs}\sum\sum\sum \Gamma_\sigma I_{mnrs} \bar{\omega}_{mn} \bar{\omega}_{rs} \phi_{mnrs} \\
\langle \sigma^2_{y,a} \rangle_t &= \sum_{mnrs}\sum\sum\sum \Gamma_\sigma I_{mnrs} \bar{\omega}'_{mn} \bar{\omega}'_{rs} \phi_{mnrs}
\end{aligned} \tag{25}$$

where

$$\begin{aligned}
\Gamma_\sigma &\equiv Q^2/Am_o^2 \\
\phi_{mr} &= \sin k_m(x-x_o) \sin k_r(x-x_o) \\
\Phi_{mnrs} &= \sin k_m(x-x_o) \sin k_n(y-y_o) \sin k_r(x-x_o) \sin k_s(y-y_o)
\end{aligned} \tag{26}$$

If response concentrations occur, then the following general expressions apply for the maximum edge and interior stresses as may be found from Eq. (25):

$$\text{Max}[\langle\sigma^2_{x,e}\rangle_t] = \sum_{mnrs}\sum\sum\sum \Gamma_\sigma I_{mnrs}\bar{\omega}_{mn}\bar{\omega}_{rs}R_{x,mn}R_{x,rs}$$

$$\text{Max}[\langle\sigma^2_{y,e}\rangle_t] = \sum_{mnrs}\sum\sum\sum \Gamma_\sigma I_{mnrs}\bar{\omega}'_{mn}\bar{\omega}'_{rs}R_{y,mn}R_{y,rs} \qquad (27)$$

$$\text{Max}[\langle\sigma^2_{x,a}\rangle_t] = \sum_{mnrs}\sum\sum\sum \Gamma_\sigma I_{mnrs}\bar{\omega}_{mn}\bar{\omega}_{rs}$$

$$\text{Max}[\langle\sigma^2_{y,a}\rangle_t] = \sum_{mnrs}\sum\sum\sum \Gamma_\sigma I_{mnrs}\bar{\omega}'_{mn}\bar{\omega}'_{rs} \quad .$$

These expressions may readily be simplified for the various modal correlation conditions discussed above. The circumstances under which these conditions apply are investigated in some detail in the following sections.

Effect of Excitation Field Correlation on Modal Coherence

In order to demonstrate the effect of parameters of the excitation field on the coherence of the modal response, it is useful to consider cross-correlation functions of the "separable" form

$$C_p = \overline{p^2}\, f(\tau)\, d_1(\xi)\, d_2(\zeta) \quad , \qquad (28)$$

where $\overline{p^2}$ denotes the mean square pressure, and where the functions d_1 and d_2 are discussed subsequently. The pressure fields to which Eq. (28) applies are nonconvecting stationary random processes having homogeneous spatial correlations, and are of considerable practical interest.

Substitution of the above correlation function into Eq. (3), and subsequent application of the last of Eqs. (9) and of Eq. (15) leads to a result which one may express as

$$I_{mnrs} = \overline{p^2}\, F_{mnrs} S_{mnrs} \quad , \qquad (29)$$

where

$$F_{mnrs} \equiv (2\pi)^{-1/2} \int_{-\infty}^{\infty} \frac{F(\omega)\, d\omega}{T_{mn} T_{rs}^*}$$

$$F(\omega) \equiv (2\pi)^{-1/2} \int_{-\infty}^{\infty} f(\tau)\, e^{-i\omega\tau}\, d\tau \qquad (30)$$

$$S_{mnrs} \equiv \int_A \int_A d_1(\xi) d_2(\zeta)\, \Phi_{mn}(x,y) \Phi_{rs}(x,y) dxdy\, dx'dy' \quad .$$

To investigate how the coherence of the excited modes depends on the spatial correlation length of the excitation field, it is useful to consider a cross-correlation function whose spatial dependence is of the form

$$d_1(\xi) d_2(\zeta) = e^{-|\xi|/\ell}\, e^{-|\zeta|/\ell} \qquad (31)$$

where the "correlation length" ℓ of the excitation field is defined as

$$\ell = \frac{1}{2} \int_{-\infty}^{\infty} d_1(\xi)\, d\xi = \frac{1}{2} \int_{-\infty}^{\infty} d_2(\zeta)\, d\zeta \quad . \qquad (32)$$

Substitution of Eq. (31) into the last of Eq. (30) and integration of the result over the entire plate area $A=L^2$ yields

$$S_{mnrs} = 4\ell^2 G_{mr}\, G_{ns}\, (K_r K_m K_n K_s)^{-1/2} \quad , \qquad (33)$$

where

$$G_{mr} \equiv \delta_{mr} + (\ell k_m)(\ell k_r)(\ell/L)(K_m K_r)^{-1/2}\ \gamma_{mr}$$

$$\gamma_{mr} \equiv 1 + (-1)^{m+r} - [(-1)^m + (-1)^r]\ e^{-L/\ell} \qquad (34)$$

$$K_m = 1 + \ell^2 k_m^2 \quad .$$

It is evident from the above expression that all the modes may be considered as incoherently responding if $\ell/L \ll 1$, and as coherently responding if $\ell/L \geq 1$.

Effect of Plate Parameters on Modal Coherence

The dependence of modal coherence on the plate damping factor and resonance frequencies may be studied by refering to Eq. (29). By combining the first two of Eq. (30) and interchanging the order of integration, one obtains

$$F_{mnrs} = \frac{1}{2\pi} \int_{-\infty}^{\infty} f(\tau) \left[\int_{-\infty}^{\infty} \frac{e^{-i\omega\tau} d\omega}{T_{mn} T_{rs}^*} \right] d\tau \quad . \qquad (35)$$

The above indicated integration with respect to ω may be carried out by the method of residues. For small damping factors η one may write the result as

$$\int_{-\infty}^{\infty} \frac{e^{-i\omega\tau} d\omega}{T_{mn} T_{rs}^*} \approx F_1(\tau, \omega_{mn}, \omega_{rs})\ F_2(\omega_{mn}, \omega_{rs}) \quad ,$$

$$F_1 = \begin{cases} \frac{2}{\omega_{rs}} e^{-\eta\omega_{rs}\tau/2} \cos(\omega_{rs}\tau) & \text{for } \tau>0 \\ \\ \frac{2}{\omega_{mn}} e^{\eta\omega_{mn}\tau/2} \cos(\omega_{mn}\tau) & \text{for } \tau<0 \end{cases} \tag{36}$$

$$F_2 = \frac{\pi\eta(\omega_{mn}^2+\omega_{rs}^2)}{(\omega_{rs}^2-\omega_{mn}^2) + \eta^2(\omega_{rs}^2+\omega_{mn}^2)} \quad .$$

One may then rewrite Eq. (35) as

$$F_{mnrs} = \frac{1}{2\pi} F_2 \int_{-\infty}^{\infty} F_1(\tau)\ f(\tau)\ d\tau \quad . \tag{37}$$

Inspection of the second of Eq. (36) shows that the magnitude of F_2 is independent of the excitation field and varies strongly with the difference between the modal natural frequencies. In fact, F_2 appears very nearly like the transfer function of a simple single-degree-of-freedom system. One may therefore approximate F_2 by

$$|F_2| = \begin{cases} \pi/\eta(\omega_{rs}^2+\omega_{mn}^2) & \text{for } |\omega_{rs}-\omega_{mn}| \leq B_e \\ \\ 0 & \text{for } |\omega_{rs}-\omega_{mn}| > B_e \end{cases} \tag{38}$$

where

$$B_e = \pi\eta(\omega_{mn}^2+\omega_{rs}^2)(\omega_{mn}+\omega_{rs})^{-1} \tag{39}$$

is the effective bandwidth.

If this effective bandwidth is narrower than the frequency spacing between modes, i.e. if $n_\omega B_e \leq 1$, where n_ω denotes the modal density (i.e., the average number of modes per unit frequency interval), then the excited modes may be considered as uncorrelated. On the other hand, if the bandwidth is wider, so that $N_o > n_\omega B_e > 1$, then one may expect all of the N_o excited modes on the average to respond as $N_g (= N_o / n_\omega B_e)$ groups of modes.

With the aid of Eq. (39) one may rewrite the condition $n_\omega B_e \leq 1$ for modal incoherence as

$$(\omega_{mn} - \omega_p)^2 + (\omega_{rs} - \omega_p)^2 \leq 2\omega_p^2 \qquad (40)$$

where

$$\omega_p = 1/2\pi\eta n_\omega \quad . \qquad (41)$$

Clearly, if the natural frequencies of all of the excited modes are below ω_p, regardless of the excitation field, then the modes are incoherent.

STRESSES PRODUCED BY BAND-LIMITED WHITE NOISE EXCITATION

For many analyses one may represent the time-correlation $f(\tau)$ by a simple function, such as a decaying exponential. (A decaying exponential correlation is particulary well suited to describe the pressure field associated with a turbulent boundary layer, for which the time correlation characterizes the generation and decay of eddies.)

In general, however, one cannot describe actual (experimentally measured) spectra by simple expressions. In such cases it is probably most convenient to consider the entire excitation spectrum as divided into a series of contiguous frequency bands, to assume the excitation in each band to be essentially of the nature of band-limited white noise, and to study the structural response in these bands separately — rather than dealing with the entire spectrum at once.

Response Characteristics

The time-correlation function $f(\tau)$ for the band-limited white noise excitation, for which the spectrum $F(\omega)$ is shown in Fig. II-1, is given by

$$f(\tau) = (2\pi)^{-1/2} \int_{-\infty}^{\infty} F(\omega)\, e^{i\omega\tau}\, d\omega$$

$$= (2/\pi)^{1/2}\, F(\omega_c)\, \tau^{-1}[\sin(\omega_2\tau) - \sin(\omega_1\tau)] \quad . \tag{42}$$

By substituting Eq. (42) into Eq. (37), and carrying out the indicated integration, one may obtain

$$\frac{F_{mnrs}}{F_2} = (2\pi^3)^{-1/2}\, F(\omega_c)\, [L_{mn}+L_{rs}] \tag{43}$$

where

$$L_{mn} \equiv \frac{1}{\omega_{mn}} \left[\pi\left(S_1-S_2\right)+\tan^{-1}\left(\theta_{2,mn}\right)-\tan^{-1}\left(\theta_{1,mn}\right)\right]$$

$$\theta_{j,mn} = \eta\, \omega_{mn}\omega_j\left[\omega_{mn}^2\left(1+\eta^2/4\right)-\omega_j^2\right]^{-1} \quad ;$$

$$S_k = \begin{cases} 1 & \text{for } \left[\omega_{mn}^2\left(1+\eta^2/4\right)-\omega_j^2\right] < 0 \\ 0 & \text{otherwise} \end{cases} \tag{44}$$

$$j,k = 1,2 \quad .$$

As has been noted previously, F_2 is independent of the excitation. From Eqs. (43) and (44) one may determine that F_{mnrs}/F_2 exhibits a sharp maximum if both ω_{mn} and ω_{rs} lie within the excitation band; this maximum corresponds to resonant response to the excitation. By making the plausible assumptions that only resonant modes are excited significantly, and that their average response characteristics are the same as those of an "average" mode having its resonance at the band-center frequency ω_c, one may determine the maximum edge and asymptotic stresses as discussed in the following sections.

The response in a given frequency band, the maximum stresses within that band, and the corresponding edge/asymptotic stress ratios, may be expected to depend on how coherently the modes in that band respond. As previously discussed, modes respond incoherently if $\omega_c<\omega_p$ (or $\ell/L<<1$). Thus, the responses in the lowest frequency bands of interest (i.e., the responses which generally are associated with the highest stresses) usually will be incoherent. On the other hand, coherent responses may be expected for high enough frequencies.

Maximum Stresses for Group of Incoherent Modes

For the case where all modal resonance responses in the band of interest are incoherent (i.e., where $\omega_c<\omega_p$ or $\ell/L<<1$), the "cross-terms" of Eq. (43) vanish, and one obtains

$$F_{mnmn} \approx (2\pi)^{-1/2}\, F(\omega_c)\cdot\Delta\omega\cdot n_\omega/\eta\ \omega_c^3 \qquad (45)$$

where $\Delta\omega = \omega_2-\omega_1$ is the excitation bandwidth.

One may then compute the maximum edge and asymptotic stresses from Eq. (27). For example, for the x-components of these stresses one finds

$$\mathrm{Max}\left[\langle\sigma_{x,\ (\underset{a}{e})}^2\rangle_t\right] \cong \Gamma_\sigma\ \frac{1}{\sqrt{2\pi}}\ \frac{F(\omega_c)}{\eta\omega_c}\ \Delta\eta_\omega\ H_{x,\ (\underset{a}{e})} \qquad (46)$$

where for the edge stress

$$H_{x,e} = \frac{2}{\pi} \int_o^\infty S_{mnmn}(\omega_c,\beta)\ R^2_{x,mn}(\omega_c,\beta)(\nu+\beta^2)^2(1+\beta^2)^{-3}\ d\beta \qquad (47)$$

and for the asymptotic stress

$$H_{x,a} = \frac{2}{\pi} \int_o^\infty S_{mnmn}(\omega_c,\beta)(\nu+\beta^2)^2(1+\beta^2)^{-3}\ d\beta \quad . \qquad (48)$$

Maximum Stresses for Group of Coherent Modes

One may deal with cases where the previous assumption of modal incoherence does not hold most simply by selecting bandwidths $\Delta\omega$ that satisfy

$$\Delta\omega = B_e \approx \frac{\pi}{2}\ \eta\ \omega_c \quad , \qquad (49)$$

so that all resonant modes within a band respond coherently. Then one finds from Eqs. (37), (43), and (49) that

$$F_{mnrs} = \begin{cases} \dfrac{\pi - 2\ \tan^{-1}(\pi/2)}{\sqrt{2\pi^3}}\ \dfrac{F(\omega_c)}{\eta\ \omega_c^3} & \text{for } |\omega_{mn}-\omega_c|, |\omega_{rs}-\omega_c| \le B_e/2 \\ 0 & \text{otherwise} \quad . \end{cases} \qquad (50)$$

One then finds from Eq. (27) that

$$\text{Max}\left[\langle\sigma^2_{x,(\vec{a})}\rangle_t\right] \approx \frac{\pi - 2\ \tan^{-1}(\pi/2)}{\sqrt{2\pi^3}}\ \frac{\Gamma_\sigma\ F(\omega_c)(\Delta\omega\cdot n_\omega)^2}{\eta\ \omega_c}\ H_{x,(\vec{a})} \qquad (51)$$

where

$$H_{x,a} = \frac{4}{\pi^2} \int_o^\infty \int_o^\infty Z_1 Z_2 \, S_{mnrs}(\omega_c, \beta_1, \beta_2) d\beta_1 \, d\beta_2$$

$$H_{x,e} = \frac{4}{\pi^2} \int_o^\infty \int_o^\infty Z_1 Z_2 S_{mnrs}(\omega_c, \beta_1, \beta_2) R_{x,mn}(\omega_c, \beta_1) R_{x,rs}(\omega_c, \beta_2) d\beta_1 d\beta_2 \tag{52}$$

$$Z_i \equiv (\nu + \beta_i)^2 (1+\beta_i^2)^{-3} \quad , \quad i = 1,2 \quad .$$

Stress Ratios

These foregoing expressions permit one to compute the stress ratios (of maximum edge stress to maximum asymptotic stress) in terms of the previously introduced rotational and translational edge stiffness parameters. The results of such computations for incoherently responding modes are plotted in Fig. II-2. This figure is qualitatively like that pertaining to the response of a single mode; the edge stress here is seen to exceed the asymptotic stress only for large rotational and translational edge stiffnesses, i.e., for the "clamped-like" edge conditions. A plot like Fig. II-2 may be developed also for coherently responding modes; such a plot also appears qualitatively like Fig. II-2.

REFERENCES FOR APPENDIX II

1. A. Powell, "On the Response of Structures to Random Pressure and to Jet Noise in Particular," in Random Vibration, S.H. Crandall, Ed. (The M.I.T. Press, Cambridge, Mass., 1958), Chap. 8.

2. R.L. Barnoski, "Response of Elastic Structures to Deterministic and Random Excitation," AFFDL-TR-64-199 (1965).

3. E.E. Ungar, "Maximum Stresses in Beams and Plates Vibration at Resonance," Trans. ASME, Series B, J. Eng. Ind. 84: 149-155 (1962).

4. R.H. Lyon, "Spatial Response Concentrations in Extended Structures," Preprint Paper No. 67-VIBR-22, to appear in Trans. ASME, Series B, J. Eng. Ind.

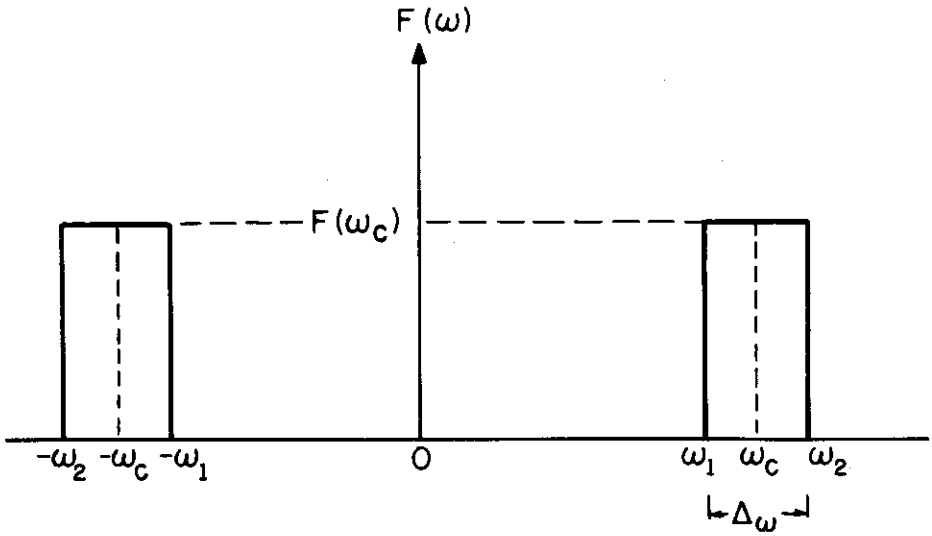

FIG. II-1 SPECTRUM OF BAND-LIMITED WHITE NOISE

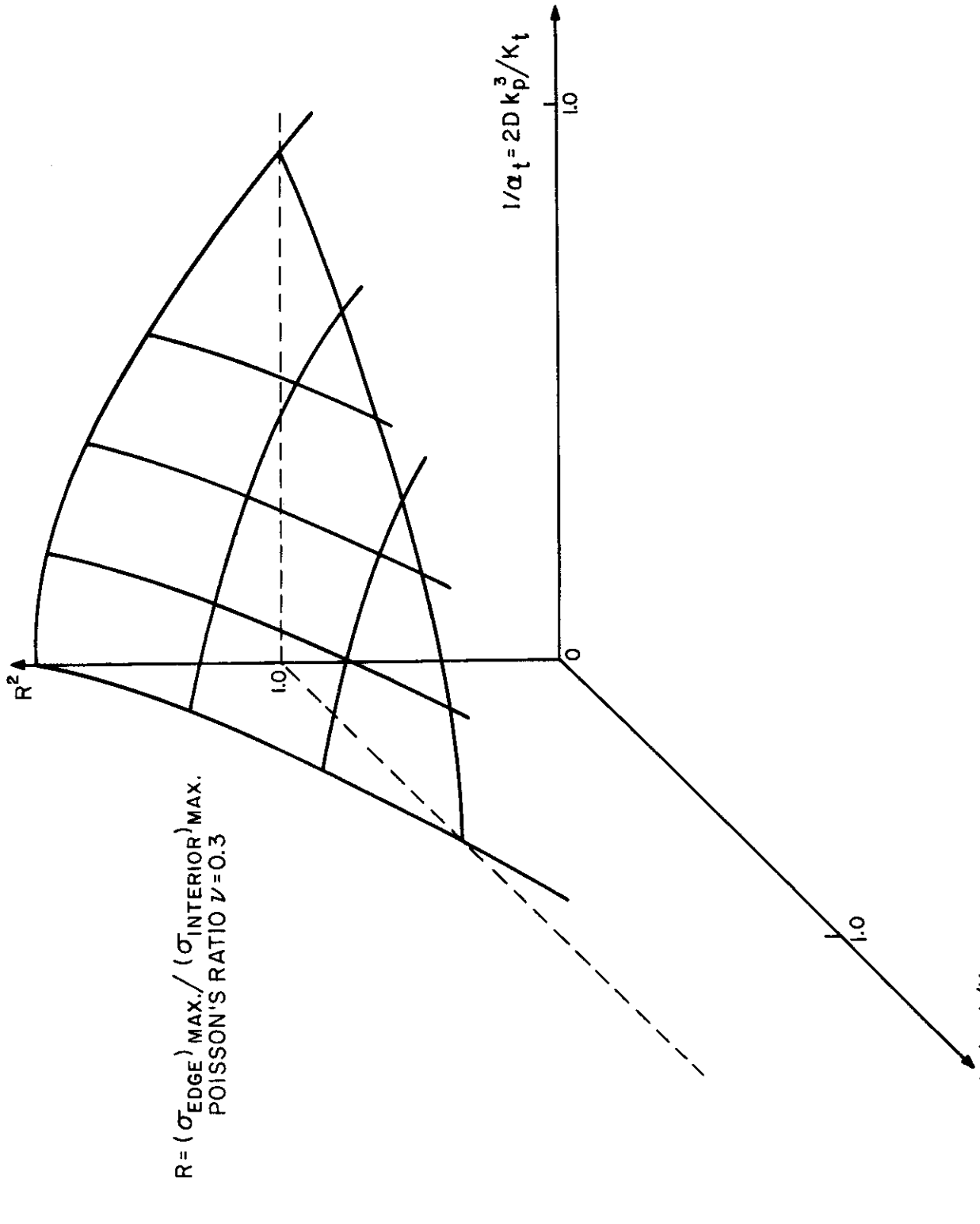

FIG. II-2 STRESS RATIO FOR INCOHERENTLY RESPONDING GROUP OF MODES

APPENDIX III

DYNAMIC EDGE EFFECT IN CYLINDRICAL SHELLS

SHELL EQUATIONS OF MOTION

General Equations

Novizhilov's well-known equations of free vibrations of thin cylindrical shells (Ref. 1) may be written in matrix form as

$$\begin{bmatrix} d_{11} & d_{12} & d_{13} \\ d_{21} & d_{22} & d_{23} \\ d_{31} & d_{32} & d_{33} \end{bmatrix} \cdot \begin{bmatrix} u \\ v \\ w \end{bmatrix} = 0$$

$$d_{11} = \frac{\partial^2}{\partial \xi^2} + \frac{1-\nu}{2} \frac{\partial^2}{\partial \theta^2} - (1-\nu) \frac{\partial^2}{\partial t^2} \tag{1}$$

$$d_{22} = \frac{1+\nu}{2} \frac{\partial^2}{\partial \xi^2} + \frac{\partial^2}{\partial \theta^2} + a^2 \left[2(1-\nu) \frac{\partial^2}{\partial \xi^2} + \frac{\partial^2}{\partial \theta^2} \right] - (1-\nu^2) \frac{\partial^2}{\partial t^2}$$

$$d_{33} = 1 + a^2 \left(\frac{\partial^2}{\partial \theta^2} + \frac{\partial^2}{\partial \xi^2} \right)^2 + \left(1-\nu^2 \right) \frac{\partial^2}{\partial t^2}$$

$$d_{12} = d_{21} = \frac{1+\nu}{2} \frac{\partial^2}{\partial \xi \partial \theta} \quad , \quad d_{13} = d_{31} = -\nu \frac{\partial}{\partial \xi}$$

$$d_{23} = d_{32} = -\frac{\partial}{\partial \theta} + a^2 \left[(2-\nu) \frac{\partial^3}{\partial \xi^2 \partial \theta} + \frac{\partial^3}{\partial \theta^3} \right]$$

where ξ is a dimensionless axial coordinate and t a dimensionless time parameter. These are related to the usual axial coordinate z' and to actual time t' as

$$\xi = z'/r \quad , \quad t = t'c_L/r \tag{2}$$

in terms of the mean radius r of the shell and the longitudinal wave velocity c_L of the shell material. The symbol θ represents the angular coordinate (in the usual cylindrical coordinate system), and u,v,w denote axial, tangential, and radial displacement components, respectively (See Fig. III-1). The parameter a is proportional to the ratio of the shell thickness h to the radius r, and obeys

$$a = h/r\sqrt{12} \quad , \tag{3}$$

and ν represents Poisson's ratio.

The problem of determining the displacements u,v,w which satisfy Eq. (1) may be reduced to that of solving one differential equation, if one lets

$$u = D_{13}\,\Phi \quad , \quad v = D_{23}\,\Phi \quad , \quad w = D_{33}\,\Phi \quad , \tag{4}$$

where the D's are the minors of the determinant Δ_d of the coefficients Eq. (1). Substitution of these expressions into Eq. (1) leads, by virtue of symmetry of Δ_d, to

$$\Delta_d\,\Phi = 0 \quad . \tag{5}$$

The differential operator Δ_d is seen to be of eighth order in ξ and θ; hence, four boundary conditions at each edge are required for the complete evaluation of Φ. Most boundary conditions of general interest may be described by specializations of the relations given below.

For a circumferential boundary (at ξ=Constant):

$$T_1 + K_1 u = 0 \quad , \quad N_1 + \frac{\partial H_1}{r\partial\theta} - K_3 w = 0 \quad ,$$
$$S_1 - \frac{H_1}{r} + K_2 v = 0 \quad , \quad G_1 + K_4 \frac{\partial w}{r\partial\xi} = 0 \quad . \tag{6}$$

For a longitudinal boundary (at θ=Constant):

$$T_2 + L_1 v = 0 \qquad N_2 + \frac{\partial H_2}{r\partial\xi} - L_3 w = 0 \quad ,$$
$$S_2 - L_2 u = 0 \qquad G_2 + L_4 \frac{\partial w}{r\partial\theta} = 0 \quad . \tag{7}$$

Here T denotes the tension force, S the tangential shear force, N the normal shear force, G the bending moment, and H the twisting moment per unit edge length; the subscript 1 refers to such loads that act on a surface of constant ξ, and subscript 2 refers to loads that act on a surface of constant θ as indicated in Fig. III-1. The K's and L's are constants that describe the stiffnesses of the edge supports.

Approximate Equations

One may simplify Eq. (5) greatly by introducing

$$\epsilon = [h^2/12r^2(1-\nu^2)]^{1/4}$$
$$x = \theta/\epsilon \quad , \quad z = \xi/\epsilon \tag{8}$$
$$\bar{u} = v/\epsilon^2 \quad , \quad \bar{v} = v/\epsilon^2 \quad , \quad \bar{w} = w/\epsilon$$
$$\nabla^2 = \frac{\partial^2}{\partial z^2} + \frac{\partial^2}{\partial x^2} \quad .$$

One may then express Eq. (5) as

$$\sum_{n=0}^{8} \epsilon^n D_n \Phi = 0 \quad , \tag{9}$$

where

$$D_0 = \frac{\partial^4}{\partial z^4} + \nabla^8 + \frac{\partial^2}{\partial t^2} \nabla^4 \quad , \quad D_1 = 0 \quad , \tag{10}$$

and the remaining D_n's are complicated operators which are not reproduced here because they are of no interest for the present purposes.

For solutions whose characteristic lengths (wavelengths) are smaller than ϵr or of the same order, one may neglect all but the initial term of Eq. (9). The resulting approximate shell equation may be written as

$$\left[\frac{\partial^4}{\partial z^4} + \nabla^8 + \frac{\partial^2}{\partial t^2} \nabla^4\right] \Phi = 0 \quad , \tag{11}$$

and the relations (4) between the displacement components and Φ may be expressed as

$$\begin{aligned} \bar{u} &= \left[-\frac{\partial^3}{\partial z \partial x^2} + \nu \frac{\partial^3}{\partial z^3}\right] \Phi \quad , \\ \bar{v} &= \left[(2+\nu) \frac{\partial^3}{\partial t^2 \partial x} + \frac{\partial^3}{\partial x^3}\right] \Phi \quad , \\ \bar{w} &= \nabla^4 \Phi \quad . \end{aligned} \tag{12}$$

Equation (11) is known as the Donnel equation for the free vibration of cylindrical shells (or in Ref. 1, as the approximate equation for states of stress with "large indices of variation").

The corresponding relations between displacements and stress components are given in Ref. 1.

EDGE EFFECT

The dynamic edge effect in thin cylindrical shells may be studied by the asymptotic method of Bolotin (Ref. 2).

Nonoscillatory and Oscillatory Edge Effects

Consider a longitudinal edge (along a line at constant z). For such an edge one requires a solution of Eq. (11) of the form

$$\Phi = \sum_{i=1}^{8} A_i \, e^{s_i z} \sin k_2(x-x_o) \, e^{i\omega t} \quad . \tag{13}$$

The above expression may be shown to satisfy Eq. (11) if the coefficients s_i are the roots of the equation

$$\omega^2 = \left(s_i^2-k_2^2\right)^2 + s_i^4\left(s_i^2-k_2^2\right)^{-2} \quad . \tag{14}$$

If the modes shapes are to approach sinusoids asymptotically, then one expects to find at least two roots of the form

$$s^2 = -k_1^2 \quad . \tag{15}$$

For such roots one may set

$$k_1 = \rho \cos \theta \quad , \quad k_2 = \rho \sin \theta \tag{16}$$

in Eq. (14) and obtain the frequency-wavenumber relation

$$\omega^2 = \rho^4 + \cos^4\theta \quad . \tag{17}$$

Figure III-2 shows two typical loci of constant frequency in the (k_1,k_2) or the (ρ,θ) plane. One may show that membrane effects in the shell are important if $\cos^4\theta>\rho^4$, but that these effects are unimportant and that the shell behaves very nearly like a flat plate if $\cos^4\theta<\rho^4$. The region where the former inequality holds has been labeled "membrane region" in Fig. III-2; the remainder of the area of Fig. III-2 has been labeled "bending region."

By equating Eqs. (14) and (17) one finds

$$\left(s^2+k_1^2\right)\left\{s^6-\rho^2\left(1+3\sin^2\theta\right)s^4+\rho^4\sin^2\theta\left(2+3\sin^2\theta+\frac{1+\cos^2\theta}{\rho^4}\right)\right.$$

$$\left.s^2-\rho^6\sin^4\theta\left(1+\sin^2\theta\right)\left(1+\frac{1}{\rho^4}\right)\right\}=0 \quad , \tag{18}$$

from which one may determine the remaining six roots of Eq. (14) in terms of ρ and θ. If $\rho>\rho_o$, where

$$\rho_o = -1 + 10\sin^2\theta + 2\sin^4\theta + \left(1+4\sin^2\theta\right)^{3/2} \quad , \tag{19}$$

all six roots are real. The corresponding solution of Eq. (11) is of the form

$$\Phi = c\, e^{i\omega t}\sin k_2\left(x-x_o\right)\left[\sin k_1 z + c_1\cos k_1 z + c_2\, e^{-\alpha z}\right.$$

$$\left. + c_3\, e^{-\beta z} + c_4\, e^{-\gamma z}\right] \quad , \tag{20}$$

where the c's are constants and α, β, and γ are real quantities. Here Φ approaches a double-sinusoid for large z, and the dynamic edge effect is termed "nonoscillatory." On the other hand, if $\rho<\rho_o$, only two of the six roots are real, the solution of Eq. (11) is of the form

$$\Phi = c\, e^{i\omega t} \sin k_2(x-x_o)\left[\sin k_1 z + c_1 \cos k_1 z + c_2\, e^{-\alpha z}\right.$$

$$\left. + c_4\, e^{-\beta z} \sin \gamma z + c_5\, e^{-\beta z} \cos \gamma z\right] \quad , \tag{21}$$

and the edge effect is called "oscillatory."

Circumferential Edges

It is instructive to examine the edge effect for a circumferential edge which is "clamped" with respect to flexure with and without axial and circumferential constraints. The boundary conditions corresponding to a fully constrained edge may be expressed as

$$\bar{u} = \bar{v} = \bar{w} = \frac{\partial \bar{w}}{\partial z} = 0 \quad \text{at} \quad z = 0 \quad , \tag{22}$$

whereas those for a clamped edge without additional constraints may be written as

$$T_1 = S_1 - \frac{H_1}{r} = w = \frac{\partial w}{\partial z} = 0 \quad \text{at} \quad z = 0 \quad , \tag{23}$$

for the clamped edge without constraints.

Edge effect at large wavenumbers. If $\rho^2 \gg 1$ and $\rho > \rho_o$, the edge effect is nonoscillatory and the roots of Eq. (18) are

$$\alpha \approx \rho\sqrt{1+\sin^2\theta} \quad , \quad \beta \approx \sin\theta\sqrt{\rho+1} \quad , \quad \gamma \approx \sin\theta\sqrt{\rho-1} \quad . \tag{24}$$

For a fully constrained edge, use of Eq. (22) permits one to evaluate the constants of integration of Eq. (20), and to find

$$c_1 \approx -\cos\theta\left[1+\sin^2\theta\right]^{-1/2} \quad , \quad c_2 \approx \cos\theta\left[1+\sin^2\theta\right]^{-1/2} \quad ,$$

$$c_3 \approx (k_1/\alpha)(F_1[\gamma]/E_1) \quad , \quad c_4 \approx -(k_1/\alpha)(F_1[\beta]/E_1) \quad , \tag{25}$$

where

$$E_1 = \beta\left(k_2^2+\nu\beta^2\right)\left\{\left(2+\nu\right)\gamma^2-k_2^2\right\} - \gamma\left(k_2^2+\nu\gamma^2\right)\left\{\left(2+\nu\right)\beta^2-k_2^2\right\} \quad ,$$

$$F_1(\gamma) = \left(k_1^2+\alpha^2\right)\left\{\gamma\left(2+\nu\right)\left(k_2^2+\nu\gamma^2\right) - \nu\gamma\left[\left(2+\nu\right)\gamma^2-k_2^2\right]\right\} \quad . \tag{26}$$

For an edge that is free of added constraints, one may apply Eq. (23) to find

$$c_1 \approx -\cos\theta\left[1+\sin^2\theta\right]^{-1/2} \quad , \quad c_2 \approx \cos\theta\left[1+\sin^2\theta\right]^{-1/2} \quad ,$$

$$c_3 \approx (k_1/\alpha)\ (F_2[\gamma]/E_2) \quad , \quad c_4 \approx (k_1/\alpha)(F_2[\beta]/E_2) \quad ,$$

where

$$E_2 = \beta^2\gamma^2(\gamma-\beta) \quad , \quad F_2(\gamma) = (\alpha-\gamma)\ \gamma^2(k_1^2+\alpha^2) \quad . \tag{28}$$

By combining Eqs. (12), (20), and (25)-(28), one finds that one may express the radial displacement w for both of the cases treated above as

$$w = c_o\, e^{i\omega t} \sin k_2(x-x_o) \left\{\left[\sin k_1 z - \frac{\cos\theta}{\sqrt{1+\sin^2\theta}} \cos k_1 z + \frac{\cos\theta}{\sqrt{1+\sin^2\theta}} e^{-\alpha z}\right] + \left[-O\left(\frac{1}{\rho^2}\right) e^{-\beta z} + O\left(\frac{1}{\rho^2}\right) e^{-\gamma z}\right]\right\} , \quad (29)$$

where O means "of the order of."

The expression in the first bracket [ ] of the above equation is identical to the solution for a flat plate clamped at one edge. The effects of curvature and of membrane-type boundary conditions (axial and circumferential constraints) are indicated by the terms contained in the second bracket; and they are negligible for sufficiently large wavenumbers.

Edge effect at small wavenumbers. If $\rho^2 \ll 1$ and $\rho < \rho_o$, the edge effects oscillate, and the roots of Eq. (18) are found to be given by

$$\alpha \approx \rho \sin\theta \left[\frac{1-\sin^2\theta}{2-\sin^2\theta}\right]^{1/2} , \quad \beta \approx \gamma \approx \left[\frac{\sin^2\theta}{4}\left(2-\sin^2\theta\right)\right]^{1/4} . \quad (30)$$

If one limits himself to considering only the case where $\beta/\rho \gg 1$, one finds from Eq. (22) that the integration constants for a fully constrained edge must satisfy

$$c_1 = E_4/E_3 , \quad c_2 = E_5/E_3 , \quad c_3 \approx c_4 = (\rho^4/\beta^4)(E_6/4E_3) \quad (31)$$

where

$$E_3 \approx \sin\theta\ A\left(1+\nu A^2\right)\left[1+\left(1+\nu\right)\cos^2\theta\right] \quad ,$$

$$E_4 \approx B\left[\left(2+\nu\right)A^2-1\right] \quad ,$$

$$E_5 \approx B\left[1+\left(1+\nu\right)\cos^2\right] \quad , \tag{32}$$

$$E_6 \approx B\left\{\left[1+\left(1+\nu\right)\cos^2\theta\right]\sin^2\theta\left(2-\sin^2\theta\right)^{-2}+\left[\left(2+\nu\right)A^2-1\right]\right\} \quad ,$$

$$A = \cos\theta\left(2-\sin^2\theta\right)^{-1/2} \quad , \quad B = \cos\theta\left(\sin^2\theta-\nu\cos^2\theta\right) \quad .$$

The integration constant for an edge without additional constraints are found by use of Eq. (23) to be given by

$$c_1 \approx -\sqrt{2-\sin^2\theta}/\sin\theta \quad ,$$

$$c_2 \approx -\left(2-\sin^2\theta\right)^{3/2}/\sin^3\theta \quad , \tag{33}$$

$$c_3 \approx c_4 \approx -\left(\rho^4/2\beta^4\right)\left(1/\sin\theta\ \sqrt{2-\sin^2\theta}\right) \quad .$$

By use of Eqs. (12), (25), (31), and (33) one finds that one may express the radial displacement w for the fully constrained edge as

$$w \approx c_o \sin k_2\left(x-x_o\right)\left[\sin k_1 z + \frac{E_4}{E_3}\cos k_1 z + \frac{\sin^4\theta}{\left(2-\sin^2\theta\right)^2}\right. \tag{34}$$

$$\left.\frac{E_5}{E_3}e^{-\alpha z} - \frac{E_6}{E_3}e^{-\beta z}\left(\cos\beta z + \sin\beta z\right) + O\left(\frac{\rho^2}{\beta^2}\right)\right] \quad ,$$

and for the edge without added constraints as

$$w \approx c_o \sin k_2(x-x_o)\left\{\sin k_1 z - \frac{\sqrt{2-\sin^2\theta}}{\sin\theta}\cos k_1 z - \frac{\sin\theta\, e^{-\alpha z}}{\sqrt{2-\sin^2\theta}}\right. \tag{35}$$

$$\left. + e^{-\beta z}\left[\frac{2(\sin\beta z + \cos\beta z)}{\sin\theta\sqrt{2-\sin^2\theta}}\right] + O\left(\frac{\rho^2}{\beta^2}\right)\right\} \quad .$$

The asymptotic forms of Eqs. (34) and (35) are not identical. As a consequence, the natural frequencies for the two types of edge constraint may differ significantly. This finding agrees with numerical results obtained by Forsberg (Ref. 3).

It is important to note that the foregoing results imply the possibility of large stress concentrations occurring at the edge: comparison of the edge and asymptotic bending moments G_e and G_a yields

$$(G_e/G_a) \approx O(\beta^2/\rho^2) \quad . \tag{36}$$

It must also be pointed out that the foregoing analysis and its results, strictly speaking, are valid only for cylindrical shells without longitudinal supports. For cylindrical shells that are stiffened by stringers, the asymptotic form of the solution may not be a simple sinusoid, and use of the asymptotic method then cannot be justified.

Longitudinal Edges

If one assumes that the solution of Eq. (11) approaches the form

$$\Phi = \sum_{i=1}^{8} A_i\, e^{i\omega t} \sin k_1(z-z_o)\, e^{s_i x} \tag{37}$$

far from the ends of the cylindrical shell and near the boundary line x=0, one finds that the coefficients s_i must be the roots of the equation

$$\omega^2 = \left(s_i^2 - k_1^2\right) + k_1^4\left(s_i^2 - k_i^2\right)^{-2} \tag{38}$$

if Eq. (37) is to satisfy Eq. (11). If two imaginary roots are $\pm i\, k_2$, the remaining six roots may be found from

$$\left(s^2\right)^3 - \rho^2\left(1+3\cos^2\theta\right)s^4 + \rho^4\cos^2\theta\left(2+3\cos^2\theta - \rho^{-4}\cos^2\theta\right)s^2 - \rho^6$$

$$\cos^4\theta\left(1+\cos^2\theta\right)\left(1-\rho^{-4}\right) = 0 \quad . \tag{39}$$

Since the discriminant of the above cubic equation in s^2 is always negative, the three solutions for s^2 are all real and either all are positive (if $\rho>1$) or one is negative and two positive (if $\rho<1$). Therefore, if ρ is greater than unity, the edge effect is nonoscillatory and uniquely defined, no matter how the edges at both ends of the cylindrical shell are supported.

$\rho^2 >> 1$, then the roots of Eq. (39) are Effect at large and small wavenumbers. For example, if

$$s^2 \approx \rho^2(1+\cos^2\theta) \quad , \quad \cos^2\theta(\rho^2 \pm 1) \quad , \tag{40}$$

and the cylindrical shell behaves like a flat plate [compare Eqs. (40) and (24)].

However, if $\rho<1$, then the roots of Eq. (39) are

$$s^2 = -k_3^2 \quad , \quad \alpha^2 \quad , \quad \beta^2 \quad ; \tag{41}$$

Equation (37) then becomes

$$\Phi = c_o\, e^{i\omega t} \sin k_1(z-z_o)\Big[A_1 \sin k_2 x + A_2 \cos k_2 x + A_3 \sin k_3 + A_4 \cos k_3 x + A_5\, e^{-\alpha x + A_6}\, e^{\alpha x + A_7}\, e^{-\beta x + A_8}\, e^{\beta x}\Big] \quad . \tag{42}$$

Clearly, Eq. (42) asymptotically approaches

$$\Phi = c_o\, e^{i\omega t} \sin k_1(z-z_o)\Big[\sin k_2(x-x_o) + c_1 \sin k_3(x-x_1)\Big] \tag{43}$$

which is a linear combination of membrane-type and bending-type solutions.

Degeneration of Dynamic Edge Effect

If Eq. (34) were the correct asymptotic form for $\rho<1$, then the edge solution would need to have the following form instead of that of Eq. (13):

$$\Phi = e^{i\omega t}[\sin k_2(x-x_o) + c_1 \sin k_3(x-x_1)]\, \Psi(z) \quad . \tag{44}$$

But substitution of Eq. (44) into Eq. (11) leads to

$$[\sin k_2(x-x_o)D_2 + c_1 \sin k_3(x-x_1)D_3]\, \Psi(z) = 0 \quad , \tag{45}$$

where

$$D_i = \frac{\partial^4}{\partial z^4} + \left(\frac{\partial^2}{\partial z^2} - k_i^2\right)^4 - \omega^2\left(\frac{\partial^2}{\partial z^2} - k_i^2\right)^2 \quad , \quad i = 2,3 \quad , \tag{46}$$

and the requirement that Ψ satisfy both $D_2\Psi=0$ and $D_3\Psi=0$, with $k_2 \neq k_3$, implies that Ψ must be of the form

$$\Psi = c \sin k_1(z-z_o) \quad . \tag{47}$$

It thus appears that the asymptotic solutions for $\rho<1$ are neither simple sinusoids nor linear combinations of simple sinusoids, unless both circumferential edges of a cylindrical shell and/or both longitudinal edges of a shell segment are simply supported. In cases where such sinusoidal asymptotic solutions do not exist, Bolotin (Ref. 2) speaks of a "degeneration" of the dynamic edge effect.

For the case where both ends of a cylindrical shell are simply supported, one finds from Eq. (42) that the solution takes the form

$$\Phi = c_o e^{i\omega t} \sin k_1(z-z_o)\left[\sin k_2 x + A_2' \cos k_2 x + A_3' \sin k_3 x + A_4' \cos k_3 x + A_5' e^{-\alpha x} + A_7' e^{-\beta x}\right] , \qquad (48)$$

where the six unknown constants A_2', A_3', A_4', A_5', A_6', A_7', and k_2 may be determined from the four boundary conditions and from the symmetry and antisymmetry of the asymptotic forms of the membrane and bending modes. It is evident from Eq. (48) that the edge effect is not degenerate in this case.

REFERENCES FOR APPENDIX III

1. A.L. Gol'denveizer, Theory of Elastic Thin Shells (Pergamon Press, London, 1961).

2. V.V. Bolotin, "The Edge Effect in the Oscillation of Elastic Shells," J. Appl. Math. Mech. 2: 1257-1272 (1960) (English Translation).

3. K. Forsberg, "Influence of Boundary Conditions on the Modal Characteristics of Thin Cylindrical Shells," AIAA J. 2: 2150-2156 (1964).

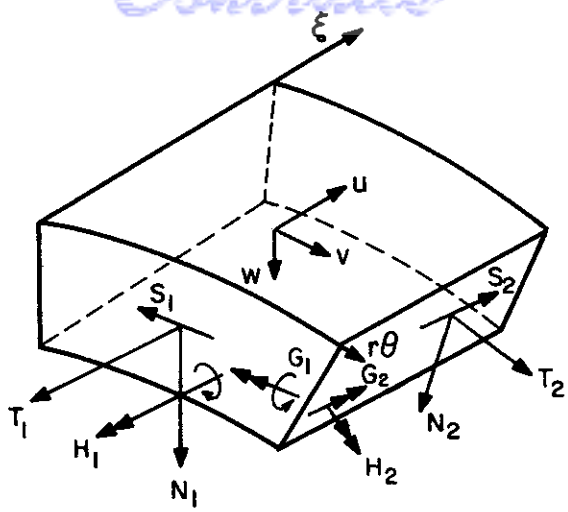

FIG. III-1 ELEMENT OF CYLINDRICAL SHELL

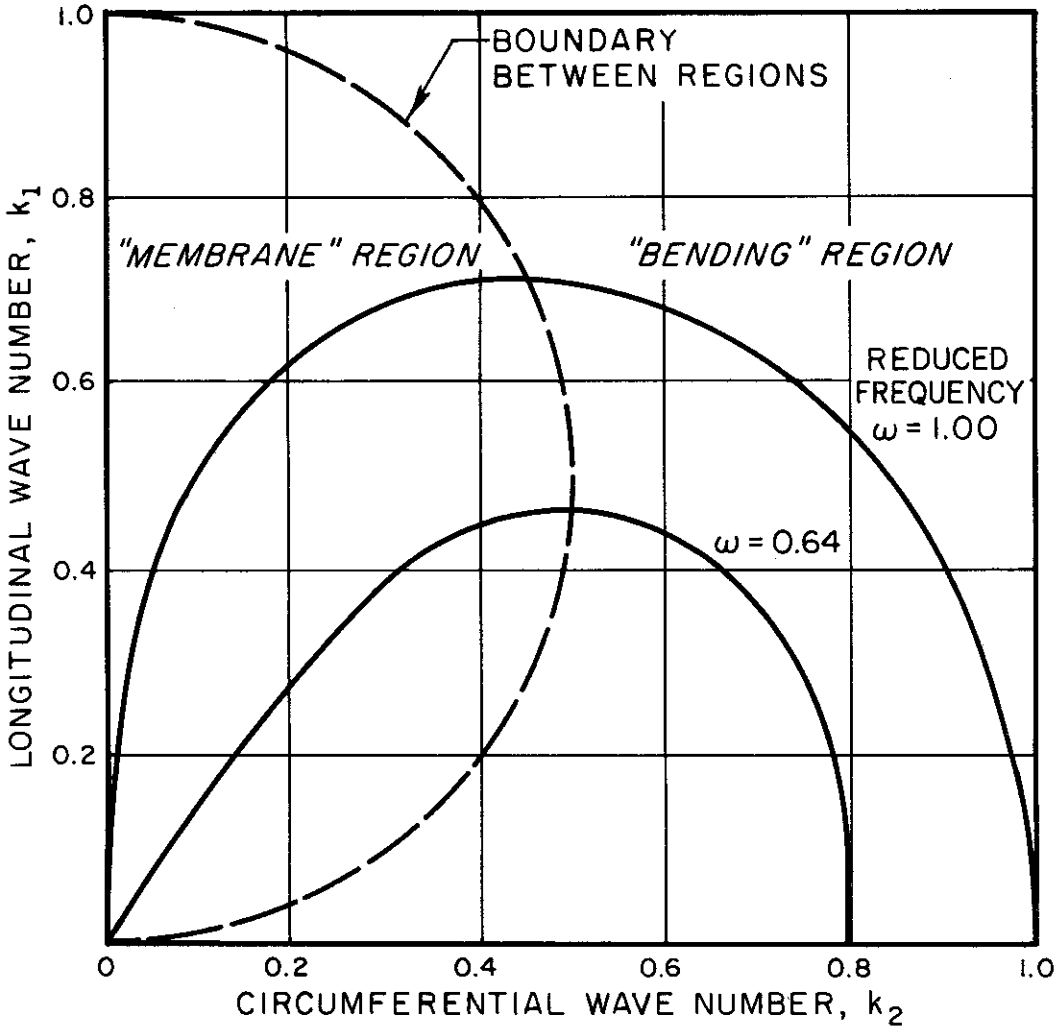

FIG. III-2 LOCI OF CONSTANT RESONANCE FREQUENCY IN REDUCED WAVE NUMBER SPACE

APPENDIX IV

EXPERIMENTAL DETERMINATION OF DAMPING AND ENERGY FLOW IN PANEL ARRAYS

INTRODUCTION

Previous investigations of vibration transmission in complex structures (Refs. 1,2,3,4) have shown that vibrational energy is removed from a given element in two ways. The first is characterized by the "internal" loss factor, which is a measure of the inherent damping of a structural element; and the second is characterized by the coupling loss factor, which is a measure of the energy flow from the element to the adjacent element. If a complete structure, such as an aircraft fuselage, is subjected essentially to uniform excitation, the response of each panel is determined by the internal loss factors alone. If, on the other hand, a panel of the complete structure is subjected to local excitation, the response of the panel depends on the coupling loss factors of the panel, as well as on its internal loss factor. This dependence of the response on internal and coupling loss factors points out the necessity of simulating the effects of both of these mechanisms in sonic fatigue tests.

Since there exist at present no useful techniques for measuring these two types of loss factors on intact built-up structures (and one needs to know these loss factors in order to simulate them), an investigation of possible simple measurement approaches was undertaken. This investigation and its results are described in the present appendix.

DETERMINATION ON BASIS OF ENERGY SHARING AND APPARENT LOSS FACTOR MEASUREMENTS

For the steady-state case where the panels of an array are subject to independent sources of random excitation, one may calculate the time-average vibrational energies from steady-state power balance relations (Refs. 2,3,4). These relations involve the internal loss factor of each panel and the coupling loss factors between adjacent panels; however, they do not provide one with enough information so that one may determine all of the internal and coupling loss factors. Additional information,

as for example obtained from measurement of apparent loss factors, is required before one can calculate all of the energy dissipation and energy transport loss factors.

A study of an array of nine panels (Figs. IV-1 and IV-2) was undertaken in order to determine the feasibility of the aforementioned approach. This study is described in the following paragraphs.

Energy Sharing Analysis

Consider the steady-state vibration problem in which each of the panels of the nine-panel array is subjected to an independent source of octave-band random noise. The time-average vibration energies of the different panels can be calculated from steady-state power balance equations, which involve the internal loss factor of each panel and the coupling loss factors between adjacent panels. For simplicity's sake one may take the internal loss factors of all nine panels to be identical, and the coupling loss factors between any two panels to be the same. This assumption is based on the uniform geometry of the experimental panel array, and is valid to the extent that the vibration characteristics of the corner, edge, and center panels are identical; it should yield good results for frequencies that are well above the first few resonance frequencies of the individual panels.

The steady-state power balance equations applicable to the nine-panel array may, by use of the foregoing simplifying approximations, be written as (Ref. 4):

$$\begin{bmatrix} \eta+2\beta & -\beta & 0 & -\beta & 0 & 0 & 0 & 0 & 0 \\ -\beta & \eta+3\beta & -\beta & 0 & -\beta & 0 & 0 & 0 & 0 \\ 0 & -\beta & \eta+2\beta & 0 & 0 & -\beta & 0 & 0 & 0 \\ -\beta & 0 & 0 & \eta+3\beta & -\beta & 0 & -\beta & 0 & 0 \\ 0 & -\beta & 0 & -\beta & \eta+4\beta & -\beta & 0 & -\beta & 0 \\ 0 & 0 & -\beta & 0 & -\beta & \eta+3\beta & 0 & 0 & -\beta \\ 0 & 0 & 0 & -\beta & 0 & 0 & \eta+2\beta & -\beta & 0 \\ 0 & 0 & 0 & 0 & -\beta & 0 & -\beta & \eta+3\beta & -\beta \\ 0 & 0 & 0 & 0 & 0 & -\beta & 0 & -\beta & \eta+2\beta \end{bmatrix} \begin{bmatrix} E_1 \\ E_2 \\ E_3 \\ E_4 \\ E_5 \\ E_6 \\ E_7 \\ E_8 \\ E_9 \end{bmatrix} = \begin{bmatrix} P_1/\omega_o \\ P_2/\omega_o \\ P_3/\omega_o \\ P_4/\omega_o \\ P_5/\omega_o \\ P_6/\omega_o \\ P_7/\omega_o \\ P_8/\omega_o \\ P_9/\omega_o \end{bmatrix} \quad (1)$$

where E_i denotes the time-average vibratory energy of the ith panel, P_i the time-average power supplied to the ith panel from an external source, ω_o the center frequency of the octave band under consideration, η the internal loss factor of the panels, and β the coupling loss factor for any two adjacent panels.

By summing all of the Eqs. (1) one obtains the additional relation

$$\sum_{i=1}^{9} P_i = \omega_o \eta \sum_{i=1}^{9} E_i \quad , \tag{2}$$

which expresses that the total time-average power input from all sources must in the steady state equal the total power dissipated in the array.

Center panel excitation. For the special case where only the center panel (panel 5 of Fig. IV-2) is externally excited, all input powers except P_5 are zero. From symmetry, the energies of all four corner panels are equal and the energies of all four edge panels are equal; that is,

$$\begin{aligned} E_1 = E_3 = E_7 = E_9 \equiv E_c \\ E_2 = E_4 = E_6 = E_8 \equiv E_e \quad . \end{aligned} \tag{3}$$

For this case Eqs. (1) and (2) yield three distinct expressions for the loss factor ratio η/β:

$$\begin{aligned} \eta/\beta &= 2(E_e/E_c - 1) \\ \eta/\beta &= (2E_c + E_5 - 3E_e)/E_e \\ \eta/\beta &= (E_5 - E_e)/(E_c + E_e) \quad . \end{aligned} \tag{4}$$

By combining Eqs. (4) one may obtain some relations which govern the distribution of vibrational energies among the panels, and which are independent of the values of the internal and coupling loss factors. These relations arise from the symmetry of the nine-panel array and the excitation, and are of no interest for the present purposes.

Edge panel excitation. In the case where only an edge panel (e.g., panel 6 of Fig. IV-2) is externally excited, all the input powers except P_6 are zero. Because of symmetry, $E_7=E_1$, $E_8=E_2$, and $E_9=E_3$. Here Eqs. (1) and (2) yield six distinct expressions for the loss factor ratio η/β:

$$\eta/\beta = (E_2+E_4-2E_1)/E_1$$

$$\eta/\beta = (E_1+E_3+E_5-3E_2)/E_2$$

$$\eta/\beta = (E_2+E_6-2E_3)/E_3 \qquad (5)$$

$$\eta/\beta = (E_5+2E_1-3E_4)/E_4$$

$$\eta/\beta = (2E_2+E_4+E_6-4E_5)/E_5$$

$$\eta/\beta = (3E_6-2E_3-E_5)/(2E_1+2E_2+2E_3+E_4+E_5) \quad .$$

Corner panel excitation. If only a corner panel, such as panel 3, is externally excited, then all input powers except P_3 vanish, and because of symmetry $E_8=E_4$, $E_9=E_1$, $E_6=E_2$. In this case Eqs. (1) and (2) again yield six distinct expressions for the loss factor ratio η/β:

$$\eta/\beta = (E_2+E_4-2E_1)/E_1$$

$$\eta/\beta = (E_1+E_3+E_5-3E_2)/E_2$$

$$\eta/\beta = (2E_3-2E_2)/(2E_1+2E_2+2E_4+E_5+E_7)$$

$$\eta/\beta = (E_1+E_5+E_7-3E_4)/E_4 \qquad (6)$$

$$\eta/\beta = (2E_2+2E_4-4E_5)/E_5$$

$$\eta/\beta = (2E_4-2E_7)/E_7 \quad .$$

Equations (4) – (6) constitute 15 distinct expressions for the ratio of coupling loss factors obtained from Eqs. (1) and (2) for different excitation cases. However, it is evident that none of these expressions permit one to calculate values of the coupling or internal loss factors separately from known values of the steady-state energies.

Apparent Loss Factor Analysis

Center panel excitation. If a panel which is part of an array is excited, and the excitation is then removed, the rate of decay of the energy in the panel then is proportional to the energy. If the center panel, panel 5, of the nine-panel array is the panel of interest, then one may express the aforementioned proportionality as (Ref. 1):

$$dE_5/dt = -\omega_o \, \eta_{app5} \, E_5 \quad . \qquad (7)$$

Here η_{app5} represents the apparent loss factor of the panel, which can be determined experimentally. This apparent loss factor depends on the internal loss factor and on the coupling loss factor between adjacent plates.

The power balance of plate 5 during decay may also be written

$$-\frac{1}{\omega_o}\frac{dE_5}{dt} = \eta E_5 + 4\beta(E_5 - E_e) = [\eta + 4\beta(1-\alpha_e)]E_5 \qquad (8)$$

where E_e denotes the energy of the edge panels and

$$\alpha_e \equiv E_e/E_5 \quad . \qquad (9)$$

By comparing Eqs. (7) and (8) one obtains

$$\eta_{app5} = \eta + 4\beta(1-\alpha_e) \quad . \qquad (10)$$

By setting all P_i's, except P_5, equal to zero in Eqs. (1), and using Eq. (3) one obtains the steady-state power balance relations, which may be written, with α_c defined by

$$\alpha_c \equiv E_c/E_5 \quad , \qquad (11)$$

as

$$\begin{aligned} (\eta+2\beta)\alpha_c - 2\beta\,\alpha_e &= 0 \\ (\eta+3\beta)\alpha_e - 2\beta\,\alpha_c - \beta &= 0 \\ \eta + 4\beta - 4\beta\,\alpha_e &= P_5/\omega_o E_5 \quad . \end{aligned} \qquad (12)$$

One may solve the first two of Eq. (12) for α_e and substitute the result into Eq. (8) to find

$$\frac{\eta_{app5}}{\eta} = 1 + \frac{4(\alpha+4)}{\alpha^2+5\alpha+2} \quad , \qquad (13)$$

where

$$\alpha \equiv \eta/\beta \quad . \qquad (14)$$

Edge and corner panel excitation. The apparent loss factors for corner plates and edge plates can be derived similarly. One obtains

$$\frac{\eta_{app.c}}{\eta} = 1 + \frac{2}{\alpha}\left(\frac{\alpha^5+13\alpha^4+59\alpha^3+113\alpha^2+84\alpha+16}{\alpha^5+14\alpha^4+69\alpha^3+144\alpha^2+114\alpha+16}\right) \qquad (15)$$

and

$$\frac{\eta_{app.e}}{\eta} = 1 + \left(\frac{3\alpha^4+69\alpha^3+176\alpha^2+322\alpha+192}{\alpha^5+14\alpha^4+70\alpha^3+151\alpha^2+128\alpha+24}\right) . \qquad (16)$$

Energy Sharing Measurements

A nine-panel array, as shown in Figs. IV-1 and IV-2, was constructed by attaching aluminum bars by means of epoxy to an aluminum plate. During the tests the panel was suspended from long strings attached to its two upper corners.

In a typical experiment one of the panels was excited with an octave band of noise via a small electromagnetic shaker, and the mean-square accelerations at a number of points on the excited and the unexcited panels were measured in the same octave band. The numbers tabulated in Tables IV-1, IV-2, and IV-3 represent the space-average values of the mean-square accelerations measured on one panel, in a single octave band.

In the experiment in which the center panel was excited, the mean-square acceleration of all nine of the panels was measured, to test the assumption that the energies of the four corner panels are equal and the energies of the four edge panels are equal in this case. The results presented in Table IV-1 indicate that this assumption is realistic.

Substitution of the energies (or mean-square accelerations, which are proportional to them) indicated in Tables IV-1, IV-2, and IV-3 into Eqs. (4), (5), and (6) respectively, yields the average ratios of the internal to coupling loss factors shown in Fig. IV-3. The curve shown in Fig. IV-3 for the case where only plate 5 is excited represents the average values of the ratios calculated from the three expressions of Eq. (4).

Similarly, the curves for excitation of plate 6 and excitation of plate 3 represent the average values calculated from Eqs. (5) and (6), respectively. It should be mentioned that for each excitation position, the values of η/β calculated from the different expressions showed quite large variation about the average values. Since the internal and coupling loss factors should show no dependence on the position of excitation, the scatter of the results shown in Fig. IV-3 probably reflects inaccuracies in the measurement techniques, as well as shortcomings in the mathematical idealization of the array and in statistical energy analysis.

Apparent Loss Factor Measurements

The apparent loss factor of a panel of interest was measured by the well-known decay-rate technique, which consists of exciting the panel with octave-band noise until it reaches steady state, then removing the excitation and observing the rate of decay of the oscillations of the panel. Such measurements were carried out on panels 5, 6, and 3 of the experimental nine-panel array, and produced the results shown in Fig. IV-4.

Internal and Coupling Loss Factors

By substituting the values of $\alpha=\eta/\beta$ indicated in Fig. IV-3 into Eqs. (13), (15), and (16), one obtains values for the ratio η_{app}/η. Use of the measured η_{app} values from Fig. IV-4 then permits one to calculate η, and once one knowns η one may use the η/β values of Fig. IV-3 once more to compute β.

Values of η and β resulting from such calculations are shown in Figs. IV-5 and IV-6, respectively. It appears that the results obtained from the three sets of measurements (with three different panels excited externally) agree reasonably well with each other, but that the spread in the results, which amounts to as much as a factor of 4.0 for β in the mid-frequency range, is somewhat excessive.

ELIMINATION OF POWER FLOW BY ENERGY MATCHING

Since the flow of power between connected panels is (under certain generally applicable random vibration conditions, Ref. 4)

proportional to the difference between the (modal) energies of the two panels, one may reduce this power flow to zero by keeping the two panels at the same energy level. With zero power flow, the panel vibrations are affected only by the internal loss factor, and not by the coupling loss factor, and one should then be able to determine the internal loss factor by itself.

The results of a corresponding study are summarized in the following paragraphs. Unlike the previous study, the present investigation was carried out for a three-panel array, for the sake of theoretical and experimental simplicity. Here the experimental array was constructed by a 1 ft × 3 ft plate, partitioned into three 1 ft × 1 ft panels by beams. All other dimensions were the same as those indicated in Fig. IV-1. Beams were also attached to the edges of the panel array.

Analysis

By a derivation similar to that which leads to Eq. (10) one may find that the apparent loss factor of the center panel of the three-panel array obeys

$$\eta_{app.c} = \eta+2\beta(1-\alpha_d) \tag{17}$$

where

$$\alpha_d = E_e/E_c \tag{18}$$

is the ratio of the energy in one (of the two symmetric) end panel to the energy in the center panel.

If the end panels are relatively highly damped, then the energy ratio α_d is very small and

$$\eta_{app.c} \approx \eta+2\beta \quad . \tag{19}$$

A similar argument, carried out for an end panel, shows that the apparent loss factor of an end panel, in presence of a highly damped center panel, obeys

$$\eta_{app.e} \approx \eta+\beta \quad . \tag{20}$$

The two foregoing equations indicate that one should be able to obtain both η and β from two apparent loss factor measurements, one carried out on the center panel, and one on an edge panel. The values of the internal loss factor η obtained in this manner may then be compared with values measured when all three panels are kept at the same energy levels. Such measurements and their results are described below.

Experiments and Results

Two sets of experiments were performed. The first set consisted of exciting all three panels equally, of observing the rate of decay when all excitations were removed, and of calculating the internal loss factor one expects to measure by this means. The second set involved measurement of the apparent loss factors of the end and center panels, and of calculating η and β from these measurements. Thus, η was determined in two ways, which should yield comparable results.

In the first set of experiments each of the three panels was excited by a separate shaker. The similarity of the shakers and of the panels leads one to expect equal power inputs and equal energies in the three panels; measurements confirmed this uniformity. Four decay rate readings were taken (at different positions) on each panel. The average of all twelve readings was used to compute the loss factor values shown in Fig. IV-7.

For apparent loss factor measurements on the center panel, the damping of the two end panels was increased by the application of six additional 2-in × 12-in strips of damping tape to each panel and of two 1-in × 12-in tapes to the edge beams of each end panel. This arrangement was intended to make α_d of Eq. (18) small enough, so that it could be neglected as compared to unity, so that Eq. (19) would apply. The experimentally obtained values of the apparent loss factor are shown in Fig. IV-8. For apparent loss factor measurements on an end panel, the panels that were not directly excited were also provided with high added damping, in order to make Eq. (20) applicable. The experimental results for this case are shown in Fig. IV-9.

Figure IV-10 shows values of the coupling loss factor obtained by combing the apparent loss factor data of Figs. IV-8 and IV-9 (one at a time) with the internal loss factor data shown in Fig. IV-7. One may observe that coupling loss factors obtained from the two different apparent loss factor measurements

differ by 10 per cent to 30 per cent, probably largely because the energy ratios that were neglected in Eqs. (19) and (20), on which the computations were based, were not small enough.

Because shakers are difficult to use on large structures, and since their attachment to inservice structures may be inadmissible, an exploratory attempt was made to excite the three-panel array acoustically, by means of loudspeakers. A chamber of 1-in × 1 ft × 3 ft, divided by 1-in high walls into three 1 ft × 1 ft chambers, was used to house the speakers, in order to isolate the sound sources from each other. By use of this device the sound pressure level on any panel due to the sound source in an adjacent chamber was about 10 dB lower than the sound pressure level on the panel directly excited by the source. This represents an energy ratio of 1 to 10, which may be too high. Nevertheless, a series of measurements using speaker excitation was completed, in order to compare the results obtained by this very convenient excitation means with those obtained with the more cumbersome shaker excitation. The various experiments discussed previously were repeated, using speaker excitation. The corresponding results are plotted on the previously mentioned figures, together with the related shaker results.

It may be noted that the speaker experiments gave smaller apparent loss factors, because of the interaction between the panels and the sound field in the speaker chambers. Also, the low coupling loss factors obtained at low exciting frequencies in the speaker experiments are probably due to the leaking of acoustic energy from the driving speaker to neighboring panel(s).

After completion of all of the previously described experiments, the end panels were cut away from the array, leaving only the center panel and a frame of beams around it. The damping (internal loss factor) of this center panel was then measured. The results of this measurement are shown in Fig. IV-11 together with the results of Fig. IV-7 obtained (with shaker excitation) on the complete array. The agreement is quite good.

Thus, determination of the internal loss factor by the energy-matching approach appears to yield good results. However, uniform excitation of all panels is required, and this implies the use of a multitude of shakers. Use of sound sources instead of shakers was found to be unsatisfactory here, but further efforts to obtain improvements in the technique (better isolation between chambers and reduced reverberation time of the chambers) may make it an acceptable one.

BLOCKING OF POWER FLOW BY STIFFENERS AND MASSES AT PANEL BOUNDARIES

If the flow of energy from the externally excited panel to its neighbors can be blocked effectively, measurements of the apparent loss factor of the excited panel should yield values that approach the internal loss factor of that panel. Some exploratory experiments were performed to investigate how well added reinforcing beams and masses can block the flow of energy. These experiments and their results are discussed below.

The configurations used in the experimental series are shown in Fig. IV-12. In the first configuration, four 5/8" × 5/8" × 12" brass beams are epoxied to the aluminum ribs of the previously used nine-panel array (Fig. IV-1), to form a stiff frame around the center panel. (The beam-rib composite is ten times stiffer in bending and six times more massive than the rib alone.) In the second configuration, six 5/8" × 5/8" × 2" brass blocks are attached to each of the four ribs, as shown in the figure. This arrangement increases the mass by the same amount as in the first configuration, but has little effect on the bending stiffness. In the third configuration, a rigid frame of four aluminum tubes (0.053" × 1" × 1" × 12") is attached to the ribs. These tubes increase the bending stiffness by a factor of 14, but have little effect on the mass.

For all three reinforcing configurations, the apparent loss factors of the center panel were measured by means of the decay rate technique. Corresponding results are presented in Fig. IV-13, together with data on the internal loss factor of the center panel and on the apparent loss factor, as measured with no reinforcing. It appears that none of the three reinforcing schemes result in the desired energy blocking, since addition of the stiffeners and masses is seen not to shift the apparent loss factor data toward those pertaining to the internal loss factor. The failure of the added elements to block energy flow may be due to: (1) the added elements' providing additional damping, and/or (2) the attached elements' improving the coupling between the center panel and its neighbors.

In order to study why the added structures resulted in increased apparent loss factors, a further series of experiments was performed, in which six damping tapes were added to each of the unexcited panels. The apparent loss factor of the center panel was again measured for each reinforcing configuration. The results are shown in Fig. IV-14, together with the apparent

loss factor measured in absence of added reinforcements (and with six damping tapes on each of the unexcited panels). The internal loss factor of the center panel is also shown for comparison.

In Fig. IV-14 the apparent loss factors of the reinforced panel are, in most cases, lower than those of the unreinforced panel — indicating that some energy blocking effect is present. By comparing Figs. IV-13 and IV-14 one may also note that the addition of damping to the unexcited panels resulted in only minor increases in the apparent loss factors of the reinforced configuration; this comparison indicates that some energy blocking has occurred due to the reinforcements. One may thus conclude that the reinforcements in the first series of experiments provided enough additional damping to offset the effect of energy blocking.

The results of all the reinforcement experiments indicate that attaching additional elements is very likely to introduce additional damping to the system and/or increase the coupling loss to the neighboring panels. These additional energy losses appear to be large enough to offset the gain in energy blocking, so that the desired aim of total energy blocking is not achieved.

ENERGY TRANSPORT ALONG RIBS

Some exploratory experiments to determine whether a significant amount of vibrational energy travels along the beams of a beam-panel structure were conducted, also on the nine-panel array. Experiments were carried out with two different loads added to the beams, as shown in Fig. IV-15. The center panel was excited by a shaker in each experiment, and the power input to the shaker was held constant in all the experiments. If energy is transported along the beams, the beam loading should be important and the vibration levels of the center panel should be different in the different experiments.

In the first experiment the beams were extended and loaded with eccentric masses. In the second experiment two of the extended beams were submerged in sand buckets to dissipate energy. In the third experiment the beams were unloaded (conventional nine-panel array).

The space-time average responses of the center panel in all three experiments are presented in Fig. IV-16. It can be seen that the response variation in the different experiments is

within 1 dB in most frequency bands. This minor change in response for different beam loads indicates that no significant amount of energy is transported along the beams.

REFERENCES FOR APPENDIX IV

1. E.E. Ungar, "Recommended Studies of Vibratory Energy Dissipation and Conduction in Aerospace Structures," Rept. FDL-TDR-64-111, August 1964.

2. R.H. Lyon and E. Eichler, "Random Vibration of Connected Structures," J. Acoust. Soc. Am. 36: 1344-1354 (1964).

3. R.H. Lyon and T.D. Scharton, "Vibrational-Energy Transmission in a Three-Element Structure," J. Acoust. Soc. Am. 38: 253-261 (1965).

4. E.E. Ungar, "Fundamentals of Statistical Energy Analysis of Vibrating Systems," Rept. AFFDL-66-52, April 1966.

TABLE IV-1

STEADY-STATE ENERGY SHARING MEASUREMENTS WITH PANEL ⑤ EXCITED WITH OCTAVE BAND NOISE

Frequency Band (Hz)	Acceleration Levels (dB)		
	PANEL ①	PANEL ②	PANEL ③
75-150	71	78.3	72.6
150-300	71.6	77.3	70.6
300-600	86.6	88	80.6
600-1200	86.6	84.6	87.6
1200-2400	84	82.3	83.3
2400-4800	81	80	80
4800-10,000	62.6	62.3	63
	PANEL ④	PANEL ⑤	PANEL ⑥
75-150	74.6	79.3	72.6
150-300	73	81.3	72.3
300-600	87.3	93	85
600-1200	93.3	92.6 ⊗ EXCIT	85.6
1200-2400	84.3	92.6	83.3
2400-4800	81	92	81.6
4800-10,000	63.3	75	64
	PANEL ⑦	PANEL ⑧	PANEL ⑨
75-150	73	76	71
150-300	72.6	76	71.3
300-600	83.3	83.3	87
600-1200	87	84	82.6
1200-2400	83	84.3	83.3
2400-4800	80	81.3	79.3
4800-10,000	63	62.6	63.3

TABLE IV-2

STEADY-STATE ENERGY SHARING MEASUREMENTS WITH PANEL ⑥ EXCITED WITH OCTAVE BAND NOISE

Frequency Band (Hz)	Acceleration Levels (dB)		
	PANEL ①	PANEL ②	PANEL ③
75-150	79	71.6	76
150-300	75.3	77.6	76.3
300-600	84.3	82	83.3
600-1200	84.3	83	83.3
1200-2400	81.6	82	82.6
2400-4800	81	82.6	82.3
4800-10,000	61.6	63	65.6
	PANEL ④	PANEL ⑤	PANEL ⑥
75-150	75.3	75.3	80.3
150-300	74	76	81.6
300-600	85.3	83.3	92.3
600-1200	88.6	84.3	93.3 ⊗ EXCIT
1200-2400	82	86.6	91
2400-4800	82	82.6	93.3
4800-10,000	63.3	63.6	74.6
	PANEL ⑦	PANEL ⑧	PANEL ⑨
75-150	79	71.6	76
150-300	75.3	77.6	76.3
300-600	84.3	82	83.3
600-1200	84.3	83	83.3
1200-2400	81.6	82	82.6
2400-4800	81	82.6	82.3
4800-10,000	61.6	63	65.6

TABLE IV-3

STEADY-STATE ENERGY SHARING MEASUREMENTS WITH PANEL ③ EXCITED WITH OCTAVE BAND NOISE

Frequency Band (Hz)	Acceleration Levels (dB)		
	PANEL ①	PANEL ②	PANEL ③
75-150	60.6	62.3	70.3
150-300	58	59.3	67.6
300-600	74	72	78.3 ⊗ EXCIT
600-1200	74	75	79
1200-2400	68.6	71.6	77.6
2400-4800	67.3	70.6	81
4800-10,000	50.3	52.6	64.3
	PANEL ④	PANEL ⑤	PANEL ⑥
75-150	59.3	56.3	62.3
150-300	56	57.6	59.3
300-600	72.3	76.3	72
600-1200	71	69.3	75
1200-2400	68	71	71.6
2400-4800	66	66.3	70.6
4800-10,000	50.3	49.6	52.6
	PANEL ⑦	PANEL ⑧	PANEL ⑨
75-150	52	59.3	60.6
150-300	55.6	56	58
300-600	70	72.3	74
600-1200	73.3	71	74
1200-2400	67.3	68	68.6
2400-4800	64.3	66	67.3
4800-10,000	49	50.3	50.3

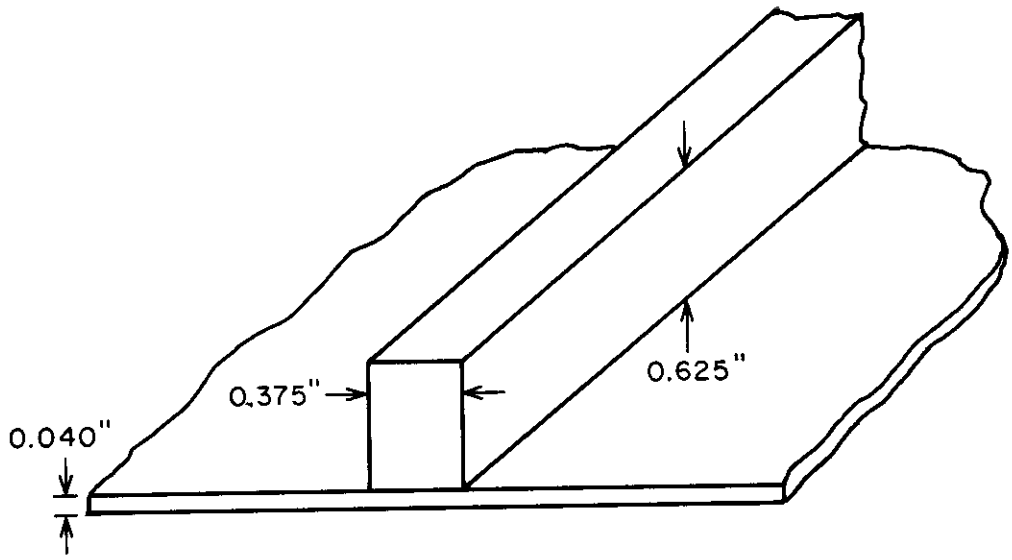

FIG. IV-1 BEAM AND PANEL DIMENSIONS

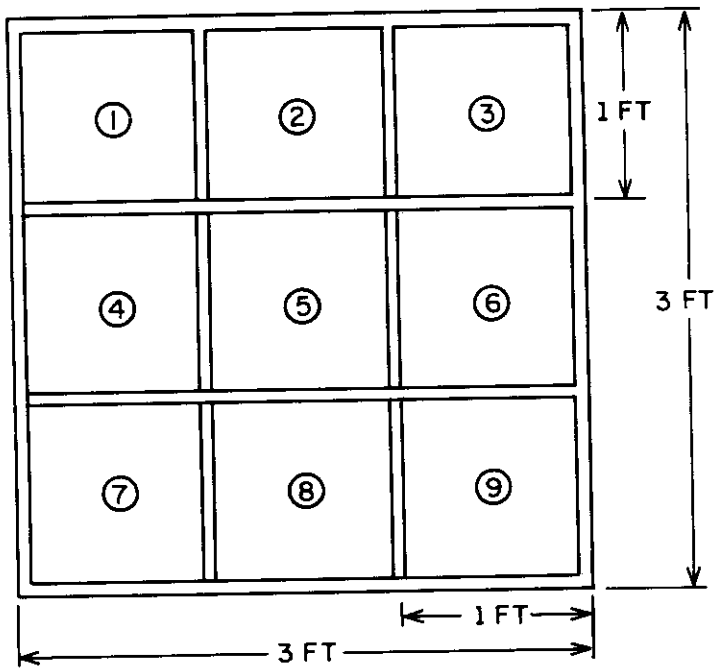

FIG. IV-2 CONFIGURATION OF EXPERIMENTAL NINE-PANEL ARRAY

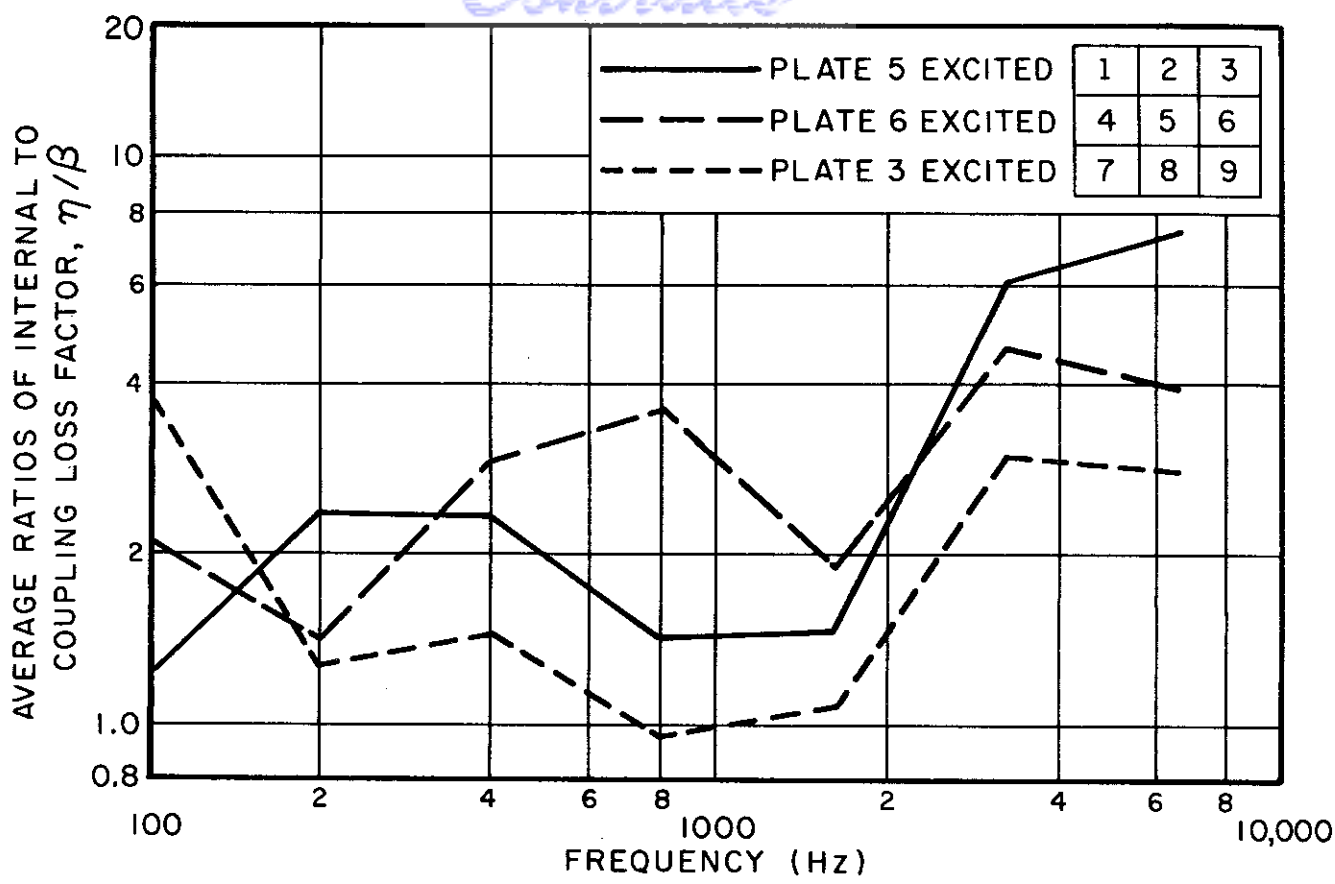

FIG. IV-3 LOSS FACTOR RATIOS CALCULATED FROM ENERGY SHARING MEASUREMENTS

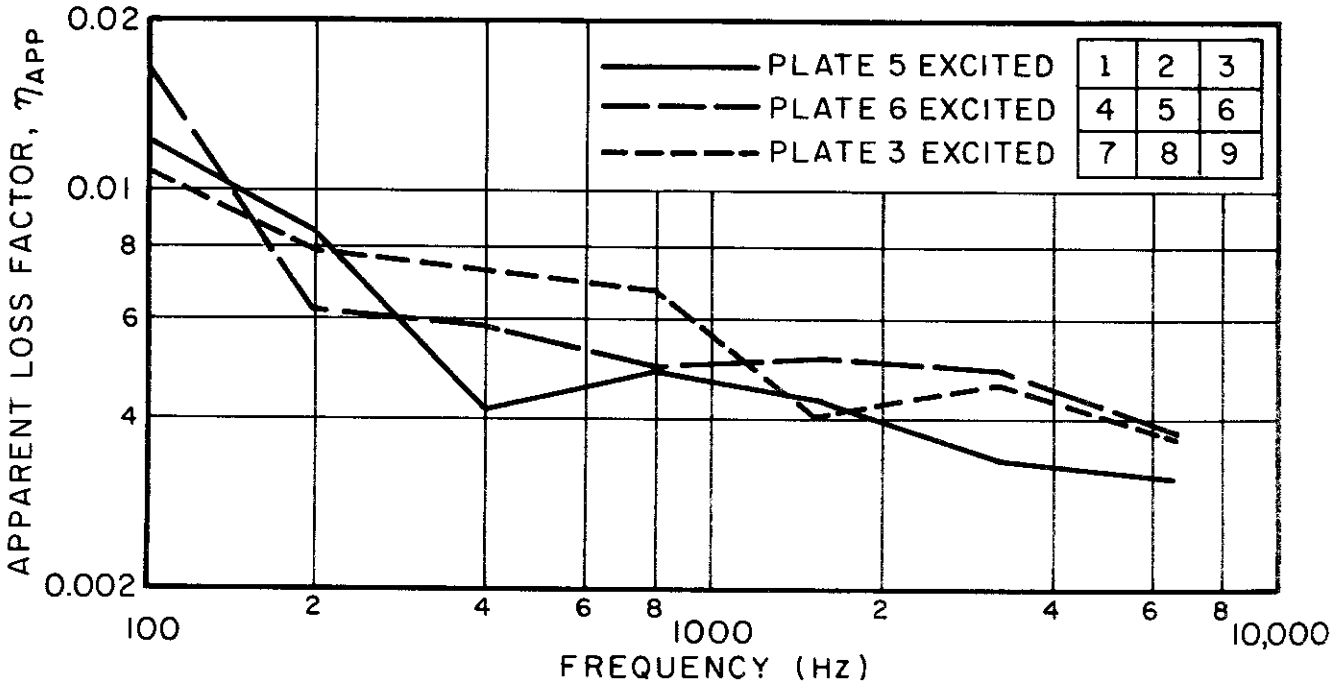

FIG. IV-4 APPARENT LOSS FACTORS CALCULATED FROM DECAY RATE MEASUREMENTS

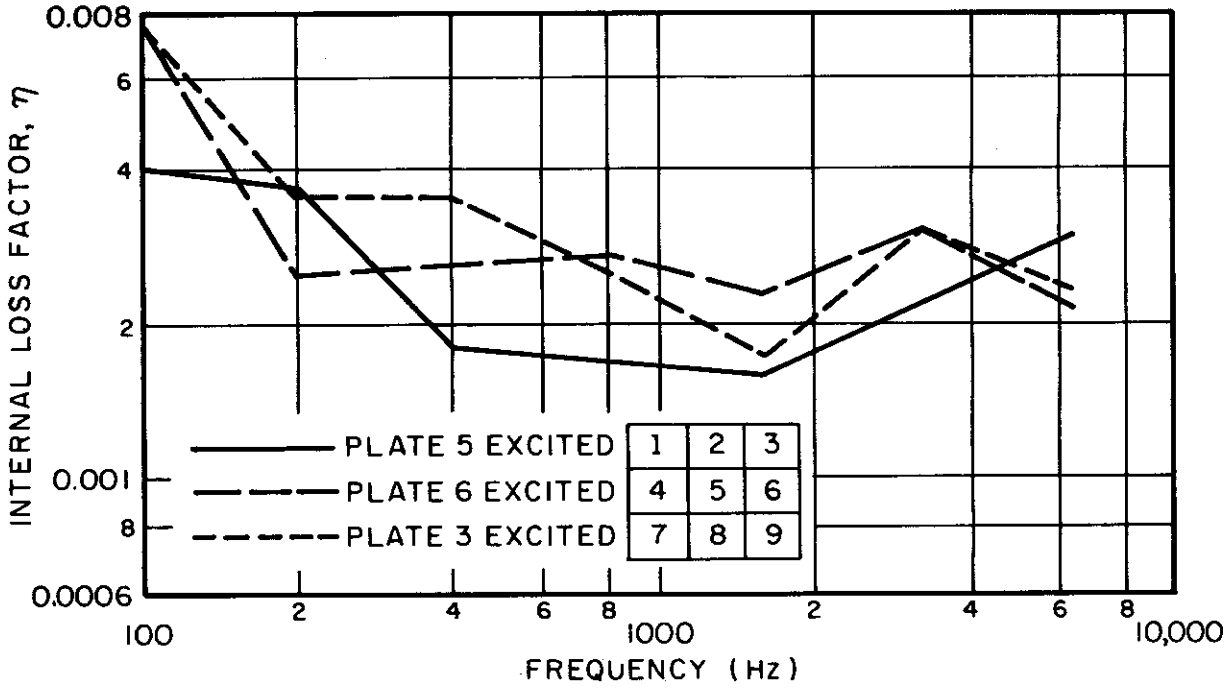

FIG. IV-5 INTERNAL LOSS FACTOR CALCULATED FROM ENERGY SHARING AND DECAY RATE MEASUREMENTS

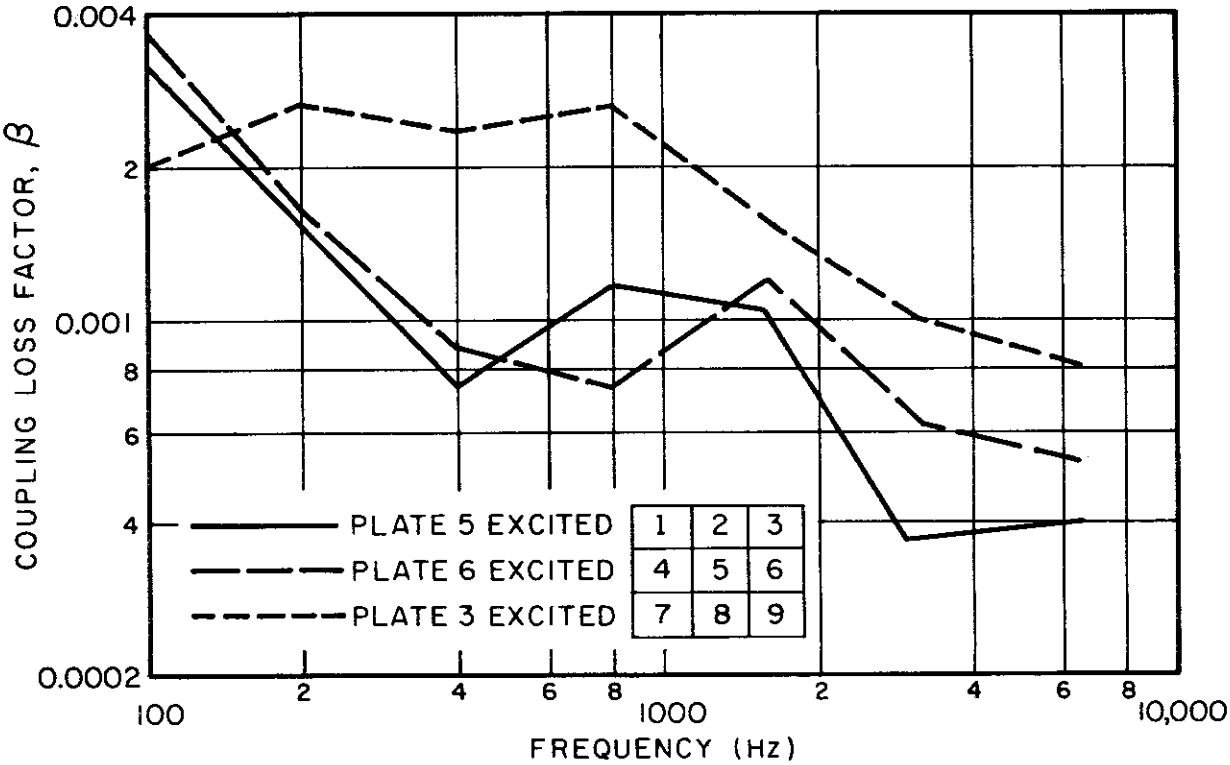

FIG. IV-6 COUPLING LOSS FACTOR CALCULATED FROM ENERGY SHARING AND DECAY RATE MEASUREMENTS

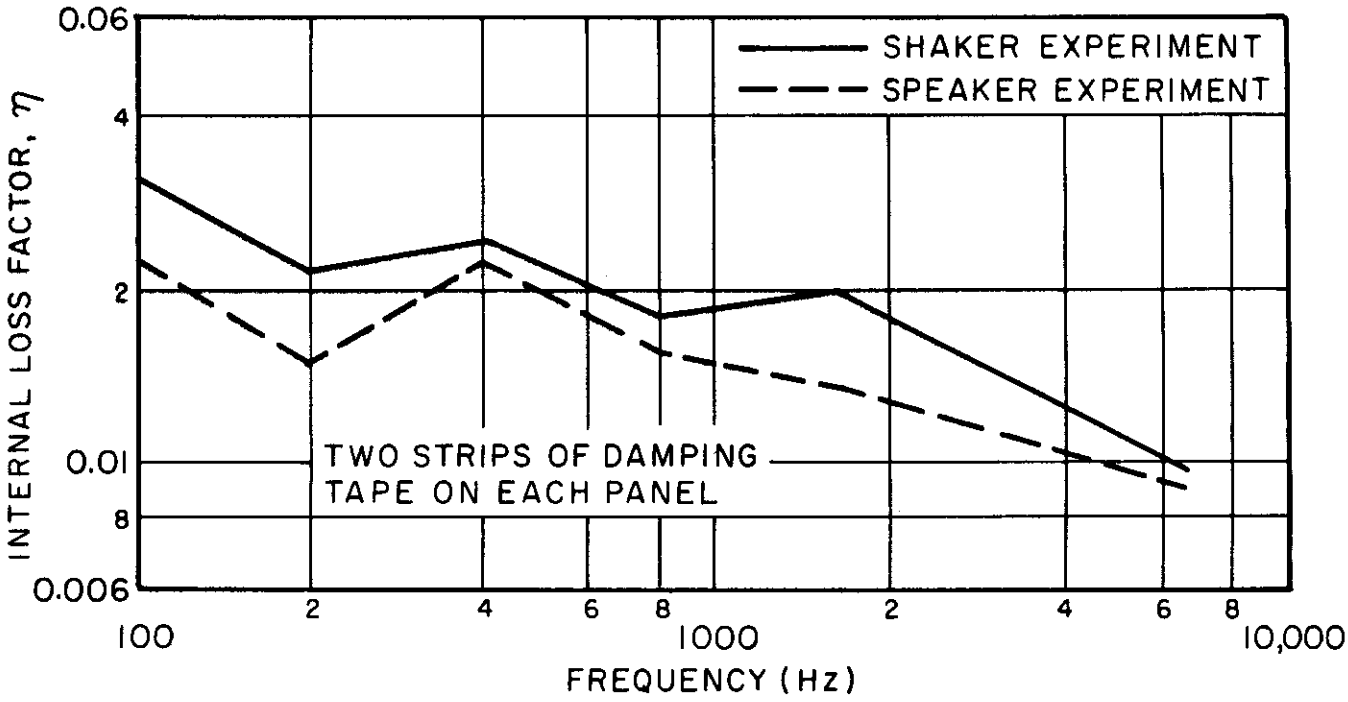

FIG. IV-7 INTERNAL LOSS FACTOR FROM ENERGY-MATCHING EXPERIMENTS ON THREE-PANEL ARRAY

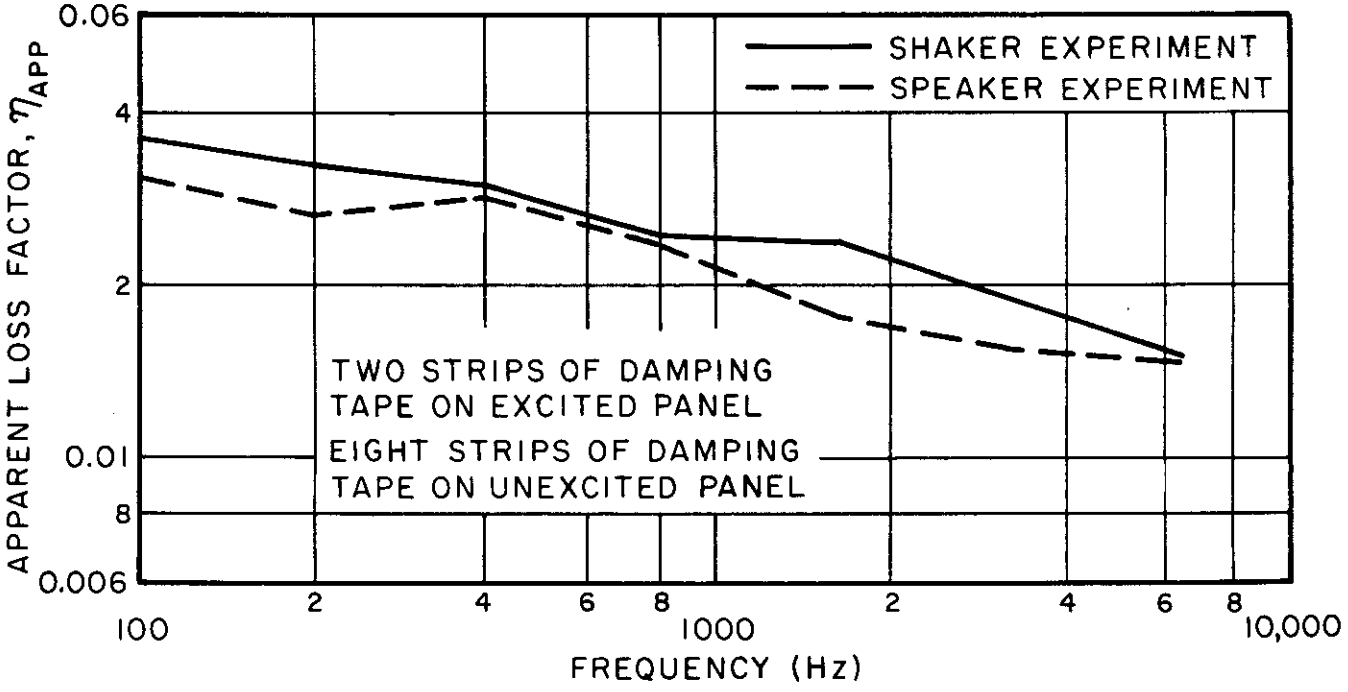

FIG. IV-8 APPARENT LOSS FACTOR MEASURED ON CENTER PANEL, WITH DAMPED END PANELS

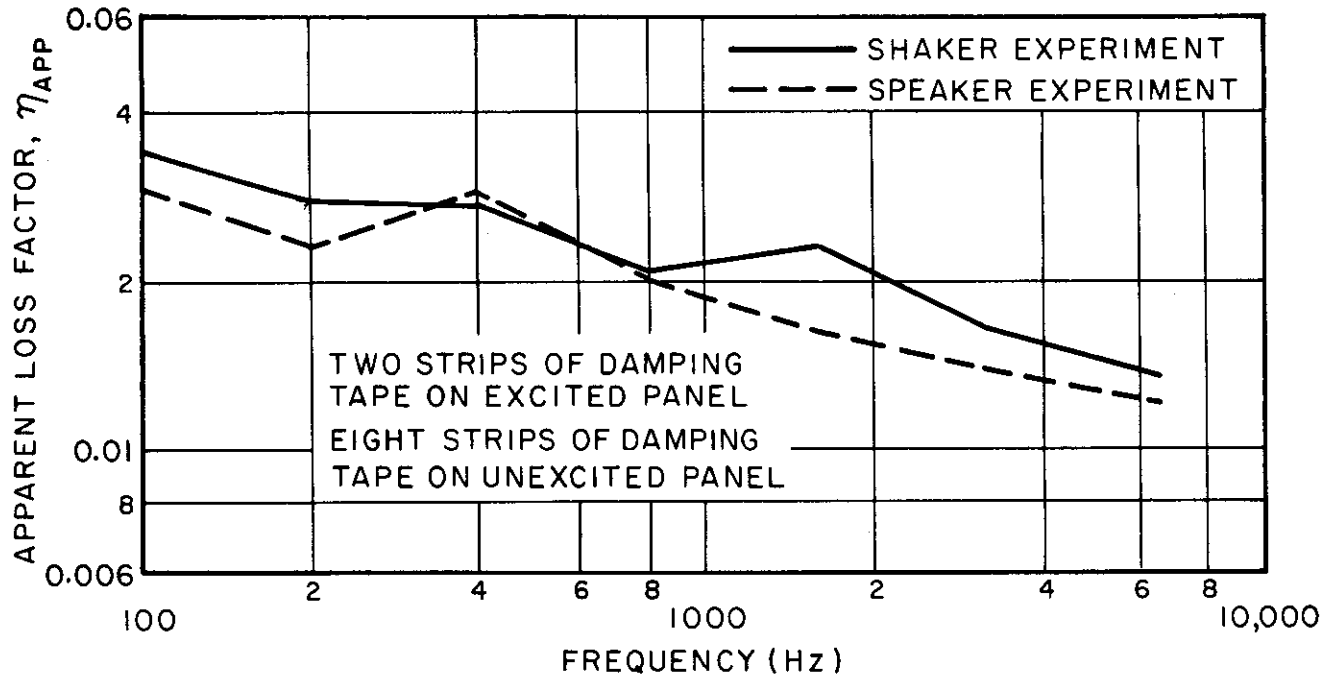

FIG. IV-9 APPARENT LOSS FACTOR MEASURED ON END PANEL, WITH OTHER PANELS DAMPED

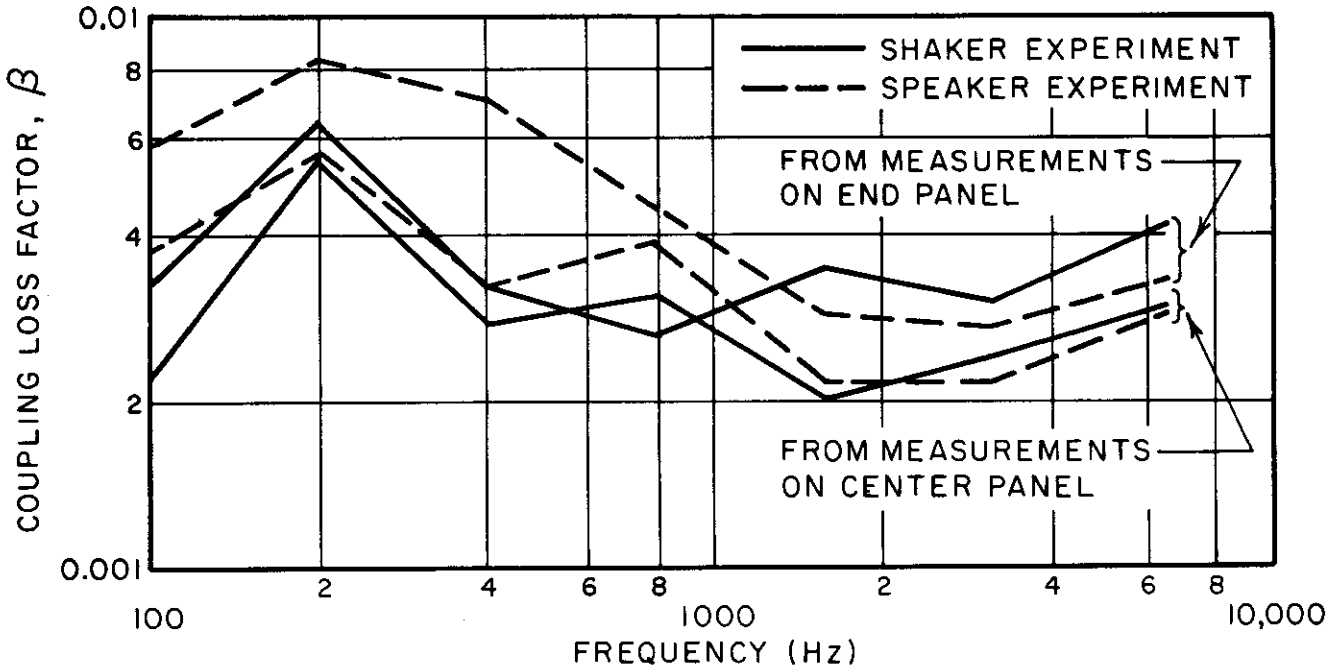

FIG. IV-10 COUPLING LOSS FACTOR, CALCULATED FROM INTERNAL LOSS FACTOR AND APPARENT LOSS FACTOR MEASUREMENTS

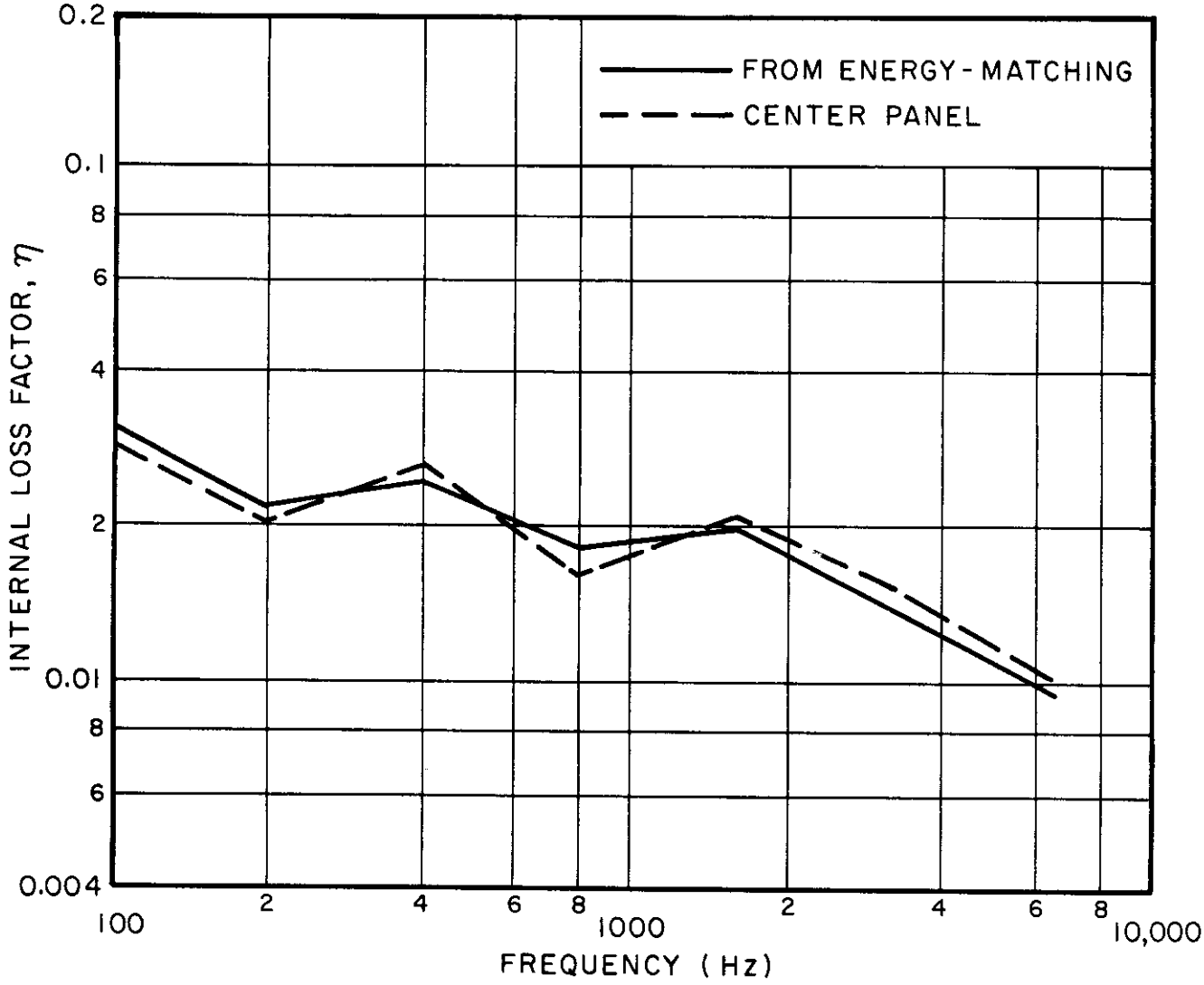

FIG. IV-11 COMPARISON OF INTERNAL LOSS FACTOR OF CENTER PANEL TO LOSS FACTOR FROM ENERGY-MATCHING EXPERIMENT

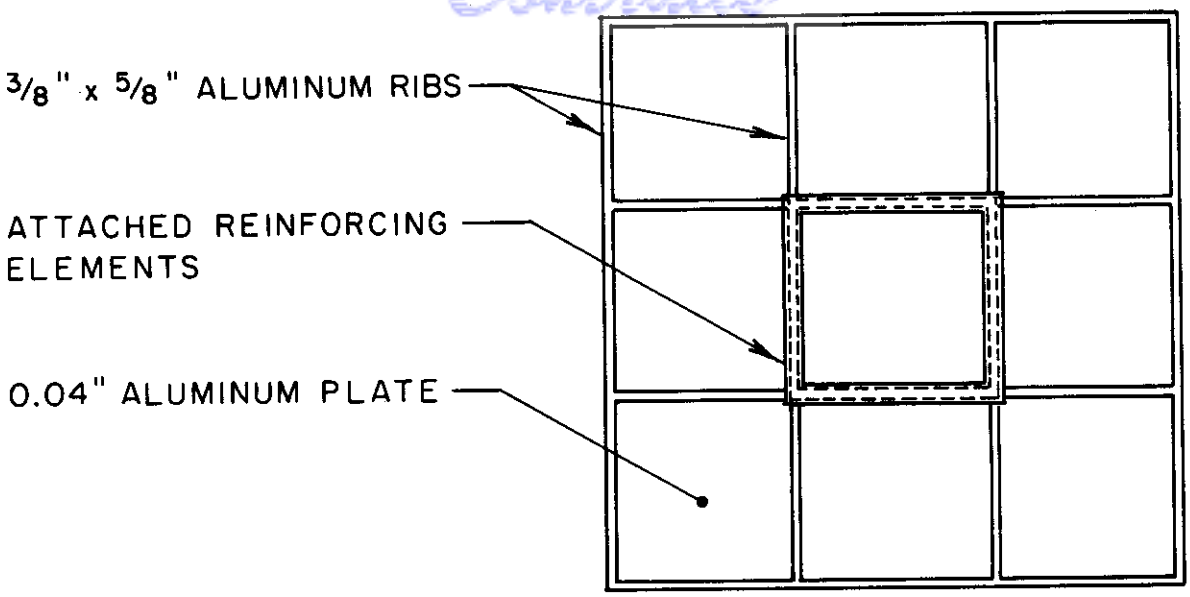

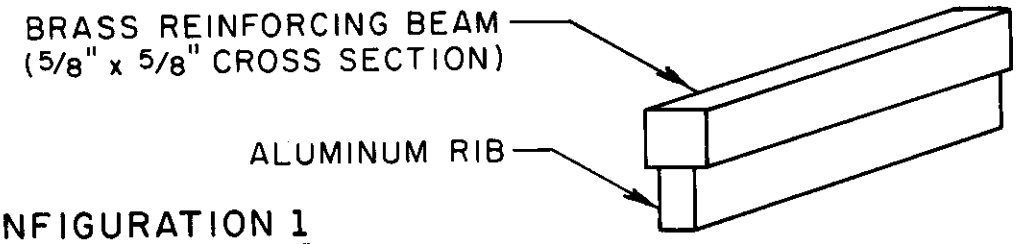

CONFIGURATION 1

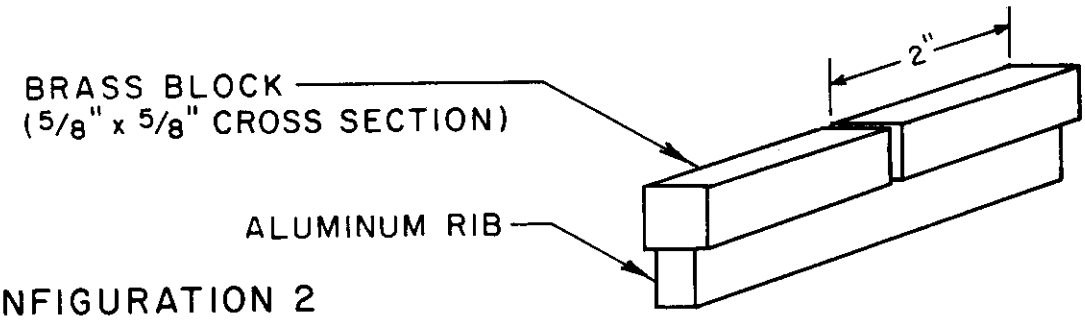

CONFIGURATION 2

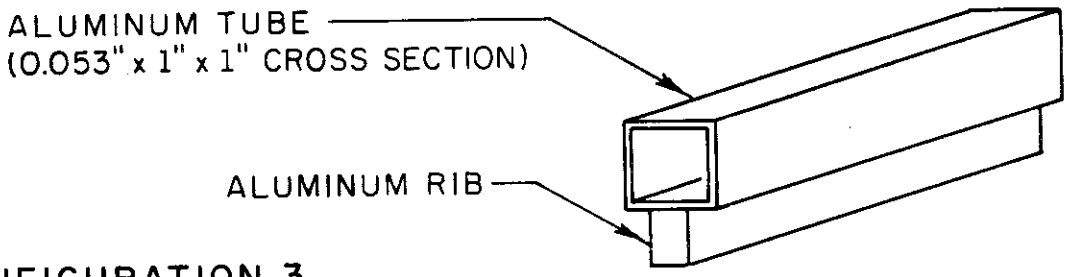

CONFIGURATION 3

FIG. IV-12 CONFIGURATIONS USED IN POWER FLOW BLOCKING EXPERIMENTS

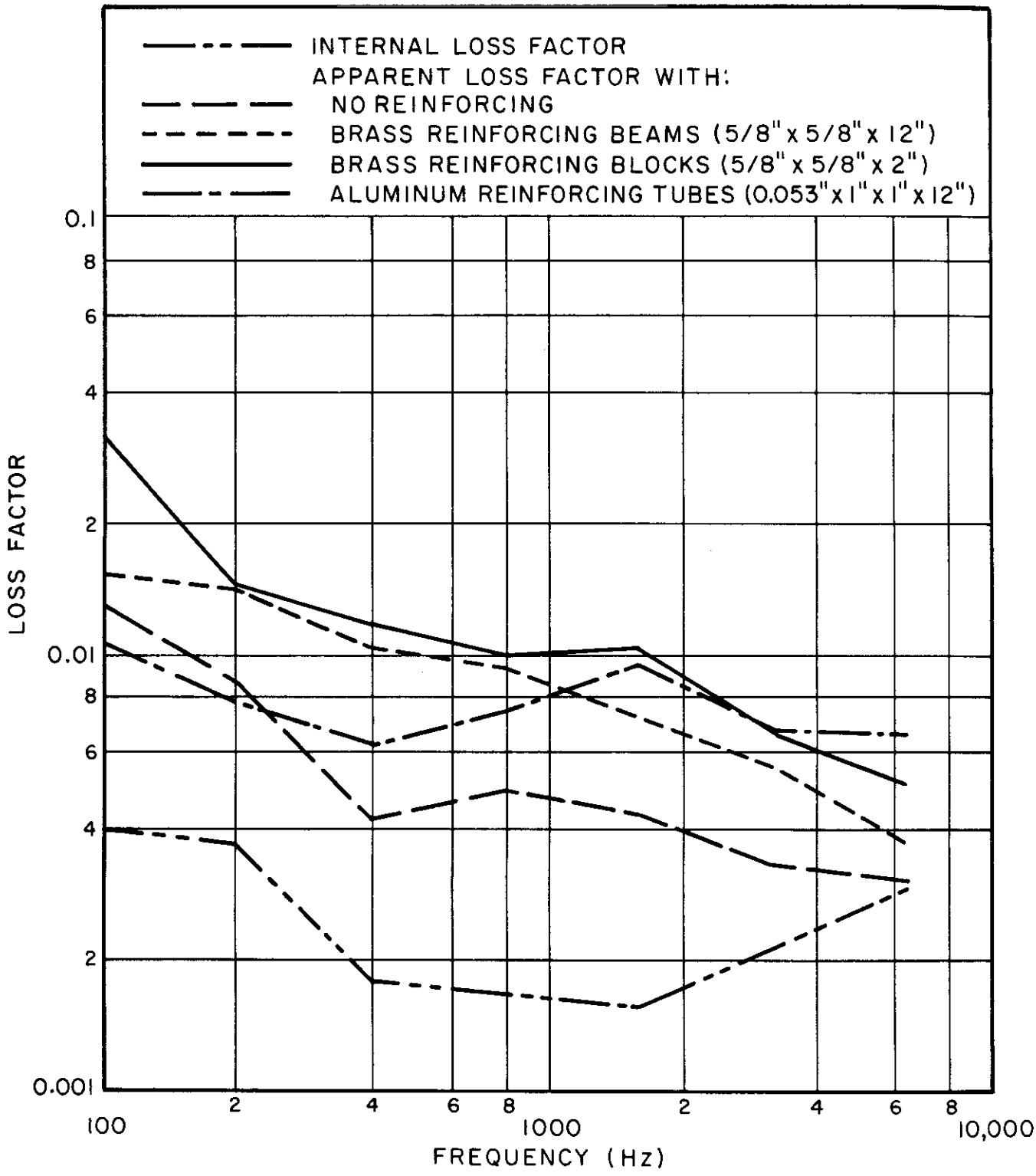

FIG. IV-13 EFFECT OF STIFFENERS AND MASSES ON APPARENT LOSS FACTOR (NO DAMPING ADDED TO UNEXCITED PANELS)

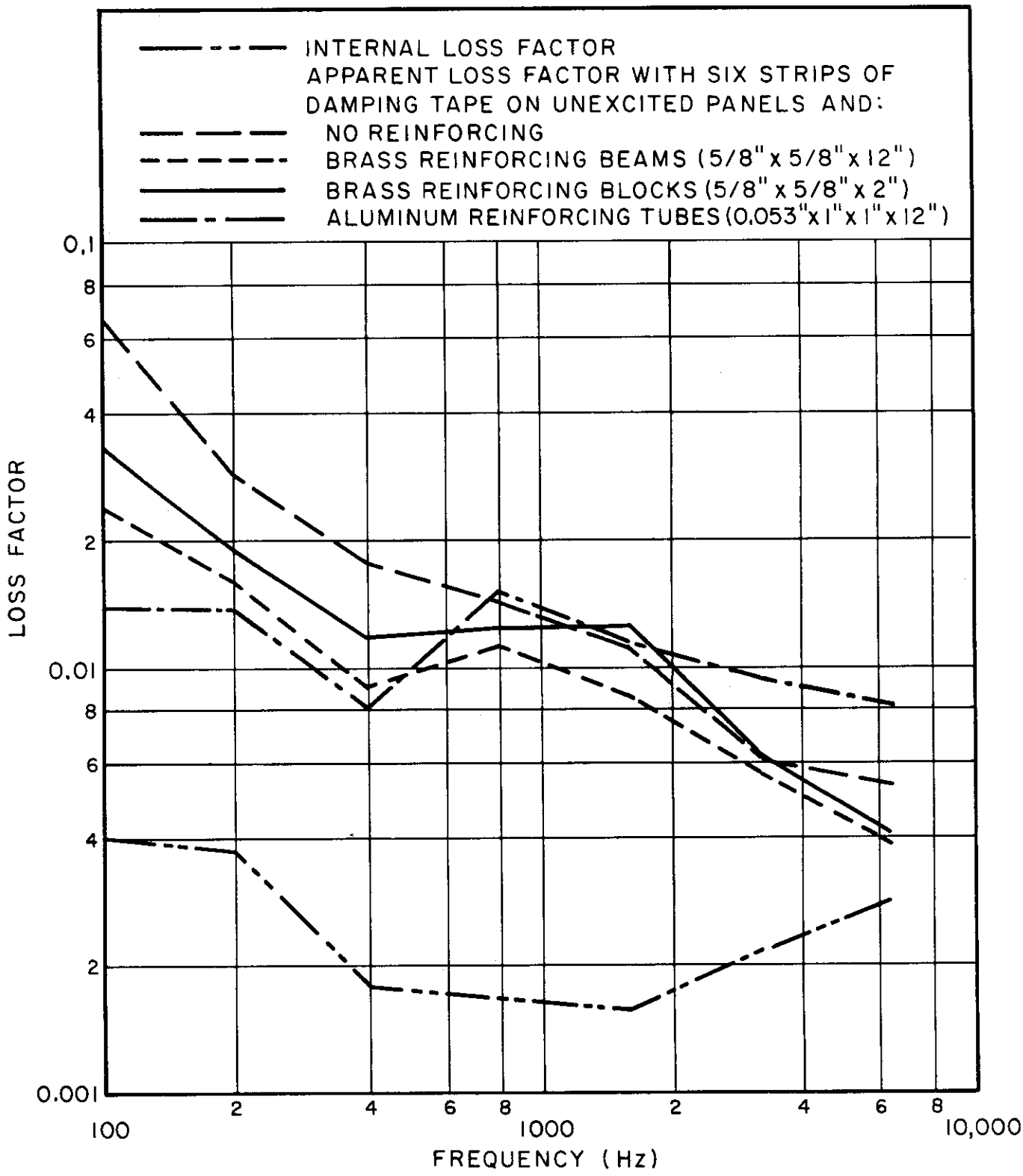

FIG. IV-14 EFFECT OF STIFFENERS AND MASSES ON APPARENT LOSS FACTOR (SIX STRIPS OF DAMPING TAPE ADDED TO UNEXCITED PANELS)

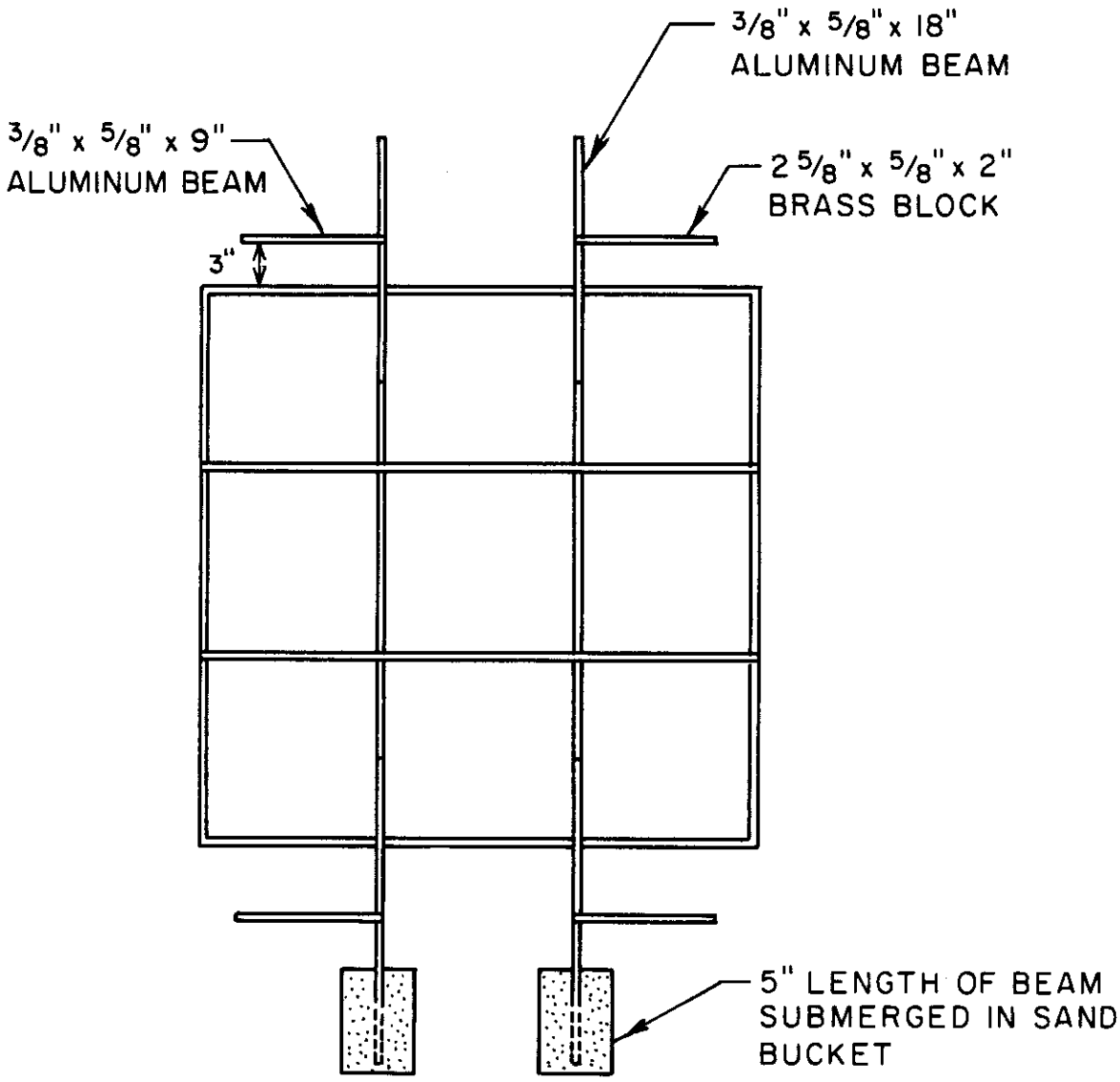

FIG. IV-15 BEAM LOADING CONFIGURATIONS

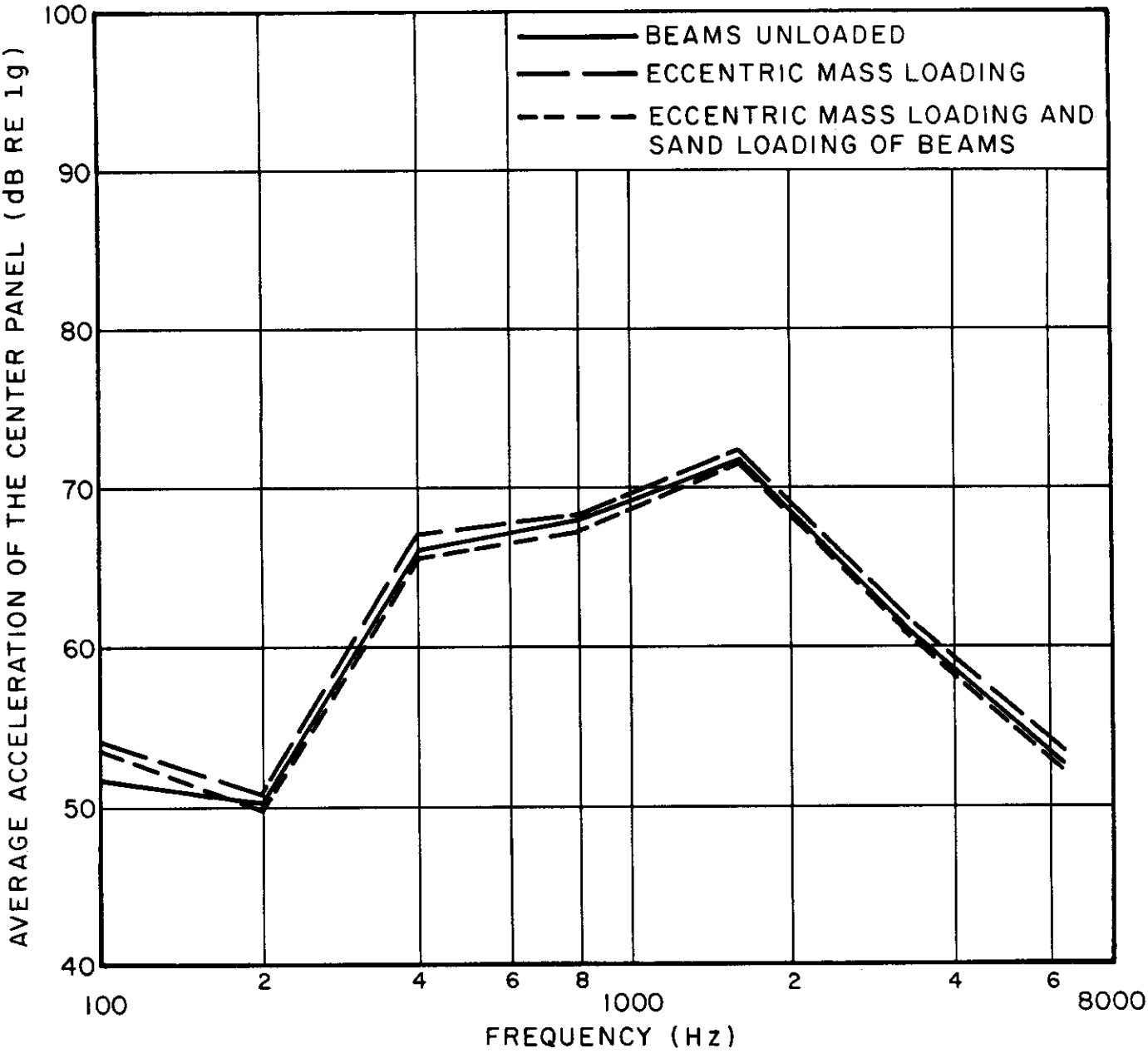

FIG. IV-16 EFFECT OF BEAM LOADING ON THE RESPONSE OF THE EXCITED CENTER PANEL

APPENDIX V

NOTES ON THE DESIGN OF SUPPORTS TO APPROXIMATE IDEAL BOUNDARY CONDITIONS

INTRODUCTION

Research tests whose purpose is to check theoretical predictions require test fixtures to simulate the ideal boundary conditions employed in theoretical calculations. The usual designs of such fixtures for dynamic tests are based on experience with static tests, and therefore often fail to take proper account of parameters related to vibration. This appendix considers some proposed fixture designs for ideal free, clamped, and simply supported boundaries from the dynamic point of view, and evaluates their feasibility and performance.

SIMULATION OF FREE BOUNDARIES

The most common method for simulating free panel edges involves suspending the test panel from long strings. This method is useful as long as the strings do not interfere significantly with the panel motion – that is, as long as the impedance of the plate at the string attachment point(s) is much greater than the impedance of string.

If one considers the generalized force which a string exerts on a plate edge to be composed of a bending moment M_B and a force F normal to the plate, then according to Eichler (Ref. 1) the edge admittance matrix Y_P of a (semi-infinite) plate is given by

$$Y_P = \frac{1}{\sqrt{\rho_P h_P D_P}} \begin{vmatrix} A_{11} & A_{12} \\ A_{21} & A_{22} \end{vmatrix} \qquad (1)$$

where Y_P is defined so as to relate the generalized force to the generalized displacement as

$$i\omega \begin{vmatrix} -\frac{\partial W_P}{\partial x} \\ W_P \end{vmatrix} = Y_P \begin{vmatrix} M_B \\ F \end{vmatrix} , \qquad (2)$$

and where

$$A_{11} \approx (0.08-0.275\ i\ \ell n\ ka/3.5)k^2$$

$$A_{12} = A_{21} \approx -(0.276+0.263\ i)k \qquad (3)$$

$$A_{22} \approx 0.403 + 0.0065\ i \quad .$$

The expressions of Eq. (3) apply in the limiting case of ka=0, where $k=[\omega^2\rho_P h_P/D_P]^{1/4}$ denotes the flexural wave number of the plate, and a the string radius. (The condition ka=0 is approached if the string radius is much smaller than a plate flexural wavelength.) In the foregoing expressions W_P denotes a plate normal mode, ρ_P the density, h_P the thickness, and D_P the flexural rigidity of the plate, and x is a coordinate perpendicular to the plate edge being considered.

The corresponding admittance matrix Y_S of semi-infinite stiff strings may be found from the equation of motion (Ref. 2),

$$E_S I_S \frac{d^4 W_S}{dx^4} - T \frac{d^2 W_S}{dx^2} + \rho_S A_S \frac{d^2 W_S}{dt^2} = 0 \qquad (4)$$

to obey

$$Y_S = \frac{\omega/E_S I_S}{k_1^3 - i\ k_2^3} \begin{vmatrix} B_{11} & B_{12} \\ B_{21} & B_{22} \end{vmatrix} \qquad (5)$$

where

$$B_{11} = (k_1^2+k_2^2)$$

$$B_{21} = B_{12} = i(k_1+i\ k_2) \qquad (6)$$

$$B_{22} = -i(k_1^2+k_2^2)/k_1k_2 \quad ,$$

and

$$k_1^2 = \alpha^2(\Gamma-1) \quad , \quad k_2^2 = \alpha^2(\Gamma+1)$$

$$\Gamma^2 = 1+(\alpha\beta)^{-2} \qquad (7)$$

$$\alpha^2 = T/2E_SI_S \quad , \quad \beta^2 = T/2\rho_SA_S\omega^2 \quad .$$

Here T represents the tension, A_S the cross-sectional area, E_S Young's modulus, I_S the cross-sectional moment of inertia, and ρ_S the density of the string. Also, W_S denotes the string's lateral deflection, and ω represents the radian frequency of the vibration.

One may obtain the impedance matrices corresponding to Eqs. (1) and (5) by inverting the admittance matrices. Then one may compare the absolute values of the corresponding elements of the impedance matrices in order to determine under what conditions the string impedance is much smaller than the plate edge impedance. However, this approach is too cumbersome, and one may obtain useful results by assuming flexural effects in the string to be negligible. Then the force components of the admittances are dominant, and one need only compare the A_{22} and B_{22} elements of the two admittance matrices. One finds that

$$\left|\frac{Y_{P22}}{Y_{S22}}\right| \approx 0.403\left[\frac{\rho_SA_S\ T}{\rho_Ph_PD_P}\right]^{1/2}\left[\frac{1+4\alpha^2\beta^2}{4\alpha\beta\sqrt{1+\alpha^2\beta^2}}\right]^{1/2} \quad . \qquad (8)$$

If tension effects in the string dominate over bending effects, then $\alpha^2\beta^2>1$; the term in the second bracket of the above equation then is always less than or equal to unity. In order for the plate impedance to be much greater than the string impedance, $|Y_{P22}/Y_{S22}|$ of Eq. (8) must be much smaller than unity, implying that the first bracketed term must be much smaller than unity.

Thus, a string support generally can approximate free edge conditions if it satisfies

$$\rho_S A_S \, T/\rho_P h_P D_P \ll 1 \quad . \tag{9}$$

However, flexural effects in the string must be considered, and additional limitations must be imposed on its design, if the condition

$$\alpha^2\beta^2 = T^2/4E_S I_S \, \rho_S A_S \, \omega^2 \gg 1 \tag{10}$$

is <u>not</u> satisfied for the entire frequency range of interest.

SIMULATION OF CLAMPED BOUNDARIES

Clamped or "built-in" boundary conditions may be simulated by supporting the test panel in two massive clamps (Fig. V-1).

In such an arrangement the lateral displacement of the panel edge deviates from the ideal zero value because the shear force exerted by the panel on the supports deforms the support structures in compression and simultaneously causes the panel-support assembly to deform in flexure. The compressional deformation of the support depends markedly on the precompression of the support assembly, as can be deduced by considering the stress distribution in a right-angle wedge with a concentrated line load P applied at the wedge corner (Fig. V-2). For two wedges that are pressed together so that the stresses and displacements are continuous across the interface (i.e., where one has essentially an elastic half-space), the stress distribution along the free surface is given (Ref. 3) by

$$\sigma_r\Big|_{\theta=0} = \frac{2P}{\pi r} \quad . \tag{11}$$

But for a single wedge (i.e., for an elastic quarter-space), one obtains

$$\sigma_r\Big|_{\theta=0} = \frac{4}{\pi(1-4/\pi^2)}\,\frac{P}{r} \quad . \tag{12}$$

The deformation of a wedge without precompression may be as much as four times as large as the deformation in a precompressed wedge. Therefore, it is clearly desirable to design support clamps so that interface contact is always maintained.

Panel Edge Displacement in Clamp

If the supports are sufficiently precompressed so that continuity of stresses and deformations is maintained, then the stress distribution in the supports is approximately that in an elastic half-space. For a parabolic stress distribution across the thickness of the test panel the stress function Φ for the support is given (Ref. 3) by

$$\Phi = \frac{S}{\pi}\left[\frac{2y^2}{3h^2}\left(\frac{3}{4}h^2-3x^2+y^2\right)\ell n\left(\frac{r_2^2}{r_1^2}\right)+\frac{hy\beta}{3}+\frac{4}{3}\,\frac{xy}{h^2}\left(x^2-3y^2-\frac{9}{4}\,h^2\right)\alpha + \frac{8}{3}\,\frac{xy^2}{h}\right] \quad , \tag{13}$$

where the coordinates x,y, and the dimension h are defined as in Fig. V-1, and

$$r_1^2 \equiv (x-h/2)^2+y^2$$

$$r_2^2 \equiv (x+h/2)^2+y^2 \tag{14}$$

$$\alpha \equiv \tan^{-1}\left(\frac{hy}{x^2+y^2-h^2/4}\right) \quad , \quad \beta \equiv \tan^{-1}\left(\frac{2xy}{x^2-y^2-h^2/4}\right) \quad ,$$

and where S is the maximum shear stress in the panel at the edge.

The corresponding stress distribution at y=0 is found to be

$$\sigma_x\Big|_{y=0} = \frac{2S}{\pi}\left[2(X+1)-X(X+2)\,\ell n\,\frac{X+2}{X}\right] \tag{15}$$

where

$$X \equiv \frac{2x}{h} - 1 \quad . \tag{16}$$

The corresponding displacement δ_S of the panel edge may be found by integrating Eq. (15) over the support height H. One finds

$$\frac{\pi\delta_S E_S}{hS} = \frac{2H_o(H_o+2)}{3} + \frac{4}{3}\,\ell n(1+H_o/2) - H_o^2(1+H_o/3)\,\ell n\left(\frac{H_o+2}{H_o}\right) \tag{17}$$

where

$$H_o \equiv 2H/h \quad . \tag{18}$$

The foregoing expression pertains only to the panel displacement that is due to compression of the support. An additional displacement δ_B occurs due to bending of the support-and-panel combination. This additional displacement may be computed approximately by assuming the panel-support assembly to be clamped rigidly at an effective distance D from its end (See Fig. V-1). From simple beam theory one finds that

$$\frac{2\delta_B E_B}{hS} = \frac{16}{3}\,\frac{D_o^3\,(1-\nu^2)}{(H_o^3+12H_o)+(E_P/E_S)(8+6H_o^2)} \tag{19}$$

where

$$D_o = 2D/h \quad , \tag{20}$$

and where E_S, E_P denote the Young's moduli of the support and panel, respectively,

The total displacement δ_T of the panel midsurface at the edge thus obeys

$$\frac{2\delta_T E_S}{hS} = \frac{16}{3} \frac{D_o^3 (1-\nu^2)}{(H_o^3+12H_o)+(E_P/E_S)(8+6H_o^2)} + \frac{2}{\pi}\left[\frac{2H_o(H_o+2)}{3}\right. \tag{21}$$

$$\left. + \frac{4}{3} \ell n(1+H_o/2) - H_o^2(1+H_o/3)\ \ell n\left(\frac{H_o+2}{H_o}\right)\right] \quad .$$

Figure V-3 shows the results of calculations based on Eq. (21) for various support widths D and support heights H. One may observe that for a given support width D (or height H) there is an optimum support height H(or width D) for which the total displacement is minimum. Figure V-4 shows how the optimum height and the corresponding minimum displacement varies with support width D.

Although at first glance the existence of conditions where increasing the support thickness results in increased deflections appears to contradict intuition, some additional thought convinces one otherwise. For small thicknesses the flexural stiffness of the support is small, and the compressive stiffness is large. As one increases the thickness one increases the flexural stiffness, while reducing the compressive stiffness. Thus, the flexural stiffness dominates at large thicknesses and the compressive stiffness at small thicknesses; therefore at some intermediate point an incremental increase in one stiffness is just balanced by a decrease in the other, resulting in a maximum stiffness and in a minimum deflection.

Bolt Tension and Spacing

In order to determine the bolt tension that is required to maintain interface contact (precompression), one must know the distribution of interface pressure that is produced by a given bolt head pressure P_B.

Rötscher (Ref. 4) has suggested the stress in an elastic body under bolt pressure may be approximated as the stress in a body limited by two truncated cones with half angles of 45° (Fig. V-5). The corresponding average pressure P(z) at different levels is found from force equilibrium to obey

$$P(z) = \frac{b^2-a^2}{(b+H-z)^2-a^2} P_B \quad . \tag{22}$$

Rötscher's method is convenient for the determination of the average contact pressure and the average deformation, but unfortunately yields misleading results for the stress and pressure distributions. An exact solution by Fernlund (Ref. 5) shows that the contact pressure decreases exponentially with increasing distance from the bolt center, and becomes vanishingly small at the Rötscher's cone surface (Fig. V-6). A fourth-order polynominal, as suggested by Fernlund, can be made to approximate the exact contact pressure distribution closely for greater axial distances from the bolt head, but fails to provide a good approximation near the bolt head. It therefore appears useful to develop a modification of Rötscher's approach, which takes account of the radial variation of stress, and to take (Fig. V-6)

$$P = \begin{cases} P_C & \text{for } a<r<b \\ P_C \dfrac{r_o-r}{r_o-b} & \text{for } b<r<r_o \end{cases} \tag{23}$$

where

$$r_o = (H-z)+b$$

$$P_C = P_B \frac{(b^2-a^2)\,(r_o-b)}{(H-z)[(H-z)^2+3b(H-z)+3(b^2-a^2)]} \quad . \tag{24}$$

The corresponding minimum compressive deformation δ_Q at the panel edge (i.e., that at point Q of Fig. V-1) for the typical case where b=2a is found to obey

$$\frac{2\delta_Q E_S}{hP_B} = 6\left(\frac{2a}{h}\right)\left[\left(1-\frac{r_Q+a}{H+3a}\right) - \frac{(r_Q-2a)}{3a}\,\ell n\,\frac{H(r_Q+a)}{(H+3a)(r_Q-2a)}\right] \tag{25}$$

where, as evident from Fig. V-1,

$$r_Q = [(a+D)^2+(L+a)^2]^{1/2} \quad . \tag{26}$$

This minimum compressive deformation δ_Q exceed or at least equal the panel edge deflection δ_T, if the support is to remain in contact with the test panel. Therefore, the minimum bolt tension for a given geometry and panel shear force S may be computed by equating Eqs. (21) and (25).

One may also show that if the supported plate vibrates, then the maximum edge shear stress S is related to the root mean square deflection w_{rms} of the panel according to

$$\frac{S}{E_P} = \frac{8}{9}\,\frac{h^2 w_{rms}}{(1-\nu^2)^{1/4}}\left[\frac{12\omega^2\rho_P}{E_P h^2}\right]^{3/4} \quad . \tag{27}$$

Sample Calculation

Consider the case where $E_P=E_S$, D/h=10, h=a=b/2. Then from Fig. V-4, the optimum support height and the corresponding displacement obey $H/h\approx 25$, $(\delta_T/h)(E_S/S)=1.75$. Substitution of the above values into Eq. (25) yields $2/\delta_\theta E_S/hP_B \approx 1.92$ and substitution

into Eq. (21) and taking the ratio of the two values indicates that the smallest acceptable bolt head pressure P_B must satisfy $P_B/S = 1.82$.

SIMULATION OF SIMPLY SUPPORTED BOUNDARIES

It has been suggested that simply supported edges may be approximated by the use of short leaf springs or "flexures," as sketched in Fig. V-7. It is clear that such a flexure will exhibit resonances and anti-resonances, and that at anti-resonances the moment it exerts on the test panel may be considerable. At anti-resonances a flexure thus fails to approximate the zero-moment condition required of a simple support; the question is whether the flexure can be designed so that its lowest anti-resonance is above the frequency range of interest.

It is instructive to consider the configuration of Fig. V-7, which shows a uniform beam supported by a short perpendicular leaf spring. The vibratory lateral deflection w_ℓ of the leaf spring may be expressed as

$$w_\ell = A_1 \sin k_\ell x + A_2 \cos k_\ell x + A_3 \sinh k_\ell x + A_4 \cosh k_\ell x \quad , \qquad (28)$$

and the lateral deflection of the beam in the vicinity of the leaf-spring-supported end may, by use of Bolotin's asymptotic method, be written as

$$w_B = B_1 \sin k_B y + B_2 \cos k_B y + B_3 e^{-k_B y} \quad . \qquad (29)$$

Here k_ℓ and k_B are the wave numbers pertaining to the leaf spring and beam, respectively.

The integration constants A_1 and B_1 of Eqs. (28) and (29) may be evaluated by application of the boundary conditions

$$w_\ell\Big|_{x=0} = dw_\ell/dx\Big|_{x=0} = w_\ell\Big|_{x=\ell} = 0$$

$$dw_\ell/dx\Big|_{x=\ell} = dw_B/dy\Big|_{y=0}$$

$$E_\ell I_\ell \, d^2w_\ell/dx^2\Big|_{x=\ell} = E_B I_B \, d^2w_B/dy^2\Big|_{y=0} \qquad (30)$$

$$E_B I_B \, d^3w_B/dy^3\Big|_{y=0} = -(E_\ell A_\ell/\ell) w_B\Big|_{y=0} \quad .$$

Here E, I, A represent Young's modulus, moment of inertia, and cross-sectional area, respectively; and the subscripts ℓ and B refer to the leaf spring and beam, respectively.

One may then compare the bending moment M_e at the supported beam end to the maximum moment M_a in the beam (asymptotic) region far from the support and find

$$M_e/M_a = 2(1-\gamma)/D_o \quad ;$$

$$\gamma = (h_\ell/\ell)^2 \, \theta^3 (\kappa\mu)^{1/4}/12$$

$$D_o^2 = (1+\beta)^2(1+\gamma^2)+(1-\gamma)^2(1+\beta^2)-2(1-\gamma)(1+\beta)(\gamma-\beta)$$

$$\beta = \kappa\alpha T \quad , \quad \alpha^4 = \mu/\kappa \qquad (31)$$

$$\kappa = E_B I_B/E_\ell I_\ell \quad , \quad \mu = \rho_B A_B/\rho_\ell A_\ell$$

$$\theta = k_\ell \ell = (\rho_\ell A_\ell \omega^2 \ell^4/E_\ell I_\ell)^{1/4}$$

$$T = (1-\cos\theta \cosh\theta)/(\sin\theta \cosh\theta - \cos\theta \sinh\theta) \quad .$$

The above function T takes on infinitely large values whenever its denominator vanishes (except for $\theta=0$, where the numerator vanishes also and T approaches zero). The smallest nonzero root of the denominator is $\theta_1 \approx 3.9$; hence a flexure can be employed usefully only for frequencies that satisfy

$$\omega < 15(E_\ell I_\ell / \rho_\ell A_\ell \ell^4)^{1/2} \quad . \tag{32}$$

REFERENCES FOR APPENDIX V

1. E.E. Eichler, "Plate-Edge Admittances," J. Acoust. Soc. Am. 36: 344-348 (1964).

2. P.M. Morse, Vibration and Sound, 2nd Ed. (McGraw-Hill Book Co., Inc., New York, 1948).

3. S. Timoshenko and J.N. Goodier, Theory of Elasticity (McGraw-Hill Book Co., Inc., New York, 1951).

4. F. Rötscher, "Die Maschinenelemente," Vol. I (Julius Springer, Berlin, 1927).

5. I. Fernlund, "A Method to Calculate the Pressure Between Bolted or Riveted Plates," Rept. No. 11, Institute of Machine Elements, Chalmers University of Technology, Gothenberg, Sweden (1961).

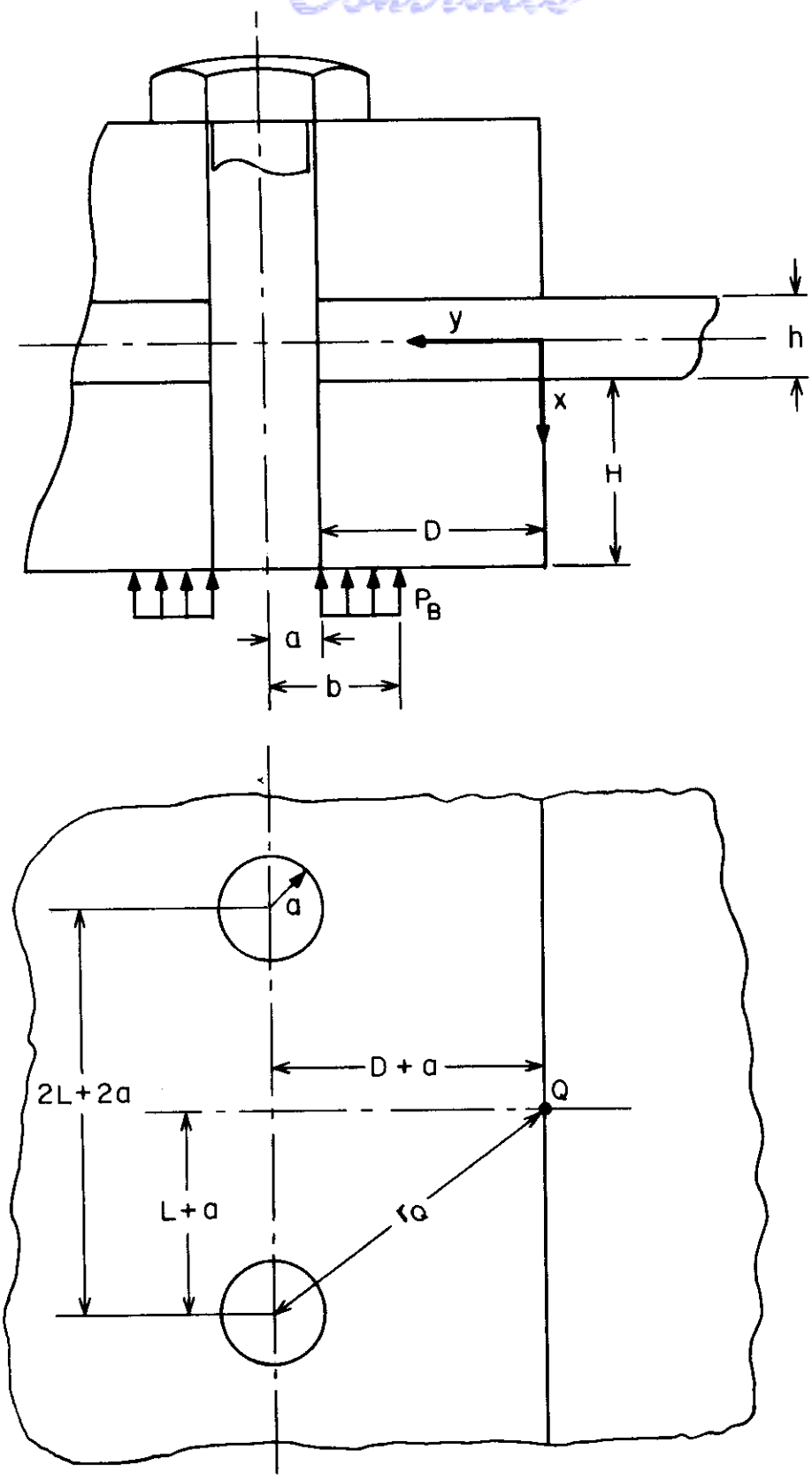

FIG. V-1 BOLTED EDGE-CLAMP GEOMETRY

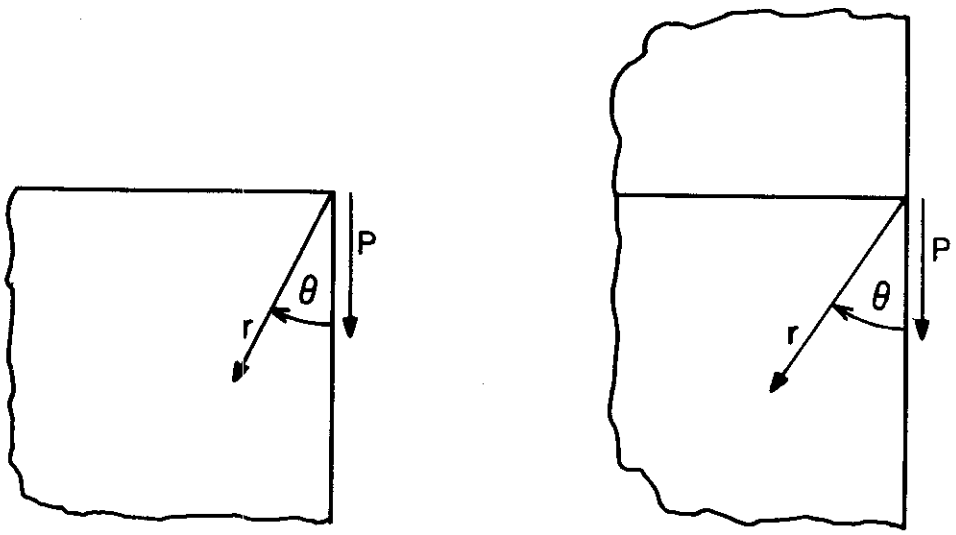

FIG. V-2 ELASTIC QUARTER- AND HALF-SPACES

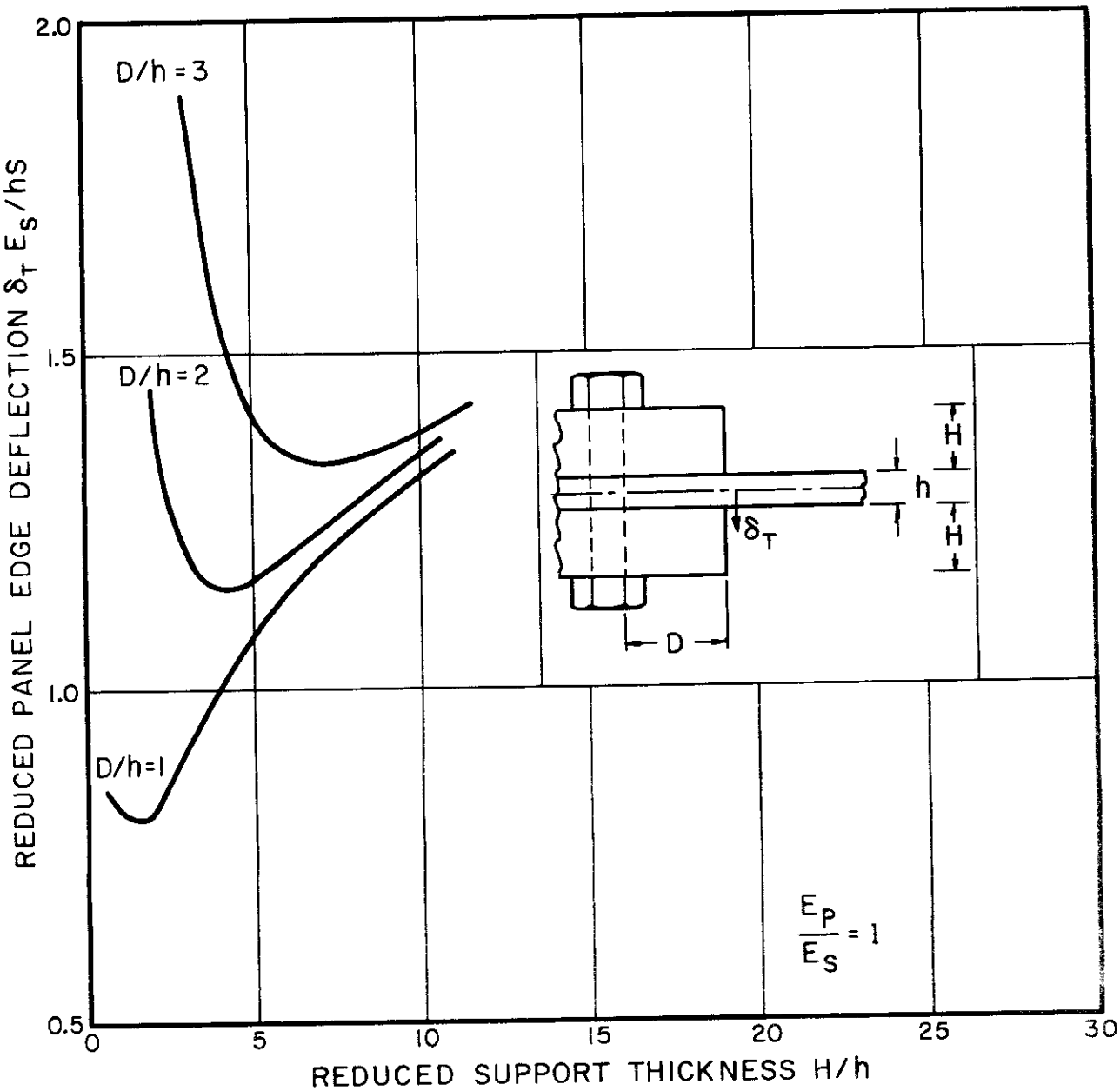

FIG. V-3 DEPENDENCE OF PANEL EDGE DEFLECTION ON SUPPORT GEOMETRY

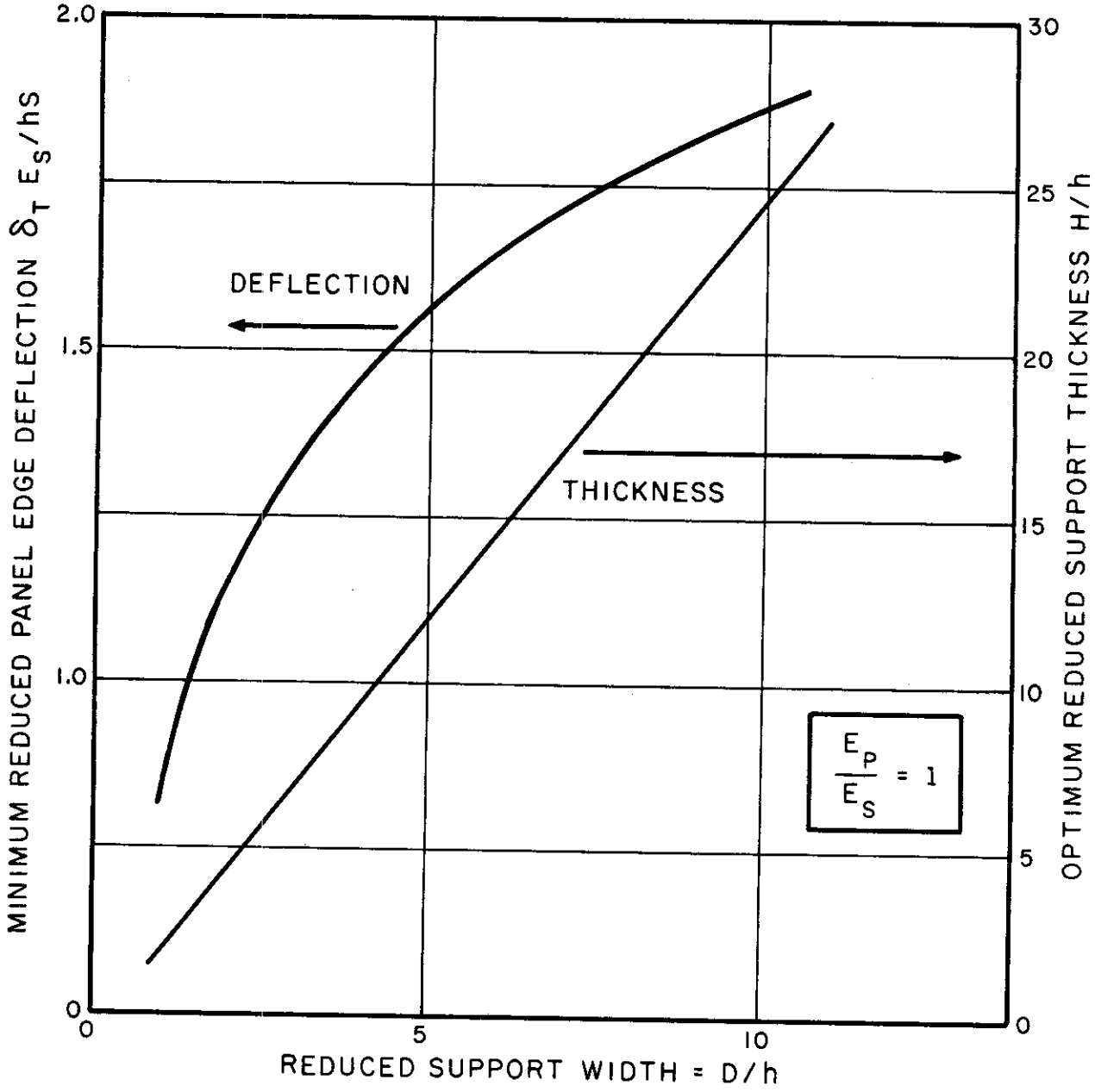

FIG. V-4 OPTIMIZATION OF EDGE CLAMP GEOMETRY

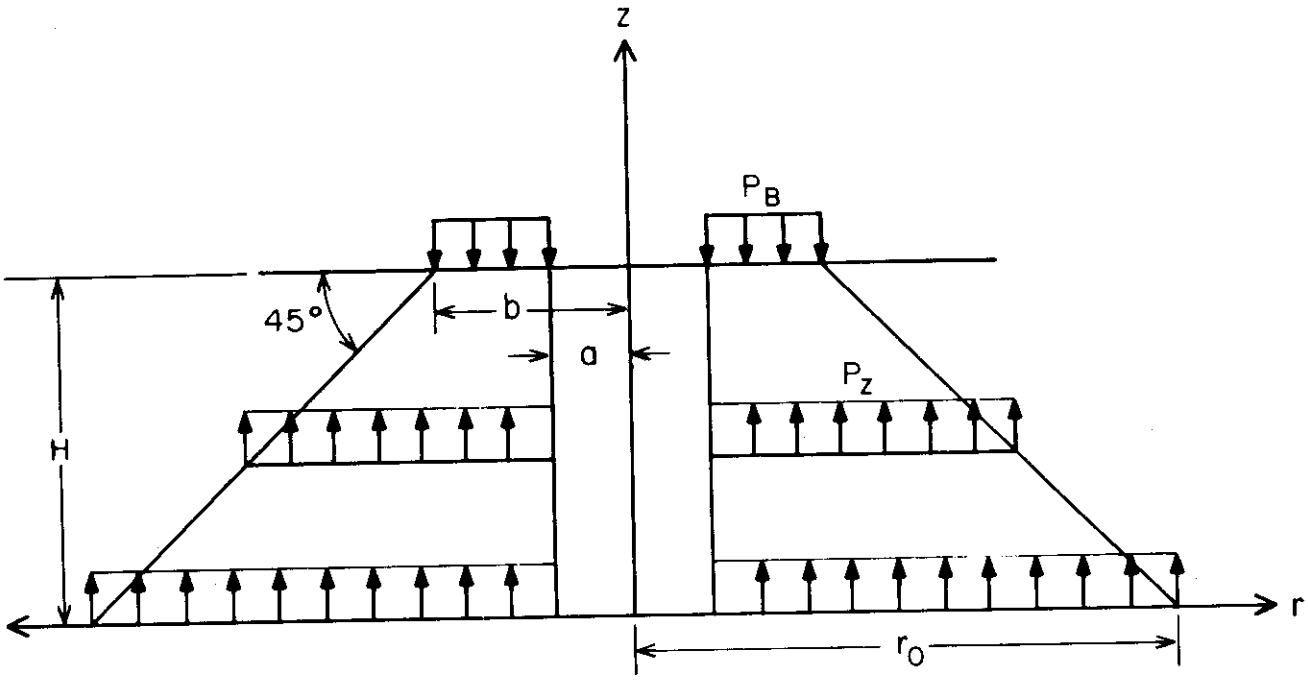

FIG. V-5 RÖTSCHER'S APPROXIMATE STRESS DISTRIBUTION UNDER A BOLT HEAD

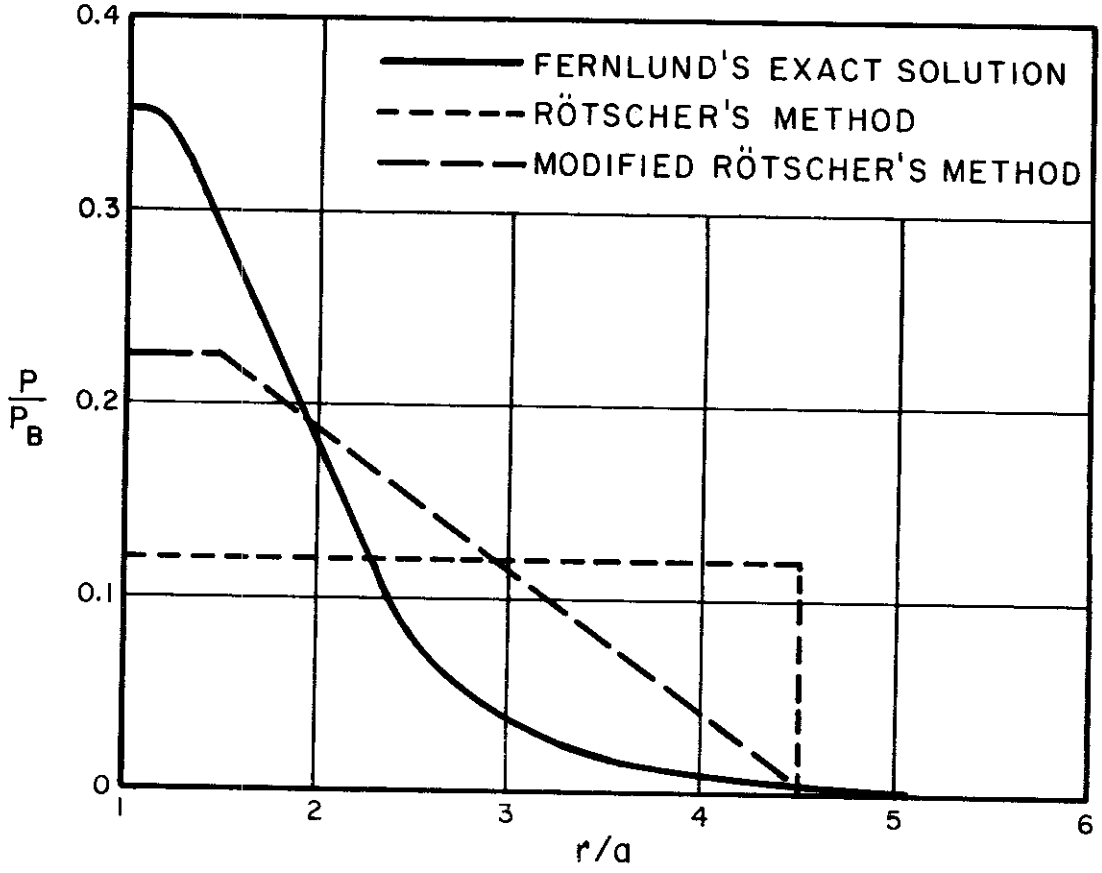

FIG. V-6 CONTACT PRESSURE DISTRIBUTION

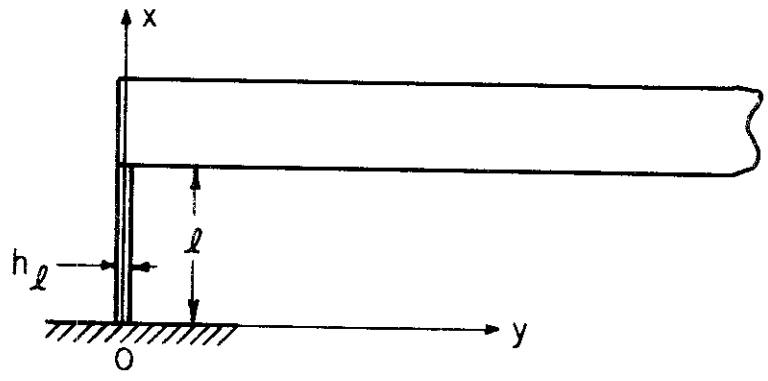

FIG. V-7 FLEXURE-SUPPORTED PANEL EDGE

Unclassified
Security Classification

DOCUMENT CONTROL DATA - R & D

(Security classification of title, body of abstract and indexing annotation must be entered when the overall report is classified)

1. ORIGINATING ACTIVITY (Corporate author)
Bolt Beranek and Newman Inc.
50 Moulton Street
Cambridge, Massachusetts 02138

2a. REPORT SECURITY CLASSIFICATION
Unclassified

2b. GROUP

3. REPORT TITLE
CONSIDERATIONS IN THE DESIGN OF SUPPORTS FOR PANELS IN FATIGUE TESTS

4. DESCRIPTIVE NOTES (Type of report and, inclusive dates)
Final Report, Work Conducted May 1966 to April 1967

5. AUTHOR(S) (First name, middle initial, last name)
Eric E. Ungar and Kyung S. Lee

6. REPORT DATE
September 1967

7a. TOTAL NO. OF PAGES
137

7b. NO. OF REFS
30

8a. CONTRACT OR GRANT NO.
AF 33(615)-5034

b. PROJECT NO.
4437

c. Task No. 443703

d.

9a. ORIGINATOR'S REPORT NUMBER(S)
AFFDL-TR-67-86

9b. OTHER REPORT NO(S) (Any other numbers that may be assigned this report)

10. DISTRIBUTION STATEMENT
This document is subject to special export controls and each transmittal to foreign governments or foreign nationals may be made only with prior approval of the Air Force Flight Dynamics Laboratory (FDD).

11. SUPPLEMENTARY NOTES

12. SPONSORING MILITARY ACTIVITY
AF Flight Dynamics Laboratory, Wright-Patterson AFB, Ohio 45433

13. ABSTRACT

The question is studied of how a test panel, which represents one of an assemblage of panels in a prototype (e.g., an aircraft fuselage), should be supported, so that a fatigue test of that panel yields the same result as a test of a complete prototype. The recommendation is developed that one should test the panel of interest at the center of a three-by-three panel array, rather than by itself, in order to obtain realistic representations of the boundary stiffness, energy dissipation, and energy transport properties. Considerations in obtaining practical supports that provide approximate free, clamped, and simply supported boundary conditions are investigated and reduced to design equations, graphs, and recommendations. Extensive analyses of the effects of boundary conditions on maximum stresses in resonantly and in randomly vibrating plates and cylindrical shells are appended, as are the results of experiments and analyses concerned with the determination of damping and energy transport in multipanel structures.

DISTRIBUTION OF THIS ABSTRACT IS UNLIMITED

DD FORM 1 NOV 65 1473 (PAGE 1)

Unclassified
Security Classification

14. KEY WORDS	LINK A		LINK B		LINK C	
	ROLE	WT	ROLE	WT	ROLE	WT
Stress Analysis						
Structural Mechanics						
Sonic Fatigue						
Vibrations						